



SCHOOL of
GRADUATE STUDIES
EAST TENNESSEE STATE UNIVERSITY

East Tennessee State University
Digital Commons @ East
Tennessee State University

Electronic Theses and Dissertations

Student Works

8-2009

Computational Investigation of Spin Traps Using Hybrid Solvation Models.

Sai Sriharsha Manoj Konda
East Tennessee State University

Follow this and additional works at: <https://dc.etsu.edu/etd>



Part of the [Analytical Chemistry Commons](#)

Recommended Citation

Konda, Sai Sriharsha Manoj, "Computational Investigation of Spin Traps Using Hybrid Solvation Models." (2009). *Electronic Theses and Dissertations*. Paper 1801. <https://dc.etsu.edu/etd/1801>

This Thesis - Open Access is brought to you for free and open access by the Student Works at Digital Commons @ East Tennessee State University. It has been accepted for inclusion in Electronic Theses and Dissertations by an authorized administrator of Digital Commons @ East Tennessee State University. For more information, please contact digilib@etsu.edu.

Computational Investigation of Spin Traps Using Hybrid Solvation Models

A thesis

presented to

the faculty of the Department of Chemistry

East Tennessee State University

In partial fulfillment

of the requirements for the degree

Master of Science in Chemistry

by

Sai Sriharsha Manoj Konda

August 2009

Dr. Scott Kirkby, Chair

Dr. Jeffery Wardeska

Dr. David Young

Dr. David Close

Keywords: Spin traps, Solvation Models, COSMO, PBN, DMPO

ABSTRACT

Computational Investigation of Spin Traps Using Hybrid Solvation Models

by

Sai Sriharsha Manoj Konda

The cyclic nitron 5,5-dimethyl-1-pyrroline-N-oxide (DMPO), and the lesser known linear phenyl-N-tert-butyl nitron (PBN) and its phosphorylated analogues have been used as spin traps for the investigation of free radicals in biological systems. Theoretical work on these molecules suggests that there are important differences in their properties between biological systems and isolated molecules in the gas phase, most likely resulting from intra and intermolecular hydrogen bonding. Most dielectric solvation models such as the polarized continuum model and COSMO are incapable of direct determination of solvent-spin trap chemical interactions. To examine this, hybrid models incorporating COSMO for long range effects and discrete solvent molecules for short range effects, at the DFT/B3LYP/6-31G* level of theory, have been used to study the stabilization and alteration of the spin trap molecules properties in protic and aprotic polar solvents. The hybrid models have been successfully implemented to support the prominent role played by hydrogen bonding interactions in the stabilization of spin traps.

ACKNOWLEDGMENTS

Foremost, I would like to express my sincere gratitude to my thesis advisor Dr. Scott Kirkby for his continuous support and encouragement for my research. I could not have asked for a more experienced and patient advisor and mentor for my thesis. I also would like to thank my thesis committee, Dr. Jeffery Wardeska, Dr. David Young, and Dr. David Close. Funding, in part, was provided by School of Graduate Studies Research Grant program. Sincere thanks to my parents for their continuous support and advice. Special thanks to my colleagues, faculty and staff of the Chemistry Department at ETSU, for their unending support and motivation.

CONTENTS

	Page
ABSTRACT	2
ACKNOWLEDGMENTS	3
LIST OF TABLES	8
LIST OF FIGURES	10
Chapter	
1. INTRODUCTION	11
Generation of Hydroxyl radicals.....	12
Fenton reaction.....	12
Photolysis.....	12
Potassium Peroxynitrite	13
Reactions of Hydroxyl radicals	13
Electron Transfer	13
Hydrogen Abstraction	14
Addition Reactions	15
Addition Reactions with Aromatic compounds	16
Detection of Radicals	17
Electron Paramagnetic Resonance	18
Hyperfine Coupling	22
Spin-trapping	23
History and Development	23
ESR Spectroscopy and Spin Trapping	25

Spin Trap Stabilities	26
C-Nitroso Spin Traps	26
Dimerization	26
Photochemical Degradation	27
Redox Reactions	27
Dissociative α -cleavage	28
Nitrones	29
Dimerization	30
Disproportionation	30
Dissociative α -cleavage	31
Addition reactions	32
Decomposition	33
Phosphorylated Nitrones	36
Applications of Spin Traps	37
2. QUANTUM MECHANICS	38
Schrödinger Equation	38
Approximations	45
The Born-Oppenheimer Approximation	45
Hartree-Fock Theory	47
Hartree's Procedure	49
Density Functional Theory	60
Hohenberg-Kohn Theorem	61
Kohn-Sham Method	63

Solvation	67
Poisson Equation	68
Self-Consistent-Reaction-Field (SCRF) Models	69
Born-Kirkwood-Onsager Method	69
Gibbs Energy of Solvation	72
Electrostatic Contribution	74
Cavitation Contribution	74
Dispersion-repulsion Contribution	76
Molecular Motion	77
Classic Continuum-Solvent Methods	77
Solvent Accessible Surface Area	77
Generalized Born Model	78
Polarized-Continuum Method (PCM).....	78
Conductor-like Solvation Model (COSMO)	80
Atomic Units	80
Basis Sets	81
3. RESULTS AND DISCUSSION	86
Computational Details	86
Input Files	86
Discussion of Results	91
DMPO Solvation Studies	93
PBN Solvation Studies	101
PBN-Me Solvation Studies	114

PPN Solvation Studies	121
Aprotic Studies	128
Conclusion	130
4. FUTURE WORK	131
REFERENCES	133
APPENDICES	141
Appendix A: Single Point Energy Tables	141
Appendix B: Structural Details of DMPO	143
Appendix C: Structural Details of PBN/PBN-OH	145
Appendix D: Structural Details of PBN-Me	149
Appendix E: Structural Details of PPN	152
Appendix F: COSMO Files	155
APPENDIX G: Output Coordinates for the Optimized Spin Traps	160
VITA	166

LIST OF TABLES

Table	Page
1. Chemical Nomenclature of the spin traps in this work.....	24
2. Advantages and disadvantages of DMPO and PBN.....	35
3. NWChem input file of DMPO.....	87
4. NWChem input file of DMPO solvation using COSMO model	89
5. Dipole moments of DMPO-type and the PBN-type Spin Traps at the COSMO/B3LYP/6-31G* level.....	91
6. Geometry changes (trends in bond lengths and bond and bond angles) in DMPO	96
7. Trends in torsion angles in DMPO	98
8. Hydrogen bond lengths in DMPO hybrid model	99
9. Trends in dipole moments for the DMPO spin trap	100
10. Calculated single point energies and dipole moments for the hydroxyl radical, spin trap and two adduct conformers at the B3LYP/6-31G* level	103
11. Geometry changes (trends in bond lengths and bond angles) in PBN-OH <i>cis</i> adduct	107
12. Trends in torsion angles for the PBN-OH <i>cis</i> adduct	109
13. Hydrogen bond lengths in PBN-OH <i>cis</i> adduct	110
14. Geometry changes (trends in bond angles) in PBN-OH <i>trans</i> adduct	111
15. Hydrogen bond lengths in PBN-OH <i>trans</i> adduct	111
16. Torsion angle comparison between <i>cis</i> and <i>trans</i> PBN-OH adducts.....	112
17. Trends in dipole moment for the PBN-OH <i>cis</i> adduct	113

18. Geometry changes (trends in bond angles) in PBN-Me adduct	117
19. Trends in torsion angles for the PBN-Me adduct	118
20. Hydrogen bond lengths in PBN-Me <i>cis</i> adduct	119
21. Trends in dipole moment for PBN-Me adduct	120
22. Geometry changes (trends in bond lengths and bond angles) in PPN spin trap	124
23. Trends in torsion angles for the PPN spin trap	125
24. Hydrogen bond lengths in PPN spin trap	126
25. Trends in dipole moment for PPN spin trap	127
26. Molecular energies of PBN in acetonitrile	129
27. Difference in single point energies of DMPO when surrounded by water molecules	141
28. Difference in single point energies of PBN-OH <i>cis</i> adduct when surrounded by water molecules	141
29. Difference in single point energies of PBN-Me adduct when surrounded by water molecules	142
30. Difference in single point energies of PPN when surrounded by water molecules	142

LIST OF FIGURES

Figure	Page
1. PBN-type and DMPO-type spin traps	18
2. DMPO spin trap	93
3. DMPO spin trap surrounded by water molecules	94
4. Plot of the difference in the single point energy of DMPO as a function of the number of water molecules in the hybrid model	95
5. PBN-OH adduct in the <i>cis</i> conformation with respect to the nitroxide group	101
6. PBN-OH adduct in the <i>trans</i> conformation with respect to the nitroxide group	102
7. Plot of the difference in single point energies of the PBN-OH <i>cis</i> -adduct as a function of the number of water molecules	104
8. PBN-OH <i>cis</i> adduct surrounded by water molecules	105
9. PBN-OH <i>trans</i> adduct surrounded by water molecules	106
10. PBN-Me <i>cis</i> adduct	114
11. PBN-Me <i>cis</i> adduct surrounded by water molecules	115
12. Plot of the difference in single point energies of the PBN-Me adduct as a function of the number of the water molecules	116
13. PPN spin trap	121
14. PPN spin trap surrounded by water molecules	122
15. Plot of the difference in single point energies of PPN as a function of the number of water molecules.....	123
16. PBN spin trap surrounded by acetonitrile molecules	128

CHAPTER 1

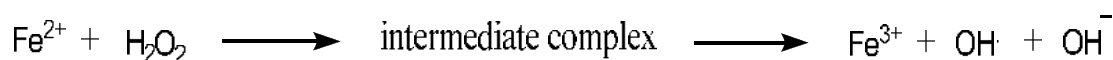
INTRODUCTION

A general definition of the term 'radical' is often defined as a group of atoms having unpaired electrons such as the methyl radical ($\text{CH}_3\cdot$) and the hydroxyl radical ($\text{OH}\cdot$). We can however define a 'free radical' as any entity possessing unpaired electrons and capable of independent existence. Free radicals may be broadly classified by the atom on which the unpaired spin is localized. Hence we can have oxygen centered radicals, carbon centered radicals, phosphorous centered radicals, nitrogen centered radicals, etc.. The role of radicals in biological systems may be both deleterious and beneficial. Many undesired processes in biological systems [1, 2] including ionizing radiation damage, aging, and many cancers are believed to be the result of free radicals. Free radicals are also believed to be the precursors for oxidative damage processes like lipid peroxidation, enzyme inactivation, and DNA cleavage.[3, 4] These damaging processes lead to various diseases like ischemic and postischemic reperfusion cell damage (a condition that results in blood flow deprivation of the tissues and organs).[5] The C-centered radicals that are generated during metabolism of certain drugs such as 1, 2-disubstituted hydrazines are considered as both carcinogenic and as antitumor agents.[4] Thiyl radicals that are generated as a result of hydrogen abstraction of thiols by C-centered and O-centered radicals are also considered as prevalent damaging agents.[4] Nitric oxide is an important mediator in processes like neurotransmission, and as a regulator of the superoxide radical ion.[5] The most damaging groups of radicals are the oxygen free radicals (OFR) and reactive oxygen species (ROS). These are considered to be precursors to heart damage, cardiovascular dysfunction, lung damage, oncogenesis, and ischemic injury. The superoxide radical anion undergoes dismutation to generate hydrogen peroxide, a source for the most reactive hydroxyl radical.[5]

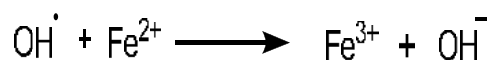
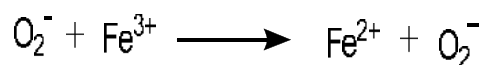
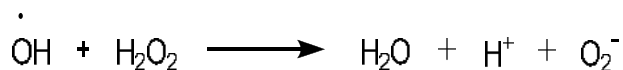
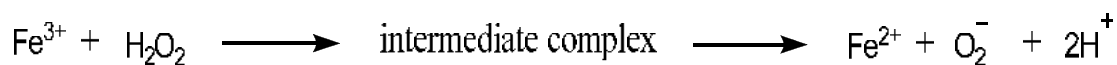
Generation of Hydroxyl radicals

Fenton Reaction

In 1894, Fenton observed that many organic molecules react with a mixture of hydrogen peroxide and Fe(II) salts.[6] The reactivity was attributed to the generation of the hydroxyl radical:



Other possible reactions are:



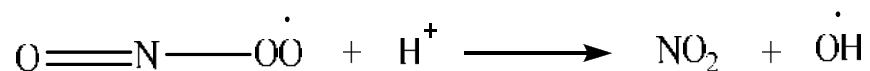
In addition to the single-electron reduction of hydrogen peroxide using Fenton's procedure, reduction by other metal ions such as Ti^{3+} also give the hydroxide ion and the hydroxyl radical.[7]

Photolysis

Hydroxyl radicals may be generated by photolysis of hydrogen peroxide or hydroperoxides.[8] The one disadvantage with this method is that the short wavelength (254 nm) used is absorbed by the substrate rather than the peroxide.[9] Hydroxyl radicals may be generated at longer wavelengths (>300 nm) by the irradiation of phthalimide hydroperoxides, but the efficiency is low.[10]

Potassium Peroxynitrite

Irradiation of potassium nitrate at 254 nm generates a solid solution of potassium peroxynitrite ($\text{O}=\text{N}-\text{OO}-\text{K}^+$) in potassium nitrate. Hydroxyl radicals are generated as a result of the homolysis of peroxynitrous acid when the solid is added to an aqueous solution at pH 7.0.

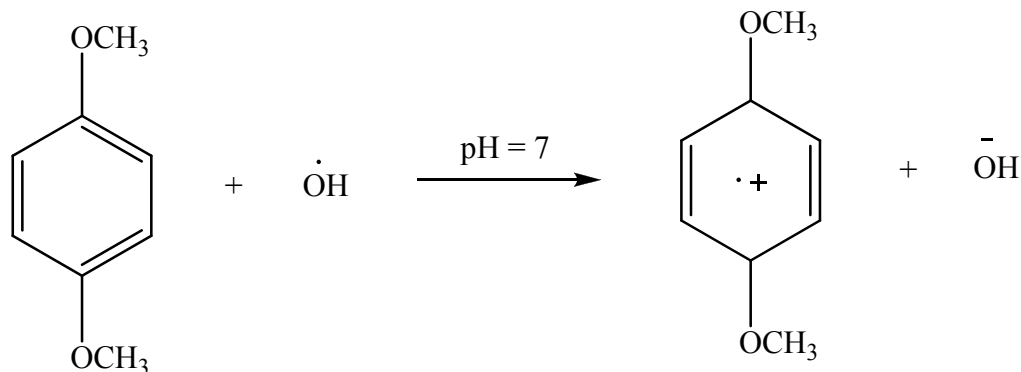
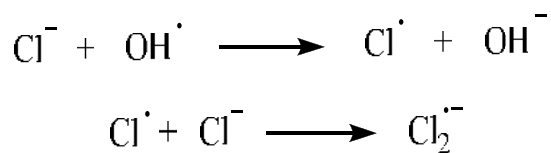


Reactions of Hydroxyl Radicals

The hydroxyl radical has a high rate-constant (on the order of $\sim 10^9 \text{ dm}^3\text{mol}^{-1}\text{s}^{-1}$ [4]) for reaction with a number of species in biological systems. The reactions may be classified as: electron transfer, hydrogen abstraction, and addition reactions.

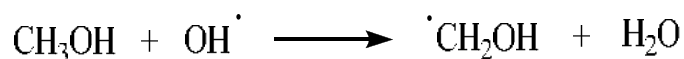
Electron Transfer

Both inorganic and organic compounds participate in electron transfer reactions with the hydroxyl radicals, e.g.

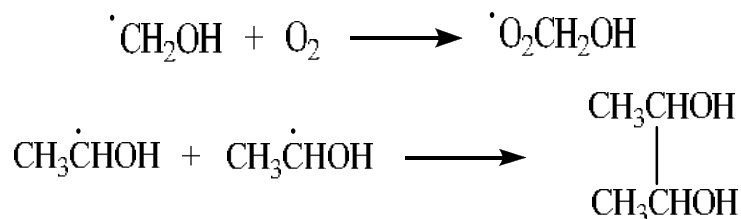


Hydrogen Abstraction

Owing to the high reactivity of the hydroxyl radical, hydrogen abstraction may take place from most organic substrates. The reactivity is much higher than its alkoxy analogues such as the *t*-butoxy radical. For example, consider the reaction of the hydroxyl radical with alcohols where the radical abstracts the H atom from the alcohol generating water and leaving a free electron on the carbon atom:



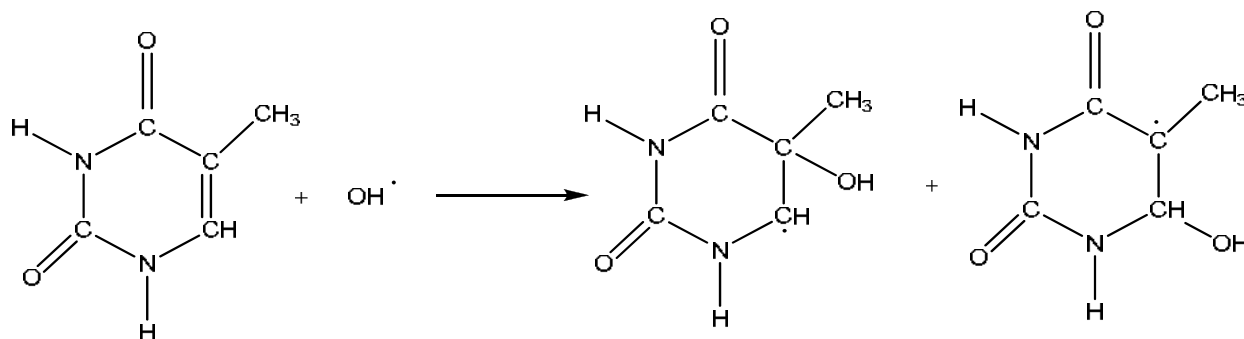
The carbon-centred radical may react further to generate radicals or non-radical species. The intermediate radical may undergo oxidation, reduction, or dimerization reactions that are responsible for the generation of non-radical species.



In the above reactions the alpha hydrogens are more readily abstracted than the beta or the gamma hydrogens.[11] The difference in the C-H bond dissociation energies is reflected in the reactivity of the alpha or beta hydrogens that increase as primary < secondary < tertiary.[12] Heteroatoms such as oxygen and nitrogen in the alcohol and amide functionalities facilitate faster abstraction of the alpha hydrogens.[13] The abstraction rate is slower in the presence of electron withdrawing groups such as aldehydes, ketones, and halogens.[13]

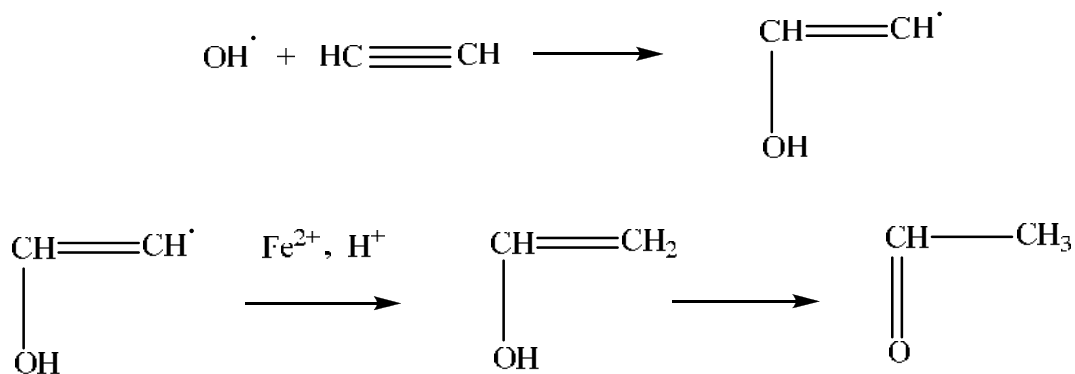
Addition Reactions

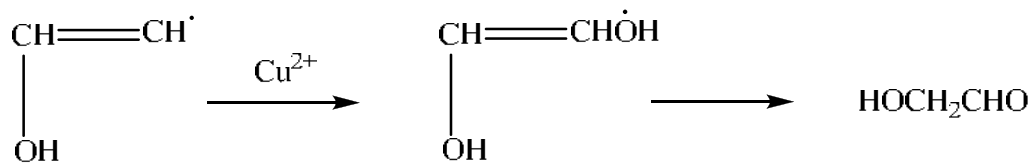
Hydroxyl radicals also have a high reactivity towards aliphatic unsaturated species and aromatic compounds. The hydroxyl radical reacts with aromatic species through an addition mechanism, and a similar reaction takes place with purine and pyrimidine bases that are the major components of DNA and RNA. The reaction with thymine occurs as follows:



The thymine radical reacts further with oxygen to generate a more reactive thymine peroxy radical. Hence the hydroxyl radical has damaging consequences for the base pairs in DNA and RNA. The irreversible nature of the damage, if unrepaired, eventually leads to the death of the cell.[14]

The hydroxyvinyl radical is generated upon the reaction with acetylene, and the radical may either be oxidized by cupric ions to give hydroxyacetaldehyde or reduced by ferrous ions to generate acetaldehyde.[14]

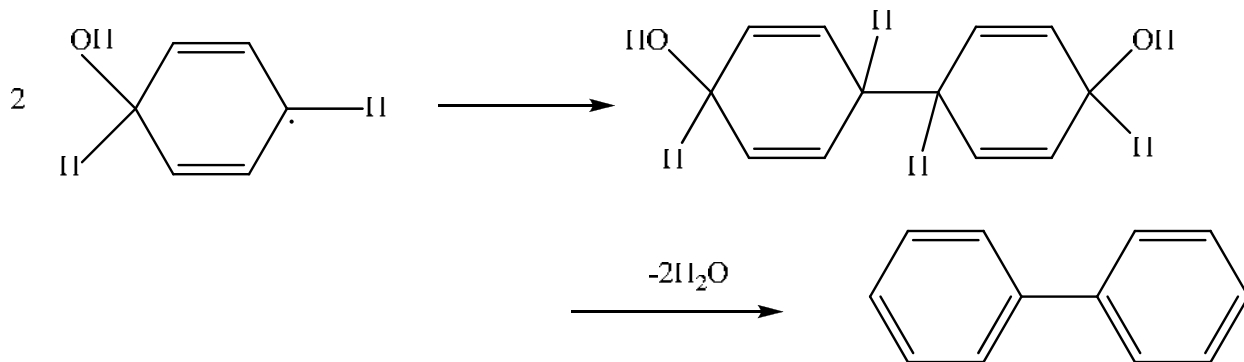
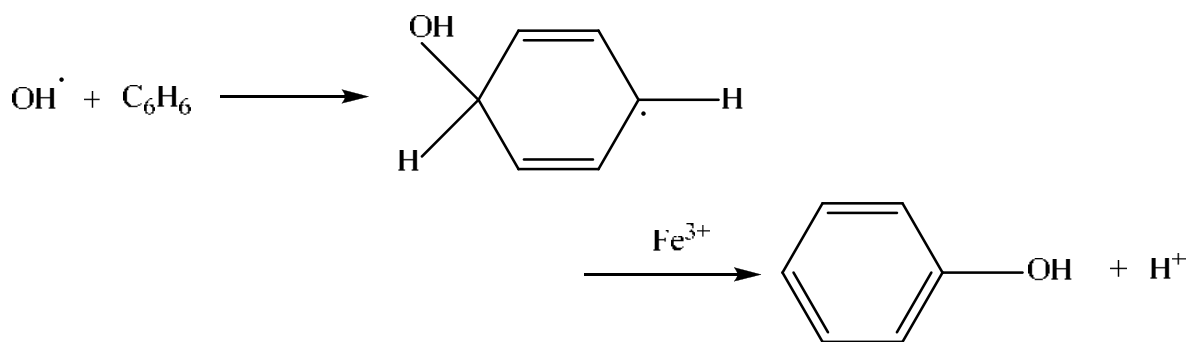




Malic acid can be generated by the ferrous ion reduction of the radical intermediate that is obtained by the addition reaction of hydroxyl radical and maleic acid.[15, 16]

Addition reaction with Aromatic compounds

Addition reactions take place with an aromatic compound



Detection of Radicals

The trapping and subsequent characterization of free radicals become very important in order to understand the various biological mechanisms. Because of their high reactivity, and hence short lifetimes, radicals and their reactions often need to be studied by indirect means. The available detection techniques are as follows:

1. Flash photolysis
2. Pulse radiolysis
3. Nuclear Magnetic Resonance
4. Electron Nuclear Double Resonance (ENDOR)
5. Chemically Induced Dynamic Nuclear Polarization (CIDNP)
6. Electron Spin Resonance (ESR)/ Electron Paramagnetic Resonance (EPR)

Of all the techniques listed above, ESR/EPR is the most commonly used. A common drawback with all these techniques is that the lifetime of the radical is often too short to be detected by any of them. Hence the challenge is to generate stable radicals that may be detected. One such route is to react the radical with a molecule that will result in a more stable product (or adduct), but one that still preserves the unpaired spin. Such species are referred to as spin traps.[17]

Spin traps have been used extensively by biochemists [18-21] for their intended purpose, but spin traps with better reactivity and selectivity among the common oxidative radicals are still needed. To improve the selectivity, details of the reaction mechanism must be properly understood so that the relevant structure property relationships may be deduced.

Most current spin traps are based on nitrones and may be divided into two families: the linear or PBN (Phenyl-N-tert-butyl-nitron) type and the cyclic or DMPO (5,5-Dimethyl-pyrrolidinium-N-oxide) type.

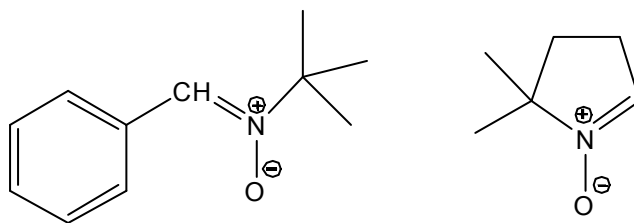


Figure 1. PBN-type and DMPO-type spin traps.

Electron Paramagnetic Resonance

The primary technique used for the detection of paramagnetic species is Electron Paramagnetic Resonance (EPR) or Electron Spin Resonance (ESR). This branch of spectroscopy is predominantly absorption spectroscopy. The energy absorbed corresponds to the electromagnetic radiation of frequencies that range from 1 megahertz (10^6 Hz) to several terahertz (10^{12} Hz), although the most common is the X-band at 9.5 GHz.

EPR spectroscopy monitors the absorption of energy when the molecule of interest is irradiated with an electromagnetic field. The electromagnetic field consists of oscillating electric and magnetic fields that are mutually perpendicular to each other. It is the magnetic field component (B_0) that interacts with the paramagnetic species resulting in the absorption of energy. This absorption can occur only when the ‘resonance’ condition is met, i.e. when the spacing between the energy levels $\Delta E = h\nu$ (which is the quanta of radiation). Spin is an inherent property of electrons and nuclei and is an intrinsic angular momentum. Electron spin states are not of equivalent energy in the presence of an external magnetic field, as any moving charge generates a magnetic field of its own. This gives rise to the magnetic moment (μ) generated as a result of the charge and the spin. The relation between the magnetic dipole moment and spin angular momentum S is:

$$\mu = \gamma S \quad (1-1)$$

where γ is the gyromagnetic ratio. The gyromagnetic ratio of a particle or a system is defined as the ratio of the magnetic moment to its angular momentum. The classical expression for γ is:

$$\gamma = q / 2m \quad (1-2)$$

where q and m are the charge and mass of the particle respectively. The electron spin is a pure quantum mechanical phenomenon and does not have a classical mechanical analogue. A dimensionless factor called the *g-factor* is introduced into the gyromagnetic ratio expression for an isolated electron

$$\gamma_e = -g_e (e / 2m_e) \quad (1-3)$$

The Bohr magneton is a constant defined in SI units as:

$$\beta = e\hbar / 2m_e \quad (1-4)$$

Hence the magnetogyric ratio may be expressed in terms of the Bohr magneton as:

$$\gamma_e = -(2\pi g_e \beta / h) \quad (1-5)$$

The magnetic dipole moment may now be expressed as:

$$\mu = -(2\pi g_e \beta / h) S \quad (1-6)$$

The Uncertainty Principle states that only a single Cartesian component may be well defined and that it can have only one of the two possible values. If we consider the component of S along the z -axis then,

$$S_z = (\hbar / M_s) \quad (1-7)$$

where $M_s = \pm 1/2$, M_s is called the spin quantum number. Substitution of this result in Equation 1-6 gives an expression for magnetic dipole moment as:

$$\mu = -g_e \beta M_s \quad (1-8)$$

The energy of interaction of the magnetic dipole moment with the external magnetic field is given as:

$$E = -\mu \cdot B \quad (1-9)$$

Hence the energy separation between the spin states may be written as:

$$\Delta E = g_e \beta B M_s = \pm g_e \beta B \quad (1-10)$$

This electronic energy is designated as the Zeeman interaction after Peter Zeeman who discovered the effects of magnetic fields on atomic spectra. In the presence of the external magnetic field, the electronic spin aligns itself in a parallel or anti-parallel configuration. The ground state corresponds to the parallel configuration and the energy separation between these configurations is given by the above expression. The spectrum is generated by varying the magnetic field and the transition occurs when the resonance condition is met. The electron present in the ground state absorbs this energy resulting in a transition to the higher level. The available energy states are described by a matrix energy function called the spin Hamiltonian. The various energy levels may be derived from this matrix. The Zeeman Hamiltonian expression can be written as

$$H_z = g_e \beta S_z B_0 \quad (1-11)$$

where the applied magnetic field is directed along the z -direction. The spin Hamiltonian is given as:

$$H = H_{elect} + H_{cf} + H_{LS} + H_{SS} + H_{Zee} + H_{hfs} + H_Q + H_N \quad (1-12)$$

where the terms are given below along with the approximate magnitude:

$$\mathcal{H}_{elect} = \text{electronic energy} \sim 10^4 - 10^5 \text{ cm}^{-1}$$

$$\mathcal{H}_{cf} = \text{crystal field energy} \sim 10^3 - 10^4 \text{ cm}^{-1}$$

$$\mathcal{H}_{LS} = \text{spin-orbit interaction} \sim 10^2 \text{ cm}^{-1}$$

$$\mathcal{H}_{SS} = \text{spin-spin interaction} \sim 0-1 \text{ cm}^{-1}$$

$$\mathcal{H}_{Zee} = \text{Zeeman energy} \sim 0-1 \text{ cm}^{-1}$$

$$\mathcal{H}_{hfs} = \text{hyperfine structure} \sim 0 - 10^2 \text{ cm}^{-1}$$

$$\mathcal{H}_Q = \text{quadrapole energy} \sim 0-10^2 \text{ cm}^{-1}$$

$$\mathcal{H}_N = \text{nuclear spin energy} \sim 0-10^3 \text{ cm}^{-1}$$

The statistical distribution of the paramagnetic species is given by the Boltzmann distribution that gives the ratio of the number of electrons in the upper and lower levels.

$$N_{upper} / N_{lower} = \exp[-h\nu / kT] \quad (1-13)$$

where h is the Planck's constant and k is the Boltzmann constant. The ratio at room temperature indicates that the higher energy state has a lower population as compared to the ground state and hence we observe a net absorption of energy.

Hyperfine Coupling

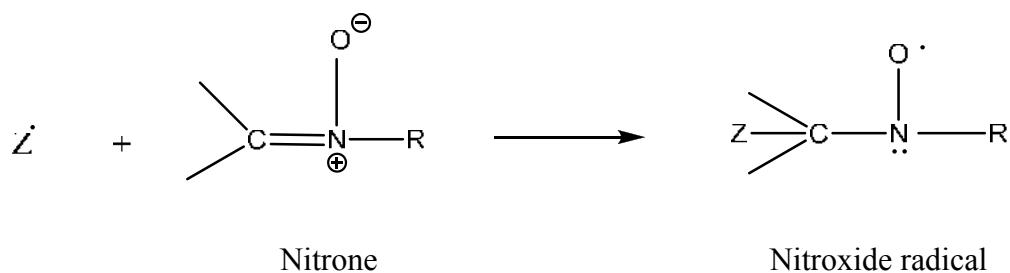
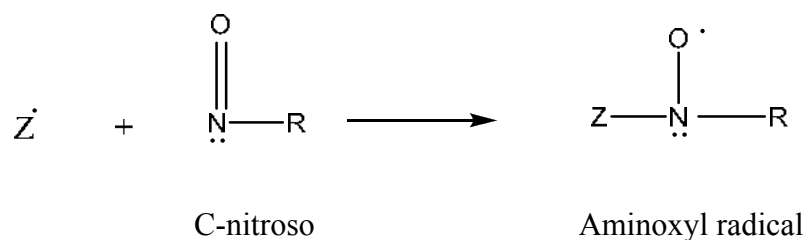
The unpaired electron is influenced by the magnetic field of neighboring spin systems such as a nucleus with spin. As a consequence, the net field experienced by the electron is slightly greater than or smaller than the field it would have experienced in the absence of the neighboring spin system. The change is dependent on the direction of the perturbing additional field. For an applied field of B_0 and a perturbing field of δB , resonance now occurs at $B_1 = B - \delta B$ and $B_2 = B + \delta B$. The spacing between the two lines is defined as the coupling constant. As the original lines are now split, the spacing between the lines is also known as the splitting constant. The splitting constant in other words indicates the degree of interaction of the unpaired electron with the spin system. The unpaired electron can experience a field generated by two different types of nuclei: equivalent and non-equivalent nuclei. For the n equivalent nuclei with a net spin of nI , the total number of lines are predicted to be $2nI + 1$. For non-equivalent nuclei the number of lines will be given by the product of individual sets of nuclei: $(2n_1I_1 + 1)(2n_2I_2 + 1) \dots$ where n_1, n_2 are the number of nuclei with spins I_1 and I_2 respectively. Historically the splitting of lines observed due to the interaction of unpaired electrons is termed as *fine splitting*. The pattern obtained from the interaction of unpaired electrons with nuclear spins is termed *hyperfine splitting*, and the pattern obtained from the interaction of unpaired electrons with nonbonded nuclei is termed as *super-hyperfine splitting*.

The predominant mechanisms by which the electrons and nuclei interact are:

- a) Fermi-contact interaction: applicable to isotropic interactions and the spectra is independent of the sample orientation in the applied magnetic field.
- b) Dipolar interaction: applicable to anisotropic interactions and the spectra is dependent on the sample orientation.
- c) Spin polarization: applicable for π – electron rich radicals such as aromatic radicals.

Spin-trapping

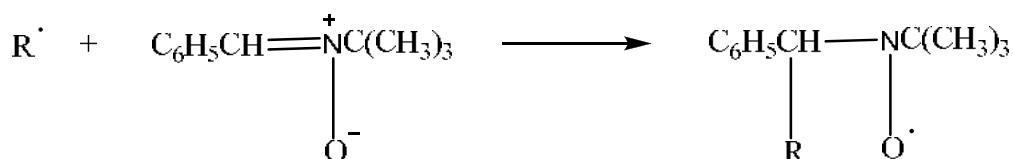
The term spin trapping refers to the method of detecting radicals wherein an addition reaction occurs between an unsaturated compound and a radical resulting in the generation of another radical with a longer lifetime. The most commonly used unsaturated compounds for spin trapping are C-nitroso and nitrones. The resultant species are aminoxyl or nitroxide radicals and are more stable than the parent radicals and may be detected by ESR spectroscopy.



The C-nitroso and the nitron compounds are known as spin traps, and the addition products are designated as spin adducts.

History and Development

The idea of spin traps originated with two papers by Iwamura and Inamoto where they reported the addition of cyano radicals to PBN generating a stable nitroxide.[22, 23]



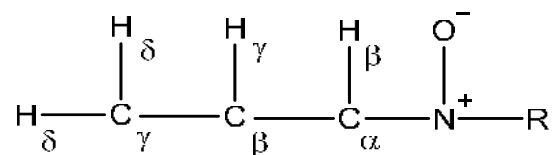
The first proposal for the use of the above addition reaction for free radical detection was given by Janzen and Blackburn [17, 24, 25] for nitrones and by Lagercrantz [26, 27] and Perkins [28] for C-nitroso compounds. Leaver and Ramsey [29] investigated the hydrogen abstraction in the photolysis of benzophenone by using the addition reaction of radicals to 2-methyl-2-nitrosopropane. Terabe and Konaka [30] used nitrosobenzene for the detection of radicals generated in nickel peroxide oxidation of hydrocarbons. Studies indicated that both nitrones and nitroso compounds were capable of trapping C-centered radicals.[31] Nitrogen-centered radicals are also trapped to give stable adducts.[32] Oxygen-centered radicals form unstable adducts with nitroso compounds but readily form stable adducts with nitrones.[33] Sulfur radicals form unstable adducts with both nitrones and nitroso compounds.[34] Phosphorus-centered radicals are readily trapped by both species of spin traps.[35] The chemical nomenclature employed in naming the spin traps is as follows (see Table 1):

Table 1. Chemical Nomenclature of the spin traps in this work.

Acronym	Formal Name
DMPO	2,2-Dimethyl-pyrrolidinium-N-oxide
DMPO-OH	2,2-Dimethyl-5-hydroxylpyrrolidine-N-oxide
PBN	Phenyl-N-tert-butylnitron
PBN-OH	Hydroxy-phenyl-N-tert-butylnitron
PBN-Me	Methyl-phenyl-N-tert-butylnitron
PPN	N-benzylidene-1-diethoxyphosphoryl-1-methylethylamine N-oxide

ESR Spectroscopy and Spin Trapping

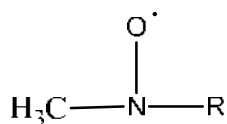
The common nomenclature employed in labeling the positions of the nuclei in the aminoxyl function is as follows



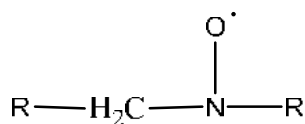
The structural characterization of the radical trapped may be deduced from the spectra. The salient features employed in characterization are as follows

1. Splitting pattern
2. Nitrogen and other nuclear hyperfine splitting constants
3. Line-widths of the individual lines
4. *g*-value

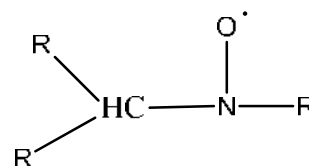
The ESR spectra of C-nitroso spin traps are more easily interpreted than the nitrones as the radical is directly bound to the aminoxyl group. This generates a characteristic pattern specific to the radical attached to the nitrogen atom.



1:3:3:1 quartets



1:2:1 triplets



1:1 doublets

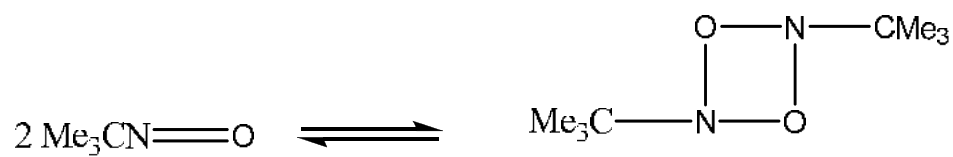
In addition, the spacing between the lines (isotropic hyperfine splitting constant (hfsc)) is also characteristic for the kind of radical trapped. If the aminoxyl nitrogen is ^{14}N , the unpaired spin interacts with the nitrogen nucleus to give three nondegenerate energy levels due to hyperfine coupling. These energy levels are further split due to the interaction with the β hydrogen nucleus. The magnitude of the ^{14}N -hfsc varies with the spin density and the planarity about the nitrogen atom. The *g*-value increases for electrons localized on atoms having higher

atomic numbers. Hence the g -value varies with the nature of the neighboring groups being either electron-withdrawing or electron-donating. In the case of nitrones, the free radical is bound in the β -position. In the presence of additional nuclei with non zero spins, the β -hfsc will provide additional information. Hence we have an additional set of unique parameters for identification of the radicals.

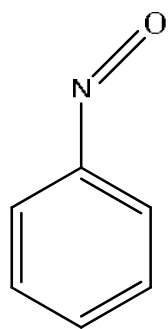
Spin Trap Stabilities

C-nitroso Spin Traps

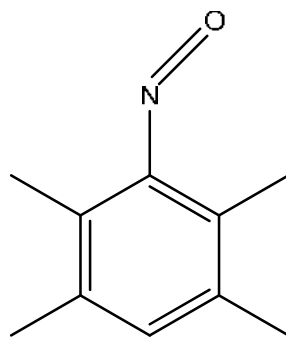
Dimerization. The C-nitroso spin trap adducts are susceptible to dimerization as is evident in the case of 2-methyl-2-nitrosopropane (MNP).[36]



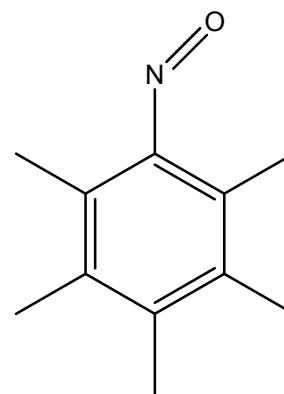
The C-nitroso aromatic spin trap adducts are more stable and tend to dimerize less. The more common nitroso aromatic compounds are as follows:



Nitroso benzene

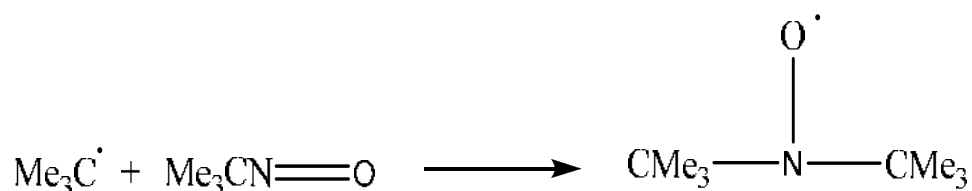
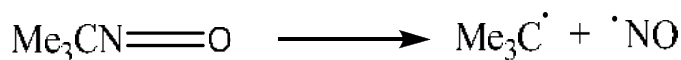


Nitroso durene



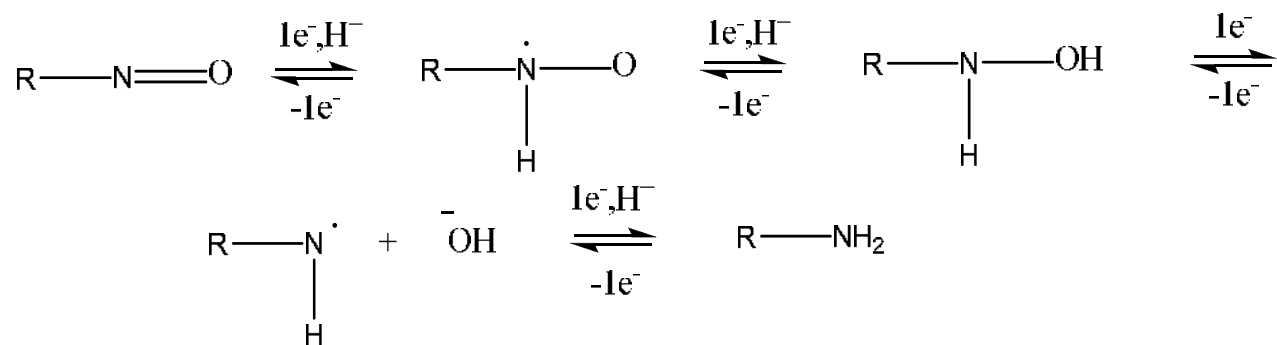
Pentamethyl nitrosobenzene

Photochemical Degradation. One of the major side reactions in using acyclic nitroso spin traps is their photo dissociation leading to the generation of NO radicals.

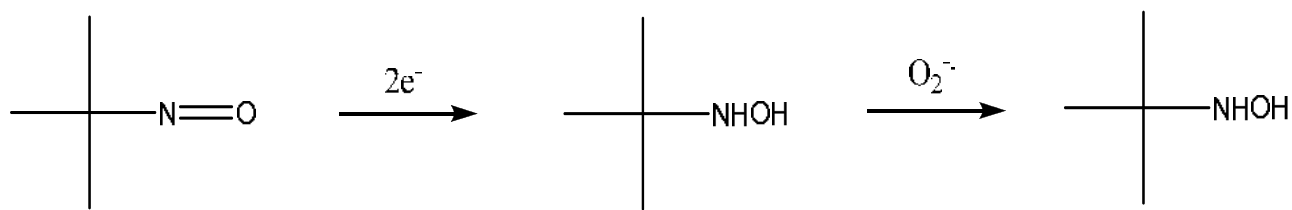


The NO[•] radicals are trapped by the nitroso spin trap present in high concentration to generate extremely stable aminoxyls. This generates a false positive as the aminoxyls are ESR active. The aromatic nitroso spin traps are less sensitive to photolysis. The structure of the nitrosoalkane often dictates the λ_{max} of the reaction. For example, the photolysis of nitrosobenzene takes place in the ultraviolet range, 320-360 nm,[37] whereas the photolysis of MNP (2-methyl-2-nitrosopropane) occurs at longer wavelengths, around 680 nm.[38] Hence the experimental conditions change according to the spin trap employed for trapping radicals.

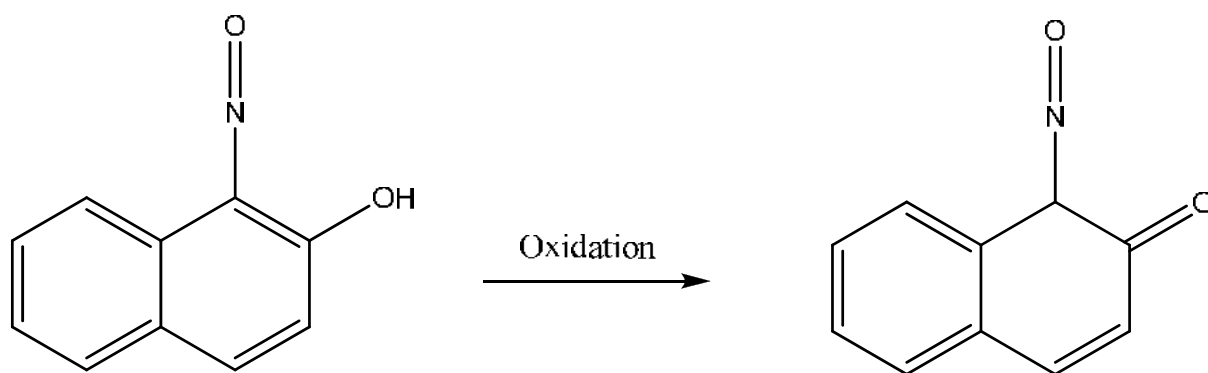
Redox Reactions. The reactions of the nitroso spin traps in biological systems are restricted because of a series of redox reactions.



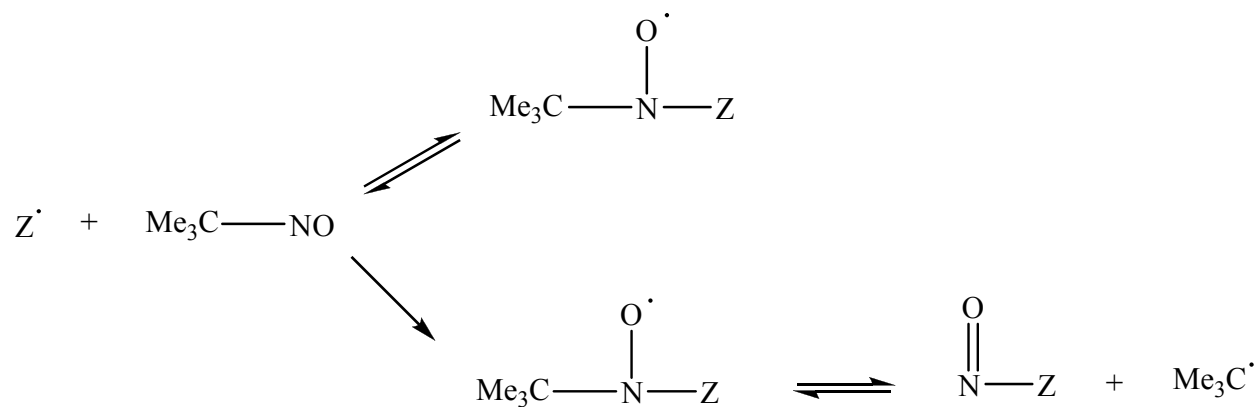
Studies on MNP have indicated a reduction to hydroxylamine, [39] and further oxidation by superoxide radical anion yielding hydronitroxide.[39]



In the biological system, aromatic nitroso spin traps are oxidized by peroxidases to iminoxyls. For example, 1-nitroso-2-naphthol is oxidized as [40]



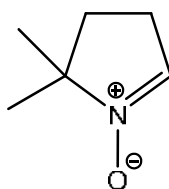
Dissociative α -cleavage. Spin traps are stabilized by the presence of bulky groups on the nitroxyl carbon. The bulky groups can however initiate dissociation reactions which reduce the lifetime of the adducts. For example, MNP dissociates to give trimethyl radical.[41]



In conclusion, C-nitroso spin traps are toxic, carcinogenic, or mutagenic, due to which they are rarely employed for *in-vivo* studies.[42-45].

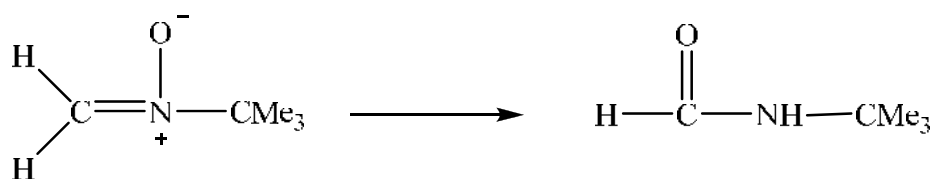
Nitrones

The most stable nitrones are the five and six carbon atom systems.

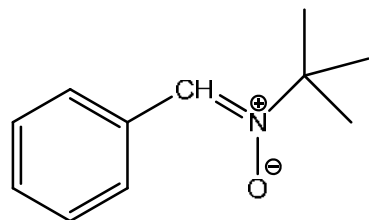


5,5- Dimethyl-pyrrolidinium-N-oxide

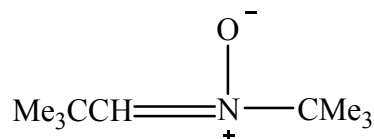
The instability of the smaller nitron systems is reflected in the case of N-tert-Butyl nitron. It rearranges on standing to N-tert-butyl formamide.



The stability of the spin trap is improved by attaching a tert-butyl or aryl group to the carbon atom adjacent to the nitron functionality.

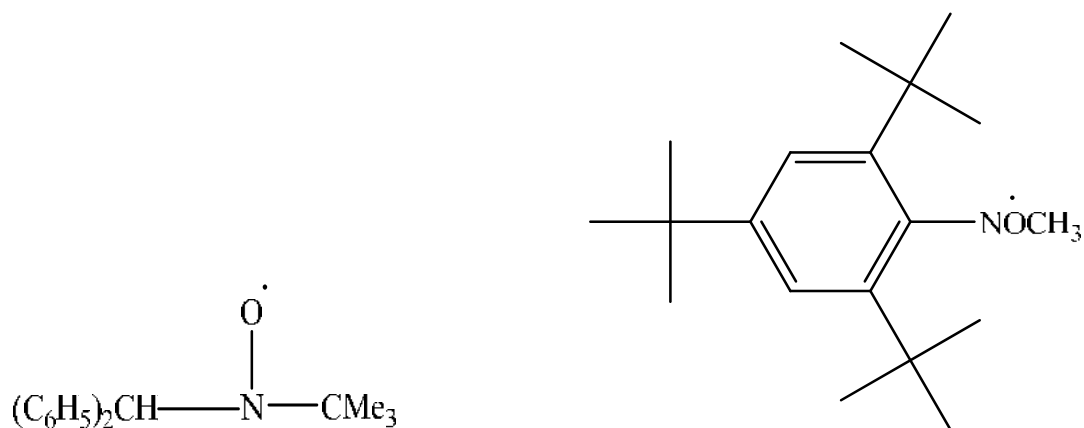


C-phenyl N-tert-butyl nitron

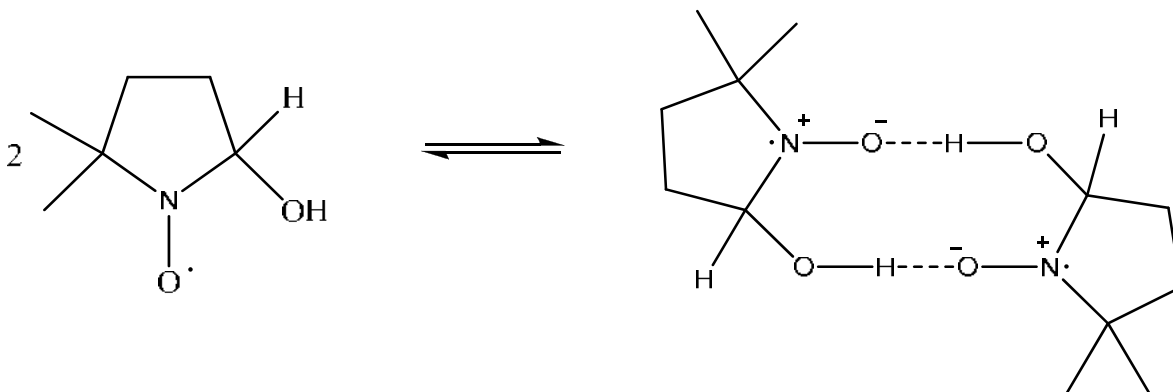


C-tert-butyl-N-tert-butyl nitron

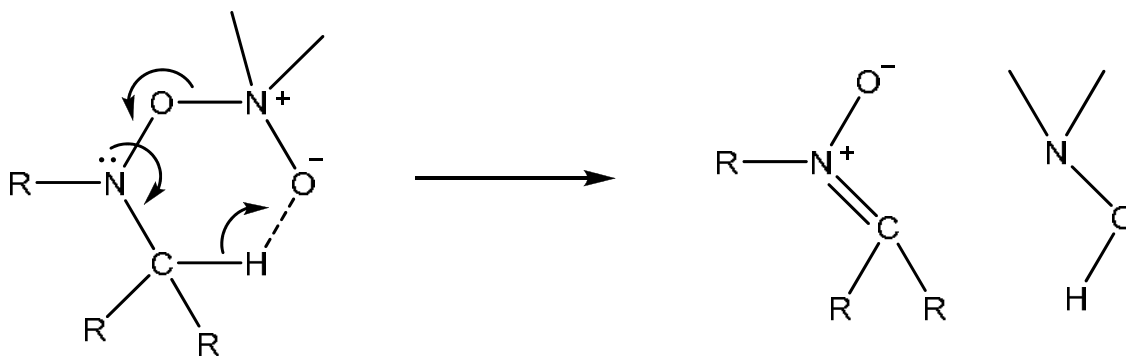
Dimerization. A loss of ESR signals for the nitrones at low temperatures is attributed to the dimerization of alkyl aryl nitrones.[46]



Intermolecular H-bonding can also facilitate dimerization in nitrones possessing heteroatoms. In the case of DMPO the dimerization occurs as [47, 48]

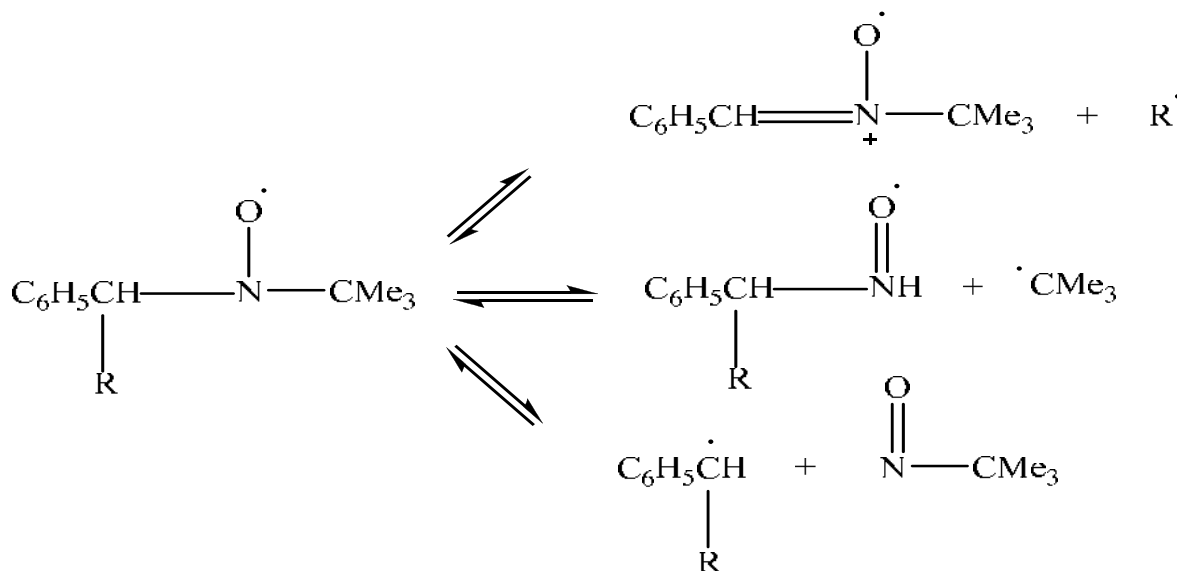


Disproportionation. Dimerization may sometimes lead to disproportionation.[49-51] Disproportionation is often induced by the presence of β -hydrogen.

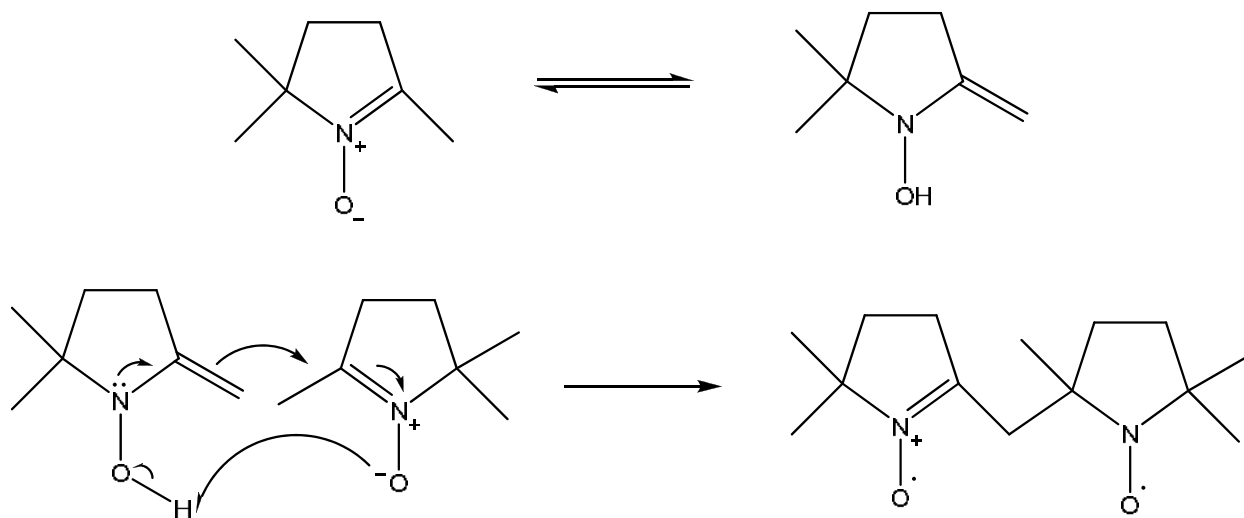


The extent of disproportionation depends on the proximity of the aminoxyls. The reactivity may be related to the dihedral angle of the β -hydrogen bond. The smaller the dihedral angle, the greater are the hyperfine splitting constants; however, there is also a greater probability of disproportionation.

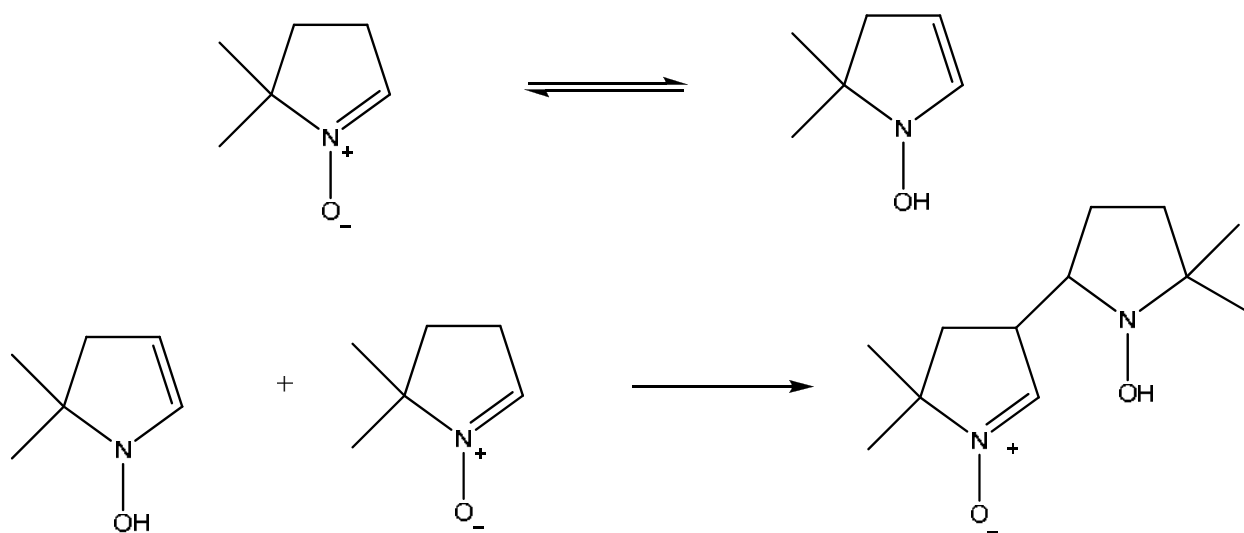
Dissociative α -cleavage. PBN spin adducts suffer from these types of reactions. The possible dissociative reactions are as follows:



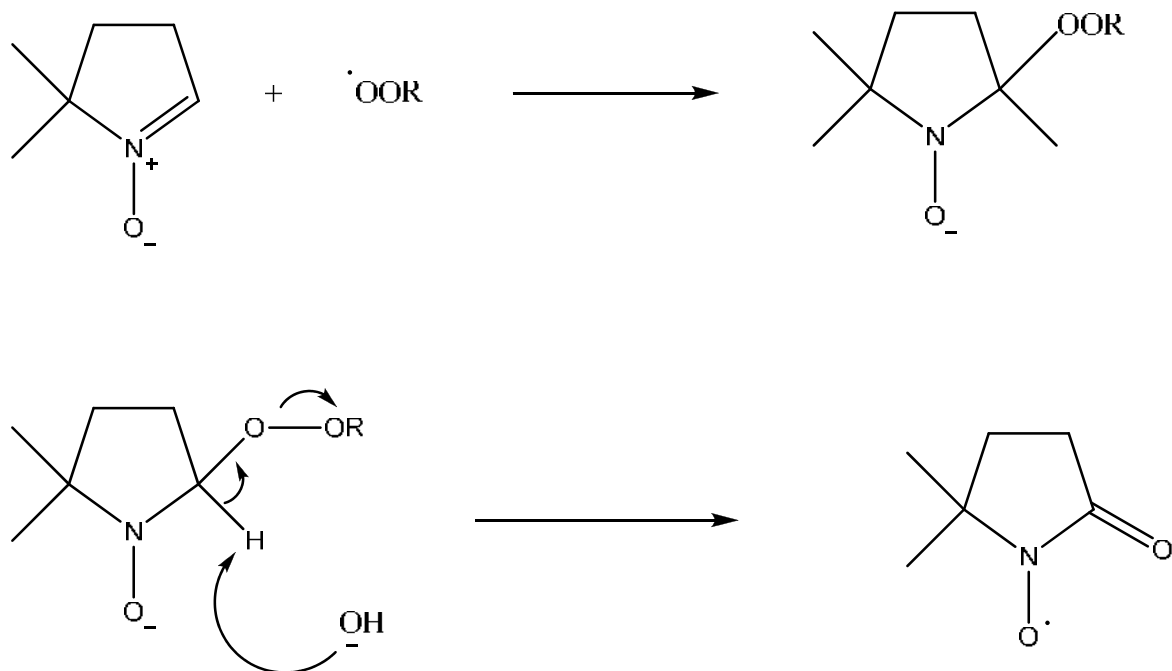
Addition Reactions. Hydride abstraction may occur in nitrones to generate stable carbanions. Intermolecular addition reactions can occur in air to generate the nitroxide triplet.[52]



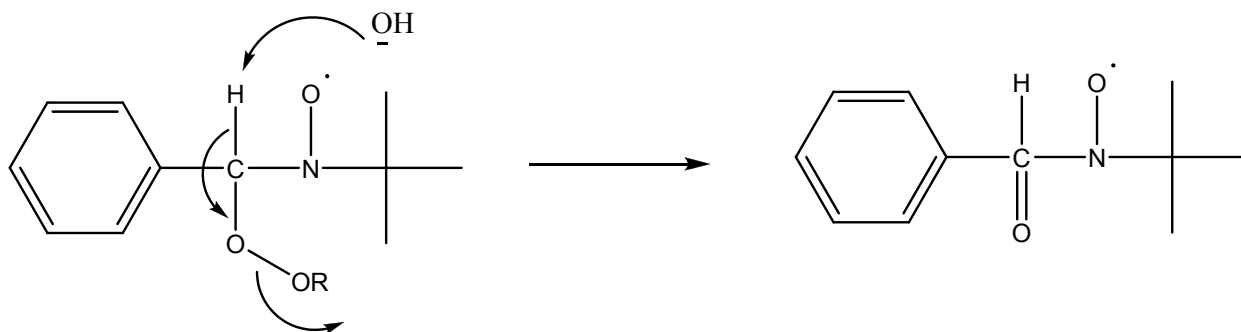
Enolization of the DMPO may lead to dimerization that generates a paramagnetic species that can contaminate the aqueous solution of the spin trap.[52]



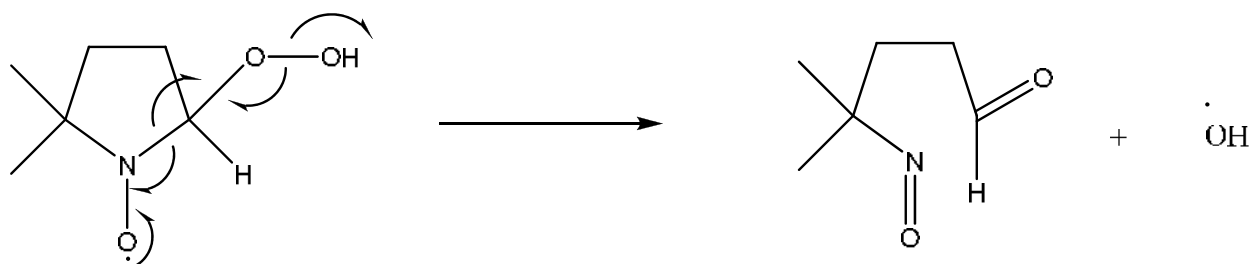
Decomposition. One of the common pathways for the decomposition of the alkylperoxyl adduct of DMPO is the rearrangement to DMPOX (2-alkylperoxyl-5,5-dimethyl-pyrrolidone-(2)-oxyl).[53, 54]



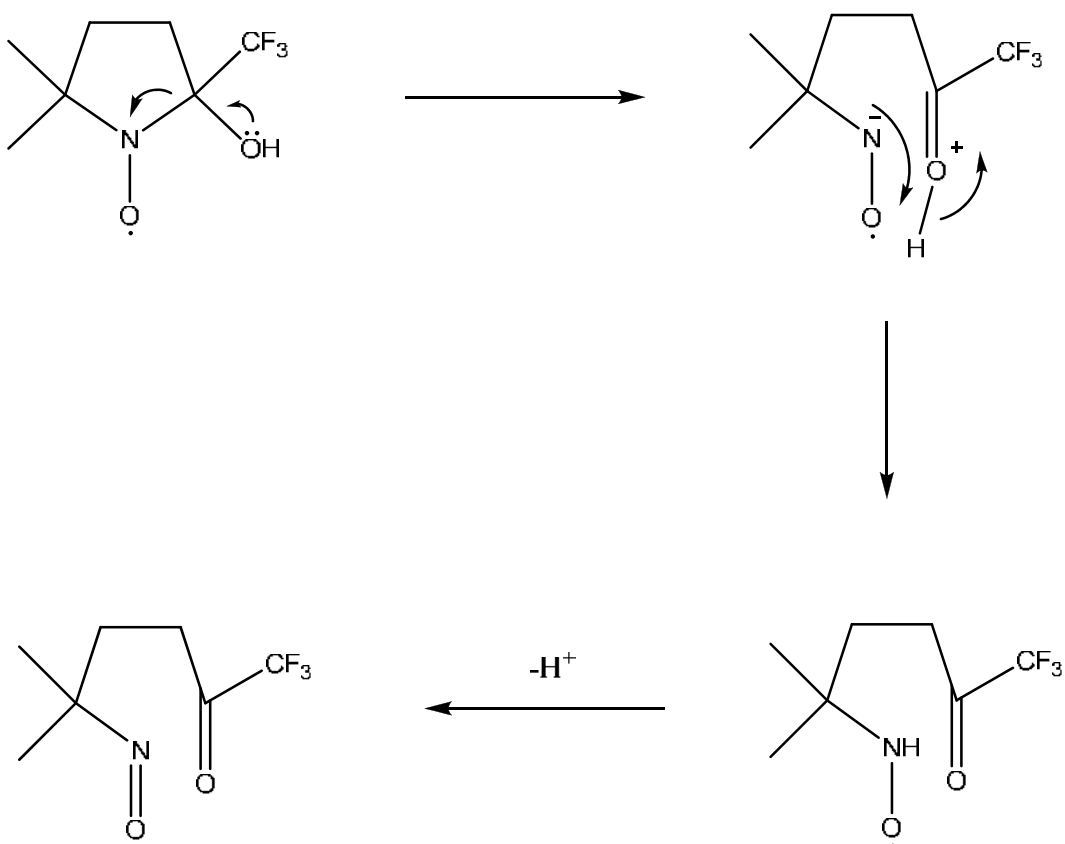
Similar decomposition reactions occur for the linear nitron PBN-OOR yielding PBNOX (benzoyl tert-butyl aminoxy radical).[55, 56]



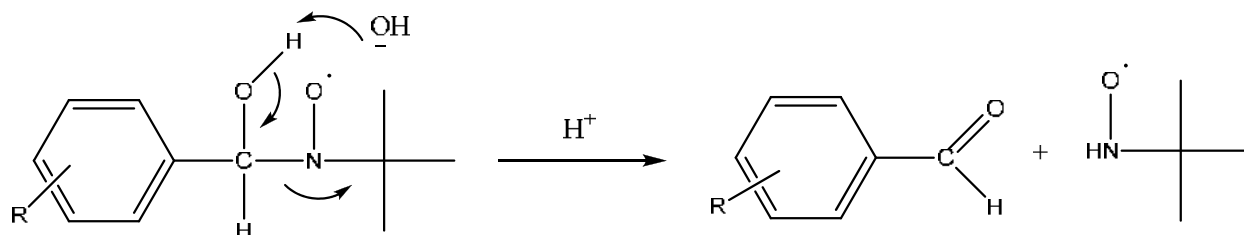
Superoxide radical ion is trapped by DMPO to yield the DMPO-OOH radical adduct. [57-59] However reports have suggested a decomposition of the DMPO-OOH to DMPO-OH. [60, 61] Based on the mechanism proposed by Finkelstein, *et al.*, DMPO-OOH rearranges to yield 4-methyl-4-nitrosopentanal and OH radical.[62]



The rearrangement reaction is facilitated by the presence of good leaving groups as is the case with TFDMPO-OH (hydroxyl adduct of trifluoro-5,5-dimethyl pyrrolidinium-N-oxide) [63]



In the case of acyclic nitrones, the decomposition rate depends on the nature of the substituent on the aromatic ring. Electron donating groups increase the rate of decomposition. In contrast, electron withdrawing groups hinder the decay process.[64, 65]



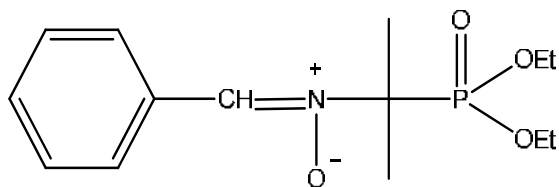
The advantages and disadvantages of the linear nitron PBN, and the cyclic nitron DMPO can be summarized as follows (see Table 2):

Table 2. Advantages and disadvantages of DMPO and PBN.[65]

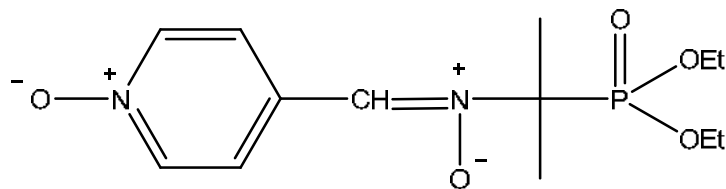
Spin Trap	Advantages	Disadvantages
PBN	<ol style="list-style-type: none"> 1. Solid at room temperature and hence relatively stable. 2. Longer lifetimes for the spin adducts. 	<ol style="list-style-type: none"> 1. Less definitive spectrum (cannot distinguish between OH and OOH radical adducts). 2. Lower rate constant of spin trapping
DMPO	<ol style="list-style-type: none"> 1. High spectrum sensitivity. 2. Higher rate constants for trapping radicals. 	<ol style="list-style-type: none"> 1. Shorter lived spin adducts.

Phosphorylated Nitrones

Aryl or tertiary alkyl nitroso compounds were initially used as scavengers for forming phosphorus substituted nitroxides.[66, 67] The resulting nitroxides were either due to an electron transfer mechanism [66] or the result of the homolytic reactivity of the nitric oxide functionality.[67] As a result, the use of nitroso spin traps in organophosphorus reactions can lead to false positive results. The alternative is to use nitrones that do not undergo homolytic dissociation in the presence of organophosphorus compounds. The added advantage is the presence of a β -phosphorus atom that provides additional hyperfine splitting and hence can be used for accurate diagnosis. Reports of phosphorylated DMPO were first published by Tordo *et al.* in 1978.[68] They have also reported long half-lives for the various β -phosphorylated nitroxides as compared to the cyclic nitroxides. The stability of the spin traps also increases when the atoms adjacent to the radical center are heteroatoms.[69, 70] Reports of phosphorylated PBN nitrone were first published by Tordo *et al.* in 1995.[71] Reports of phosphorylated analogues like N-benzyl-idene-1-diethoxyphosphoryl-1-methylethylamine N-oxide (PPN), 1-diethoxyphosphoryl-1-methyl-N-[(1-oxidopyridin-1-ium-4-yl)methylidene]ethylamine n-oxide (4-PyOPN) were made for the first time. The authors reported longer half-lives of the radical adducts as compared to PBN, and also reported additional hfsc from the β -phosphorus atom.



PPN



4-PyOPN

The phosphorylated PBN nitrones were shown to be efficient spin traps for trapping oxyl radicals in polar environments.[72] Theoretical studies describing the spin trapping of superoxide radical by the phosphorylated PBN nitrone were published in 2006.[73] All the above mentioned studies indicate the potential capability of phosphorylated nitrones in spin trapping.

Applications of Spin Traps

Nitrones and nitroxides have been recognized as versatile functional groups with a broad spectrum of applications.

Nitrones

1. Extensively used in 1,3-dipolar cycloaddition reactions for natural product synthesis.[74]
2. Spin trapping radicals for *in vivo* and *in vitro* studies.[75]

Nitroxides

1. Widely employed as biophysical probes and contrast agents in magnetic resonance spectroscopy [76]
2. Employed in enantioselective oxidation processes [77]
3. Living radical polymerizations [78]
4. Used as spin labels [79]

Other areas of applications of spin traps can be broadly categorized as

1. Sonolysis [80]
2. Lipid peroxidation studies [81]
3. Smoke toxicity studies [82]
4. Fenton-type reactions [83]
5. *In vivo* and *in vitro* enzymatic reactions [84, 85]

CHAPTER 2

QUANTUM MECHANICS

Schrödinger Equation

Classical mechanics is deterministic in nature. This means that we can predict the future state of the classical mechanical system given an exact knowledge of its present state. This concept is very feasible and practicable when we deal with macroscopic particles. However in order to deal with microscopic particles we need a new tool called quantum mechanics. In the early 19th century, phenomena like black body radiation and the photoelectric effect could not be explained by classical mechanics. These phenomena could be successfully explained by quantum mechanics by considering the wave-particle duality of light. The same concept was attributed to matter, and this effect was more pronounced for microscopic particles. Heisenberg came up with his Uncertainty Principle that implied the act of measurement introduced a perturbation in the system being measured. In other words we cannot simultaneously predict the exact position and velocity of a microscopic particle. This is a direct consequence of the wave-particle duality. Hence the basic knowledge required by classical mechanics cannot be obtained for microscopic particles.

Quantum mechanics postulates the existence of a function called the wave function or the state function (Ψ) in order to describe the state of the system. The wave function contains all the possible information about the state of the system. The evolution of the wave function with time is governed by the time-dependent Schrödinger equation:[86-89]

$$\frac{-\hbar}{i} \frac{\partial \psi(x,t)}{\partial t} = \frac{-\hbar^2}{2m} \nabla^2 \psi(x,t) + V(x,t) \psi(x,t) \quad (2-1)$$

where m is the mass of the particle, ∇^2 is the second order differential operator known as the Laplacian operator, and \hbar is the reduced Planck's constant equal to $h/2\pi$. The Laplacian operator is given as:

$$\nabla^2 = \frac{\partial^2}{\partial x^2} + \frac{\partial^2}{\partial y^2} + \frac{\partial^2}{\partial z^2} \quad (2-2)$$

The Schrödinger equation enables us to obtain information about the wave function at a time t given the information about the initial wave function. The probability density for locating the particle at a certain position is given as

$$|\Psi(x, t)|^2 dx \quad (2-3)$$

which is the probability of finding the particle at a given time t located between x and $x + dx$. This was proposed by Max Born and is known as Born's postulate.[90] However the simpler time-independent Schrödinger equation is widely employed in quantum mechanics. When the potential energy is independent of time, that is it is a function of distance only, the total energy of the system remains constant and is said to be conserved. Hence the wave function may be separated into spatial and time functions.

$$\Psi(x, t) = \psi(x)f(t) \quad (2-4)$$

Substituting this expression in Equation 2-1 and differentiating with respect to time gives

$$\frac{-\hbar^2}{2m} f(t) \frac{d^2\psi(x, t)}{dx^2} + V(x)\psi(x)f(t) = \frac{-\hbar}{i} \frac{df(t)}{dt} \psi(x) \quad (2-5)$$

dividing both sides by $\Psi(x,t) = \psi(x)f(t)$ gives

$$\frac{-\hbar^2}{2m} \frac{1}{\psi(x)} \frac{d^2\psi(x)}{dx^2} + V(x)\psi(x) = \frac{-\hbar}{i} \frac{1}{f(t)} \frac{df(t)}{dt} \quad (2-6)$$

The left hand side of the equation is time independent and the right hand side is position independent. Hence the two terms should be equal to E . Equating the left hand side of the equation to E gives the time-independent Schrödinger equation for a particle of mass m .

$$\frac{-\hbar^2}{2m} \frac{d^2\psi(r)}{dr^2} + V(r)\psi(r) = E\psi(r) \quad (2-7)$$

The classical-mechanical Hamiltonian function is the total energy expressed in terms of Cartesian coordinates and conjugate momenta. This Hamiltonian function gives an expression for the total energy, which is the sum of potential and kinetic energies. The Hamiltonian function is

$$H = \frac{p_x^2}{2m} + V(x) \quad (2-8)$$

For every physical property there corresponds a quantum mechanical operator. This is a fundamental postulate of quantum mechanics. Hence corresponding to the Hamiltonian function we have the operator:

$$\hat{H} = \frac{-\hbar^2}{2m} \frac{d^2}{dx^2} + V(x) \quad (2-9)$$

The Schrödinger equation is an eigenvalue problem with the wave function being the eigenfunction and the energy being the eigenvalue. The operator corresponding to these eigenvalues and eigenfunctions is known as the Hamiltonian operator.

$$\hat{H} \psi = E \psi \quad (2-10)$$

The total energy contains contributions from the kinetic energy and potential energy components. The kinetic energy is the sum total of the individual kinetic energies of all the particles constituting the system.

$$T = \frac{-\hbar^2}{2m} \sum_n \left[\frac{\partial^2}{\partial x^2} + \frac{\partial^2}{\partial y^2} + \frac{\partial^2}{\partial z^2} \right] \quad (2-11)$$

and the potential energy is the sum of the electrostatic interactions between the particles.

$$V = \frac{1}{4\pi\epsilon_0} \sum_l \sum_{m < l} \frac{q_l q_m}{r_{lm}} \quad (2-12)$$

where ϵ_0 is the permittivity of free space, q_l, q_m are the charges on the l^{th} and m^{th} particle separated by a distance r_{lm} .

In addition to the orbital angular momentum, the electron also possess an intrinsic angular momentum arising from its spin. This is defined as the spin angular momentum, or simply, spin. The concept of spin is a purely quantum mechanical phenomenon, and does not have any classical-mechanical analogue. In the nonrelativistic picture of quantum mechanics, spin is introduced as an additional hypothesis. The wave function is now dependent upon the spin of the electron apart from the Cartesian coordinates. As an approximation, the Hamiltonian

is considered independent of the spin variables. Hence the state function may now be expressed as a product of the spatial and spin functions.

$$\Psi(x, y, z, m_s) = \psi(x, y, z)g(m_s) \quad (2-13)$$

where $g(m_s)$ is either one of the spin eigenfunctions denoted as α or β depending on m_s , which can take either of the two values, i.e. $+1/2$ or $-1/2$. The Schrödinger equation can then be expressed as

$$\hat{H}[\psi(x, y, z)g(m_s)] = g(m_s)\hat{H}[\psi(x, y, z)] = E[\psi(x, y, z)g(m_s)] \quad (2-14)$$

The energy of the system is not affected by the introduction of the spin; however the number of possible energy states is doubled. The energy states are now given as $\psi(x, y, z)\alpha$ and $\psi(x, y, z)\beta$. The effect created by the spin can be seen in the degeneracy of the hydrogen-atom energy levels that is $2n^2$ rather than n^2 .

The Uncertainty Principle [91] imposes a constraint on the identification of the path of a microscopic particle. The restriction imposed on the wave function due to the fundamental indistinguishability is that the wave function for a system of electrons must be antisymmetric with respect to the interchange of any two electrons. The antisymmetric condition means that

$$\psi(q_1, q_2, q_3, q_4, \dots, q_n) = -\psi(q_2, q_1, q_3, q_4, \dots, q_n) \quad (2-15)$$

This postulate is known as the Pauli Principle when applied to a system of electrons.[92] Particles described by antisymmetric wave functions are called fermions (e.g. electrons) and those requiring symmetric wave functions are called bosons (e.g. pions). An application of the Pauli Principle to the helium atom wave function can be described as follows

$$\psi(r_1, r_2) = 1s\alpha(r_1)1s\beta(r_2) \quad (2-16)$$

where $1s\alpha$ and $1s\beta$ are abbreviated notations for the hydrogen-atom like wave functions with α and β as the respective spin eigenfunctions. The arguments r_1 and r_2 denote the coordinate system (x, y, z, σ) of electrons 1 and 2 respectively. The indistinguishability of the electrons gives rise to the equivalent wave function

$$\psi(r_2, r_1) = 1s\alpha(r_2)1s\beta(r_1) \quad (2-17)$$

Mathematically, indistinguishability imposes the condition of linear combination of all possible configurations. For the helium atom, the wave function can now be written as:

$$\Psi_1 = \psi(r_1, r_2) + \psi(r_2, r_1) = 1s\alpha(r_1)1s\beta(r_2) + 1s\alpha(r_2)1s\beta(r_1) \quad (2-18)$$

$$\Psi_2 = \psi(r_1, r_2) - \psi(r_2, r_1) = 1s\alpha(r_1)1s\beta(r_2) - 1s\alpha(r_2)1s\beta(r_1) \quad (2-19)$$

Ψ_2 has the unique property of being antisymmetric in that it changes sign when the electrons are interchanged

$$\Psi_2(r_2, r_1) = \psi(r_2, r_1) - \psi(r_1, r_2) = -\Psi_2(r_1, r_2) \quad (2-20)$$

Hence the ground state of the helium atom may be described by the antisymmetric wave function Ψ_2 .

Many approximations have to be made in order to solve a many particle Schrödinger equation. For example the Hamiltonian for a helium atom may be written as follows

$$\hat{H} = -\frac{\hbar^2}{2M} \nabla^2 - \frac{\hbar^2}{2m_e} \nabla_1^2 - \frac{\hbar^2}{2m_e} \nabla_2^2 - \frac{2e^2}{4\pi\epsilon_0 |R-r_1|} - \frac{2e^2}{4\pi\epsilon_0 |R-r_2|} + \frac{e^2}{4\pi\epsilon_0 |r_1-r_2|} \quad (2-21)$$

where ∇^2 is the Laplacian operator with respect to the helium nucleus, ∇_1^2 and ∇_2^2 are the operators corresponding to the coordinates of the two electrons, M is the mass of the nucleus, m_e is the electronic mass, R is the position of the helium nucleus and r_1, r_2 are the positions of the two electrons. Assuming that the nucleus is at a fixed position with respect to the electron's motion and neglecting relativistic effects, the Hamiltonian can be simplified to:

$$\hat{H} = -\frac{\hbar^2}{2m_e} (\nabla_1^2 + \nabla_2^2) - \frac{2e^2}{4\pi\epsilon_0} \left(\frac{1}{r_1} + \frac{1}{r_2} \right) + \frac{e^2}{4\pi\epsilon_0 |r_1-r_2|} \quad (2-22)$$

and the Schrödinger equation can be written as

$$-\frac{\hbar^2}{2m_e} (\nabla_1^2 + \nabla_2^2) \psi(r_1, r_2) - \frac{2e^2}{4\pi\epsilon_0} \left(\frac{1}{r_1} + \frac{1}{r_2} \right) \psi(r_1, r_2) + \frac{e^2}{4\pi\epsilon_0 |r_1-r_2|} \psi(r_1, r_2) = E \psi(r_1, r_2) \quad (2-23)$$

However this simplified equation cannot be solved. The $\frac{e^2}{4\pi\epsilon_0 |r_1-r_2|}$ term, known as the interelectronic term, is responsible for the difficulty associated with solving the above equation. In the absence of this term, the Schrödinger equation would have been separable and the Hamiltonian would be the product of the Hamiltonian operators for two hydrogen-like atoms. The total energy would have been the sum of the individual hydrogen-like atoms and the wave function would be a product of two hydrogen-like atomic orbitals. Hence we need approximation methods in order to solve the many body Schrödinger equation.

Some of the mathematical approximations are as follows: the Variational method, Perturbation theory, the Born-Oppenheimer approximation, Hartree-Fock Self Consistent theory, and Density Functional Theory (DFT).

Approximations

The Born-Oppenheimer Approximation

Approximating the nuclei and electrons as point masses, and ignoring relativistic interactions, the molecular Hamiltonian can be written as

$$\hat{H} = -\frac{\hbar^2}{2} \sum_i \frac{1}{m_i} \nabla_i^2 - \frac{\hbar^2}{2m_e} \sum_l \nabla_l^2 + \sum_i \sum_{j>i} \frac{Z_i Z_j e^2}{r_{ij}} - \sum_i \sum_l \frac{Z_i e^2}{r_{li}} + \sum_m \sum_{l>m} \frac{e^2}{r_{lm}} \quad (2-24)$$

where i and j refer to nuclei and l and m refer to electrons. The first term is the kinetic energy operator for the nuclei, and the second term is the kinetic energy operator for electrons. The third term is the electrostatic energy of repulsion between the nuclei separated by a distance r_{ij} . The fourth term is the electrostatic energy for attraction between nucleus i and electron l separated by a distance r_{li} . The fourth term is the potential energy of the repulsions between electrons l and m . The H_2 molecular Hamiltonian is

$$\hat{H} = -\frac{\hbar^2}{2m_p} \nabla_i^2 - \frac{\hbar^2}{2m_p} \nabla_j^2 - \frac{\hbar^2}{2m_e} \nabla_1^2 - \frac{\hbar^2}{2m_e} \nabla_2^2 + \frac{e^2}{r_{ij}} - \frac{e^2}{r_{1i}} - \frac{e^2}{r_{1j}} - \frac{e^2}{r_{2i}} - \frac{e^2}{r_{2j}} + \frac{e^2}{r_{12}} \quad (2-25)$$

The Schrödinger equation can be written as

$$\hat{H} \psi (q_l, q_i) = E \psi (q_l, q_i) \quad (2-26)$$

The approximation lies in the fact that the nuclei are much heavier than electrons. As electrons move much faster than the nuclei, the nuclei can be considered to be fixed with respect to the motion of the electrons. Omitting the nuclear kinetic energy terms in Equation 2-24 the Schrödinger equation for electronic motion is

$$(\hat{H}_{el} + V_{NN})\psi_{el} = U\psi_{el} \quad (2-27)$$

where the electronic Hamiltonian is

$$\hat{H}_{el} = -\frac{\hbar^2}{2m_e} \sum_i \nabla_i^2 - \sum_i \sum_l \frac{Z_l e^2}{r_{li}} + \sum_m \sum_{l>m} \frac{e^2}{r_{lm}} \quad (2-28)$$

The nuclear repulsion term V_{NN} is given as

$$V_{NN} = \sum_i \sum_{j>i} \frac{Z_i Z_j e^2}{r_{ij}} \quad (2-29)$$

The energy U is the total energy inclusive of the internuclear repulsion experienced by the nuclei i and j . The internuclear distance r_{ij} is fixed at a constant value and hence the electronic wave functions and energies depend parametrically on the nuclear coordinates

$$\psi_{el} = \psi_{el,n}(q_l, q_i) \quad (2-30)$$

$$U = U_n(q_n) \quad (2-31)$$

The electronic Hamiltonian is dependent on electronic coordinates and is independent of nuclear coordinates. The nuclear repulsion term V_{NN} is constant for a particular nuclear configuration and is independent of the electronic coordinates. Hence V_{NN} can be omitted from the electronic Schrödinger equation to give

$$\hat{H}_{el} \psi_{el} = E_{el} \psi_{el} \quad (2-32)$$

The purely electronic energy E_{el} is related to the total energy as

$$U = E_{el} + V_{NN} \quad (2-33)$$

The electronic Schrödinger equation is solved for a fixed nuclear configuration to obtain E_{el} . The total energy is then found using Equation 2-33, whereas the constant V_{NN} is calculated from Equation 2-29. Thus the nuclei in the Born-Oppenheimer approximation move on a potential energy surface defined by the solutions to the electronic Hamiltonian. Hence the solutions to the nuclear Schrödinger equation are:

$$\hat{H}_{nucl} \psi_{nucl} = U \psi_{nucl} \quad (2-34)$$

The approximation yields reasonable results for the ground electronic states of diatomic molecules.[93]

Hartree-Fock Theory

The exact wave function for the hydrogen atom is known. For systems like helium and lithium the wave function may be calculated to a high degree of accuracy by incorporating the interelectronic distance as a variable in the variational function. The Hartree-Fock procedure is employed in order to find the wave functions for many-electron systems. The Hamiltonian for an n -electron system is given as

$$\hat{H} = -\frac{\hbar^2}{2m_e} \sum_{i=1}^n \nabla_i^2 - \sum_{i=1}^n \frac{Ze^2}{r_i} + \sum_{i=1}^{n-1} \sum_{j=i+1}^n \frac{e^2}{r_{ij}} \quad (2-35)$$

The first summation includes the kinetic energy terms for n -electrons. The second summation is the potential energy for attraction between the electrons and the nucleus of charge Ze . The last sum is the interelectronic repulsion term, and the restriction $j=i+1$ avoids double counting of the same repulsions and terms like e^2/r_{ij} . As an initial approximation the zeroth-order wave function can be obtained by ignoring the interelectronic repulsion term, which makes the Hamiltonian separable. The zeroth-order wave function can then be written as a product of n hydrogen-like orbitals. An orbital by definition is a one-electron wave function.

$$\psi^{(0)} = f_1(r_1, \theta_1, \phi_1) f_2(r_2, \theta_2, \phi_2) f_3(r_3, \theta_3, \phi_3) \dots f_n(r_n, \theta_n, \phi_n) \quad (2-36)$$

where the hydrogen-like wave functions are given as

$$f = R_{nl}(r) Y_l^m(\theta, \phi) \quad (2-37)$$

where $R_{nl}(r)$ is the radial component of the hydrogen-like orbitals given as:

$$R_{nl}(r) = - \left\{ \frac{(n-l-1)!}{2n[(n+l)!]} \right\}^{1/2} \left(\frac{2}{na_0} \right)^{l+3/2} r^l e^{-r/na_0} L_{n+l}^{2l+1} \left(\frac{2r}{na_0} \right) \quad (2-38)$$

where $L_{n+l}^{2l+1} \left(\frac{2r}{na_0} \right)$ are called the associated Laguerre polynomials, and n and l are quantum numbers. $Y_l^m(\theta, \phi)$ are called the spherical harmonics, given as

$$Y_l^m(\theta, \phi) = \left[\frac{(2l+1)(l-|m|)!}{4\pi(l+|m|)!} \right]^{1/2} P_l^{|m|}(\cos \theta) e^{im\phi} \quad (2-39)$$

where $P_l^{|m|}(\cos \theta)$ are known as the associated Legendre functions.

The quantitative problem associated with Equation 2-36 is that all the orbitals use the same nuclear charge. The approximation can be made more accurate by employing different effective atomic numbers for different orbitals to account for the screening effect. This leads to the use of a variational function that is not restricted to any form of orbitals. The new variational function can now be written as

$$\phi = g_1(r_1, \theta_1, \phi_1) g_2(r_2, \theta_2, \phi_2) g_3(r_3, \theta_3, \phi_3) \dots g_n(r_n, \theta_n, \phi_n) \quad (2-40)$$

The functions g_i are then defined so as to minimize the variational integral given as

$$E_1 \leq \frac{\int \phi^* \hat{H} \phi d\tau}{\int \phi^* \phi d\tau} \quad (2-41)$$

where E_1 is the ground state energy for the system. The procedure for calculating the g_i 's is known as the Hartree self-consistent-field (SCF) method.[94]

Hartree's Procedure. The first step involves an initial guess for the product wave function

$$\phi = s_1(r_1, \theta_1, \phi_1) s_2(r_2, \theta_2, \phi_2) s_3(r_3, \theta_3, \phi_3) \dots s_n(r_n, \theta_n, \phi_n) \quad (2-42)$$

where the s_i 's are products of the normalized radial functions multiplied by the respective spherical harmonics. The primary approximation that is made is the central field approximation. This means that the electrostatic electron-electron repulsion term is averaged. The first electron experiences an averaged field created by smearing out the other electrons. Coulomb's law gives the potential energy of interactions between two charges q_1 and q_2 as (in atomic units)

$$V_{12} = \frac{q_1 q_2}{r_{12}} \quad (2-43)$$

The electrons are approximated to be averaged out as a continuous charge distribution with ρ_2 as the charge density. Considering the infinitesimal charge $\rho_2 dv_2$ in an infinitesimal volume dv_2 , the average interactions between q_1 and the infinitesimal elements of charge q_2 is given as

$$V_{12} = \frac{q_1}{4\pi\epsilon_0} \int \frac{\rho_2}{r_{12}} dv_2 \quad (2-44)$$

where r_{12} is the distance between the first electron with charge q_1 and the charge distribution with charge density ρ_2 . The probability density of electron i is $|s_i|^2$, hence $\rho_2 = -e|s_2|^2$, and for electron 1, $q_1 = -e$. Hence

$$V_{12} = \frac{e^2}{4\pi\epsilon_0} \int \frac{|s_2|^2}{r_{12}} dv_2 \quad (2-45)$$

Summing the interactions with other electrons

$$V_{12} + V_{13} + \dots + V_{1n} = \sum_{j=2}^n \frac{e^2}{4\pi\epsilon_0} \int \frac{|s_j|^2}{r_{1j}} dv_j \quad (2-46)$$

The potential energy of interaction between electron 1 and the other electrons and the nucleus is given as

$$V(r_1, \theta_1, \phi_1) = \sum_{j=2}^n \frac{e^2}{4\pi\epsilon_0} \int \frac{|s_j|^2}{r_{1j}} d\nu_j - \frac{Ze^2}{4\pi\epsilon_0 r_1} \quad (2-47)$$

The central-field approximation uses the result that the effective potential acting on an electron is a function of r only. Hence, averaging out $V_1(r_1, \theta_1, \phi_1)$ over the angles θ and ϕ we get

$$V_1(r_1) = \frac{\int_0^{2\pi} \int_0^{\pi} V(r_1, \theta_1, \phi_1) \sin \theta_1 d\theta_1 d\phi_1}{\int_0^{2\pi} \int_0^{\pi} \sin \theta d\theta d\phi} \quad (2-48)$$

Substituting for $V_1(r_1)$ in the one-electron Schrödinger equation, we have

$$\left[-\frac{\hbar^2}{2m_e} \nabla_1^2 + V_1(r_1) \right] t_1(1) = \epsilon_1 t_1(1) \quad (2-49)$$

The Schrödinger equation is then solved to obtain the improved wave functions t_l and the orbital energy ϵ_l . This procedure is repeated iteratively until the input and output wave functions match, or are self-consistent. The orbitals obtained by this method are known as Hartree-Fock orbitals. The effective Hamiltonian operator is known as the Fock operator, and the Schrödinger equation is given as

$$\hat{F} t_i(i) = \varepsilon_i t_i(i) \quad (2-50)$$

The orbital energies in the SCF approximation are obtained by iteratively solving the one-electron Schrödinger equation. However a correction term has to be introduced in order to avoid double counting of the repulsion terms. The corrected energies are given as

$$E = \sum_{i=1}^n \varepsilon_i - \sum_{i=1}^{n-1} \sum_{j=i+1}^n \iint \frac{e'^2 |g_i(i)|^2 |g_j(j)|^2}{r_{ij}} d\nu_i d\nu_j \quad (2-51)$$

The approximation to the exact wave function should take Pauli's principle into consideration and should be antisymmetric with respect to the interchange of electrons. Hence we consider anti-symmetrized spin-orbitals and the SCF calculation that employs them is known as the Hartree-Fock calculation.[95, 96]

The differential equation for evaluating the Hartree-Fock orbitals is:

$$\hat{F} u_i = \varepsilon_i u_i \quad i = 1, 2, \dots, n \quad (2-52)$$

where the operator F is once again the Fock (or Hartree-Fock) operator and u_i is the spin orbital corresponding to the orbital energy ε_i .

In the early 1930s Slater used determinants to construct antisymmetric wave functions.[97] For example, the wave function for helium can be written as a linear combination of terms in order to generate the antisymmetric wave function.

$$\Psi = \psi(r_1, r_2) - \psi(r_2, r_1) = 1s\alpha(r_1)1s\beta(r_2) - 1s\alpha(r_2)1s\beta(r_1) \quad (2-53)$$

The wave function can be expressed in determinant form as

$$\Psi = \begin{vmatrix} 1s\alpha(r_1) & 1s\beta(r_1) \\ 1s\alpha(r_2) & 1s\beta(r_2) \end{vmatrix} \quad (2-54)$$

where $1s\alpha$ and $1s\beta$ are the hydrogen atom-like wave functions with α and β being the spin eigenfunctions. The arguments 1 and 2 denote the coordinates (x, y, z, σ) of electrons 1 and 2 respectively. Upon expanding the above determinant we obtain the antisymmetric wave function Equation 2-53. These determinants are known as the Slater determinants and the wave function Ψ given by the Slater determinant is known as the determinantal wave function. The N-electron determinantal wave function may be written as

$$\Psi = \begin{vmatrix} a_1(1) & \dots & a_N(1) \\ \vdots & \ddots & \vdots \\ a_1(N) & \dots & a_N(N) \end{vmatrix} \quad (2-55)$$

where the a_n 's are the orthonormal spin orbitals.

The Hartree-Fock wave function for molecules is written as a Slater determinant of spin orbitals, each orbital being a product of the spatial wave function dependent on the coordinates (x, y, z) and the spin function (α or β).

Variation theorem predicts the Hartree-Fock molecular energy as

$$E_{HF} = \left\langle S \left| H_{el} + V_{NN} \right| S \right\rangle \quad (2-56)$$

where S is the Slater determinant HF-wave function, H_{el} and V_{NN} are the electronic Hamiltonian and potential energy term for nuclear repulsion respectively. The electronic Hamiltonian is the sum of one-electron Hamiltonians given as

$$f_i = -\frac{1}{2} \nabla_i^2 - \sum_{\alpha} \frac{Z_{\alpha}}{r_{i\alpha}} \quad (2-57)$$

and the two electron operator given as

$$g_{ij} = \frac{1}{r_{ij}} \quad (2-58)$$

The SCF energy for a closed-subshell configuration is given as

$$E = \left\langle S \left| \hat{H} \right| S \right\rangle = 2 \sum_{i=1}^{n/2} \langle \phi_i(1) | f_i | \phi_i(1) \rangle + \sum_{j=1}^{n/2} \sum_{i=1}^{n/2} (2J_{ij} - K_{ij}) \quad (2-59)$$

The HF energy for diatomic or polyatomic molecule is modified as

$$E_{HF} = 2 \sum_{i=1}^{n/2} H_{ii}^{core} + \sum_{j=1}^{n/2} \sum_{i=1}^{n/2} (2J_{ij} - K_{ij}) + V_{NN} \quad (2-60)$$

where

$$H_{ii}^{core} = \left\langle \phi_i(1) \left| H^{core}(1) \right| \phi_i(1) \right\rangle = \left\langle \phi_i(1) \left| -\frac{1}{2} \nabla_i^2 - \sum_{\alpha} \frac{Z_{\alpha}}{r_{i\alpha}} \right| \phi_i(1) \right\rangle \quad (2-61)$$

$$J_{ij} = \left\langle \phi_i(1) \phi_j(2) \left| 1 / r_{12} \right| \phi_i(1) \phi_j(2) \right\rangle \quad (2-62)$$

$$K_{ij} = \left\langle \phi_i(1) \phi_j(2) \left| 1 / r_{12} \right| \phi_i(1) \phi_j(2) \right\rangle \quad (2-63)$$

H_{ii}^{core} is the one-electron core Hamiltonian, J_{ij} and K_{ij} are the Coulomb and exchange integrals respectively integrated over the spatial coordinates for electrons 1 and 2 respectively. The objective of the Hartree-Fock method is to minimize the variation integral by obtaining suitable orbitals ϕ_i . The orbitals are assumed to be orthogonal and hence satisfy the differential equation

$$\hat{F}(1) \phi_i = \varepsilon_i \phi_i \quad (2-64)$$

where ϵ_i is the orbital energy and the Hartree-Fock operator is given as

$$\hat{F}(1) = \hat{H}^{core}(1) + \sum_{j=1}^{n/2} [2J_j(1) - K_j(1)] \quad (2-65)$$

and the Coulomb operator and exchange operator are:

$$J_{ij}f(1) = f(1) \int |\varphi_j(2)|^2 \frac{1}{r_{12}} d\nu_2 \quad (2-66)$$

$$K_{ij}f(1) = \varphi_j(1) \int \frac{\varphi_j^*(2)f(2)}{r_{12}} d\nu_2 \quad (2-67)$$

Where f is an arbitrary function and the definite integrals are integrated over all space. The Coulomb operator J_{ij} is the potential energy of interaction between electron 1 and the smeared out charge distribution with charge density $|\varphi_j(2)|^2$. The exchange integral K_{ij} is however a purely quantum-mechanical effect and has no classical mechanical analogue. It arises from the antisymmetric nature of the wave function with respect to electron exchange.

In order to obtain expressions for the orbital energies ϵ_i , Equation 2-64 is multiplied by $\varphi_i^*(1)$, and integrating over all space we have

$$\varepsilon_i = \int \phi_i^*(1) \hat{F}(1) \phi_i(1) d\nu_1 \quad (2-68)$$

and

$$\varepsilon_i = \left\langle \phi_i(1) \left| H^{core}(1) \right| \phi_i(1) \right\rangle + \sum_j \left[2 \left\langle \phi_i(1) \left| \hat{J}_j(1) \right| \phi_i(1) \right\rangle - \left\langle \phi_i(1) \left| \hat{K}_j(1) \right| \phi_i(1) \right\rangle \right] \quad (2-69)$$

that simplifies to

$$\varepsilon_i = \hat{H}_{ii}^{core} + \sum_{i=1}^{n/2} (2J_{ij} - K_{ij}) \quad (2-70)$$

Summing the above equation over $n/2$ occupied orbitals gives:

$$\sum_{i=1}^{n/2} \varepsilon_i = \sum_{i=1}^{n/2} \hat{H}_{ii}^{core} + \sum_{j=1}^{n/2} \sum_{i=1}^{n/2} (2J_{ij} - K_{ij}) \quad (2-71)$$

Solving for $\sum H_{ii}^{core}$, the Hartree-Fock energy is given as

$$E_{HF} = 2 \sum_{i=1}^{n/2} \varepsilon_i - \sum_{j=1}^{n/2} \sum_{i=1}^{n/2} (2J_{ij} - K_{ij}) + V_{NN} \quad (2-72)$$

If the initial guess for the molecular orbitals can be taken as a linear combination of atomic orbitals then we can have a more accurate molecular SCF wave function. Roothaan proposed that the spatial orbitals φ_i be taken as linear combination of one-electron basis functions. [98]

$$\varphi_i = \sum_{j=1}^s c_{ji} \chi_j \quad (2-73)$$

In order to correctly represent the molecular orbitals φ_i , the basis functions χ_j should form a complete set. The number of basis functions, s , should be as large as possible to minimize the error. Substituting the expression for φ_i in Equation 2-64 gives

$$\sum_j c_{ji} \hat{F} \chi_j = \varepsilon_i \sum_j c_{ji} \chi_j \quad (2-74)$$

Multiplication by χ_p and integration gives

$$\sum_{j=1}^s c_{ji} (F_{pj} - \varepsilon_i S_{pj}) = 0 \quad p = 1, 2, \dots, s \quad (2-75)$$

where

$$F_{pj} = \left\langle \chi_j \left| \hat{F} \right| \chi_p \right\rangle \quad (2-76)$$

and

$$S_{pj} = \langle \chi_j | \chi_p \rangle \quad (2-77)$$

For the solutions to be nontrivial the coefficients of the secular determinant should vanish, hence

$$\det(F_{pj} - \varepsilon_i S_{pj}) = 0 \quad (2-78)$$

The roots of the secular equation provide the orbital energies ε_i . The Hartree-Fock-Roothan equations Equation 2-75 are solved iteratively to yield the unknown coefficients c_{ji} .

The Hartree-Fock-SCF wave function averages out the interactions between electrons. However electrons tend to repel each other and the concept of a Coulomb hole comes into the picture. This is a region in which the probability of finding another electron is small. Hence the motions of electrons are correlated, and the wave function should be corrected for instantaneous electron correlation. The correlation energy is defined as

$$E_{corr} = CE = E_{exact} - E_{HF} \quad (2-79)$$

Many theories have been developed to compute the correlation energies. One example is that of the perturbation schemes where the HF orbital can be considered as the zeroth-order wave function and the correlation energy can be solved as a first order perturbation.

Density Functional Theory

The probability distribution function of finding an electron in a given volume element in terms of spatial and spin coordinates may be given as

$$\rho(x, y, z) = \left| \varphi(x_1, \dots, z_n, m_{s1}, \dots, m_{sn}) \right|^2 dx_1 dy_1 dz_1 \dots dx_n dy_n dz_n \quad (2-80)$$

This distribution function gives the probability of finding electron n with spin m_{sn} in the volume element $dx_n dy_n dz_n$ at (x_n, y_n, z_n) . Ignoring the spin, the probability of finding each electron in a given volume element is:

$$\rho(x, y, z) = \sum_{m_{s1}} \dots \sum_{m_{sn}} |\varphi|^2 dx_1 \dots dz_n \quad (2-81)$$

The probability density for finding electron 1 in a given region (x, y, z) is

$$\rho(x, y, z) = n \sum_{m_s} \int \dots \int \left| \varphi(x, y, z, x_2, \dots, z_n, m_{s1}, \dots, m_{sn}) \right|^2 dx_2 \dots dz_n \quad (2-82)$$

and in vector notation this is:

$$\rho(r) = n \sum_{m_s} \int \dots \int \left| \varphi(r, r_2, \dots, r_n, m_{s1}, \dots, m_{sn}) \right|^2 dr_2 \dots dr_n \quad (2-83)$$

For an electron i , the function, $f(r_i)$ is assumed to be dependent on the spatial coordinates (x_i, y_i, z_i) . For an n -electron system the average is defined as

$$\left\langle \varphi \left| \sum_{i=1}^n f(r_i) \right| \varphi \right\rangle = \int \varphi^* \sum_{i=1}^n f(r_i) \varphi d\tau = \sum_{i=1}^n \int \varphi^2 f(r_i) d\tau \quad (2-84)$$

Due to the indistinguishability of the electrons, the value of the last integral should be the same for any value of n . Hence

$$\left\langle \varphi \left| \sum_{i=1}^n f(r_i) \right| \varphi \right\rangle = \int n |\varphi|^2 f(r_i) d\tau \quad (2-85)$$

The probability density is introduced using Equation 2-83. Hence the equation transforms as

$$\int \varphi^* \sum_{i=1}^n f(r_i) \varphi d\tau = \int \rho(r) f(r) d\tau \quad (2-86)$$

Hohenberg-Kohn Theorem. In 1964, Pierre Hohenberg and Walter Kohn proposed the use of electron density for the calculation of molecular properties. They proved the theorem for systems possessing a nondegenerate ground state and proposed that the wave function and the molecular electronic properties may be uniquely determined by the ground state electron probability density $\rho_0(x, y, z)$. [99] One defines a functional as being a function of another function. According to the Hohenberg-Kohn theorem, the ground state electronic energy, E_0 , is a functional of the electron probability density and is written as:

$$E_0 = E_0(\rho_0) \quad (2-87)$$

This idea was termed as the Density-functional theory, wherein the ground state electronic energy and other ground state properties are calculated from the electron density and not from the wave function of the system. The pure electronic Hamiltonian for the ground state electronic wave function in atomic units is:

$$\hat{H} = -\frac{1}{2} \sum_{i=1}^n \nabla_i^2 + \sum_{i=1}^n v(r_i) + \sum_i \sum_{j>i} \frac{1}{r_{ij}} \quad (2-88)$$

$$v(r_i) = -\sum_{\alpha} \frac{Z_{\alpha}}{r_{i\alpha}} \quad (2-89)$$

The term, $v(r_i)$, is the Coulomb potential for the interaction between electron i and the nuclei. Because the Hamiltonian is solved for fixed nuclear coordinates, $v(r_i)$ is dependent only on the electronic coordinates. This quantity is known as the external potential, as the potential is developed by charges external to the electrons. The wave function and the energy of the system are determined as a solution to the Schrödinger equation with a prior knowledge of the external potential and the number of electrons. The Hohenberg-Kohn theorem states that the external potential and the number of electrons are given by the ground state electron probability density. Hence the electron density yields the wave functions and energy of the system under consideration. The number of electrons is given by integrating Equation 2-83 to obtain

$$\int \rho_0(r) dr = n \quad (2-90)$$

As the name suggests, the ground state electronic energy is a functional of the electron probability density written as

$$E_0 = E_v[\rho_0] \quad (2-91)$$

The ground state energy is given as

$$E_0 = E_v[\rho_0] = \bar{T}[\rho_0] + \bar{V}_{Ne}[\rho_0] + \bar{V}_{ee}[\rho_0] \quad (2-92)$$

where the energy is the sum of the average kinetic-energy term, average electron-nuclear attraction term, and the average electron-electron repulsion term. The electron-nuclear attraction term is given as

$$\bar{V}_{Ne} = \left\langle \varphi_0 \left| \sum_{i=1}^n v(r_i) \right| \varphi_0 \right\rangle = \int \rho(r) v(r) d\tau \quad (2-93)$$

The unknowns in the expression for the ground state energy term are $T[\rho]$ and $V_{ee}[\rho]$.

Kohn-Sham Method. The disadvantage with Hohenberg-Kohn theorem was the lack of information regarding the evaluation of the ground state energy term from the electron density. In 1965, Kohn and Sham devised a technique for finding ρ_0 and for evaluating E_0 from ρ_0 . [100] They considered a fictitious non-interacting system of n electrons wherein the external potential $v_s(r)$ is adjusted to make the electron probability density of the reference system $\rho_s(r)$ equal to the exact ground state electron density $\rho_0(r)$ of the molecule of interest. The Hamiltonian for the reference system is:

$$\hat{H} = -\frac{1}{2} \sum_{i=1}^n \left[-\frac{1}{2} \nabla_i^2 + v_s(r_i) \right] = \sum_{i=1}^n \hat{h}_i^{KS} \quad (2-94)$$

where h_{KS} is the Kohn-Sham Hamiltonian. The reference system can be related to the real one by including an extra term in the Hamiltonian as

$$\hat{H} = \hat{T} + \sum_i v(r_i) + \lambda \hat{V}_{ee} \quad (2-95)$$

where the variable λ can vary from 0 (no interelectronic repulsions that is the reference system) to 1 (the real system). The ground state wave function may be written as the Slater determinant of Kohn-Sham spin orbitals given as

$$\varphi_{s,0} = |u_1 u_2 \dots u_n| \quad (2-96)$$

where,

$$u_i = \theta_i^{KS}(r_i) \sigma_{(i)} \quad (2-97)$$

and the Schrödinger equation is:

$$\hat{h}_i^{KS} \theta_i^{KS} = \varepsilon_i^{KS} \theta_i^{KS} \quad (2-98)$$

Kohn and Sham modified Equation 2-92, and defined the new terms as follows

$$\Delta \bar{T}[\rho] = \bar{T}[\rho] - \bar{T}_s[\rho] \quad (2-99)$$

where the quantity on the left hand side is the difference between the average ground state kinetic energy of the real system and the average kinetic energy of the reference system.

$$\Delta \bar{V}_{ee}[\rho] = \bar{V}_{ee}[\rho] - \frac{1}{2} \iint \frac{\rho(r_1)\rho(r_2)}{r_{12}} dr_1 dr_2 \quad (2-100)$$

The second term on the right is the classical mechanics expression for interelectronic repulsion energy for electrons smeared out as a continuous charge distribution with density ρ . Combining Equations 2-99, 2-100 and 2-92

$$E_v[\rho_0] = \int \rho(r)v(r)d\tau + \bar{T}_s[\rho] + \Delta\bar{T}[\rho] + \frac{1}{2} \iint \frac{\rho(r_1)\rho(r_2)}{r_{12}} dr_1 dr_2 + \Delta\bar{V}_{ee}[\rho] \quad (2-101)$$

The unknowns in the equation are ΔT and ΔV_{ee} , the summation of which is defined as exchange-correlation energy functional given as

$$E_{xc}[\rho] = \Delta\bar{T}[\rho] + \Delta\bar{V}_{ee}[\rho] \quad (2-102)$$

The expression for ground state energy transforms as

$$E_v[\rho_0] = \int \rho(r)v(r)d\tau + \bar{T}_s[\rho] + \frac{1}{2} \iint \frac{\rho(r_1)\rho(r_2)}{r_{12}} dr_1 dr_2 + E_{xc}[\rho] \quad (2-103)$$

$$E_v[\rho_0] = -\sum_{\alpha} Z_{\alpha} \int \frac{\rho(r_1)}{r_{1\alpha}} dr_1 - \frac{1}{2} \sum_{i=1}^n \langle \theta_i^{KS}(\mathbf{1}) | \nabla_1^2 | \theta_i^{KS}(\mathbf{1}) \rangle + \frac{1}{2} \iint \frac{\rho(r_1)\rho(r_2)}{r_{12}} dr_1 dr_2 + E_{xc}[\rho] \quad (2-104)$$

The first three terms in the above equation can be evaluated from a known value of the electron density. The main step in a KS-DFT calculation is a good approximation of the exchange-correlation energy functional.

In defining the reference system, it was assumed that the fictitious system had the same electron density as the real system. The Slater-Condon rules [101, 102] give the electron probability density for an n -particle system having anti-symmetrized wave function as

$$\rho_0 = \rho_s = \sum_{i=1}^n \left| \theta_i^{KS} \right|^2 \quad (2-105)$$

where θ^{KS} is the spatial part of the anti-symmetric wave function. The Hohenberg-Kohn variational theorem states that the true ground state energy term can be found by varying ρ so as to minimize the ground state energy functional $E_v[\rho]$. Alternatively θ^{KS} (spatial part of the Kohn-Sham orbitals) can be varied to determine the ground state electron probability density, the relation given by (2-106). The Kohn-Sham orbitals that minimize (2-104) satisfy the equation

$$\left[-\frac{1}{2} \nabla_1^2 - \sum_{\alpha} \frac{Z_{\alpha}}{r_{1\alpha}} + \int \frac{\rho(r_2)}{r_{12}} dr_2 + v_{xc}(1) \right] \theta_i^{KS}(1) = \varepsilon_i^{KS} \theta_i^{KS}(1) \quad (2-106)$$

where v_{xc} (exchange-correlation potential) is defined as the functional derivative of the exchange-correlation potential

$$v_{xc}(r) = \frac{\delta E_{xc}[\rho(r)]}{\delta \rho(r)} \quad (2-107)$$

Solvation

Gas-phase calculations assume that there is no interaction between the various molecules. Hence the studies involve stationary-state quantum mechanics of isolated molecules. However, most biochemical and laboratory studies occur in solution where the interaction between the molecule of interest and the solvent is not negligible. Simulation in solvents can be broken down into two categories: (1) simulation of the bulk solvent and (2) solvation effect.

Modeling of bulk liquids involves computing properties that are not defined for individual molecules such as viscosity, diffusion rates, etc. One of the effective ways of simulating bulk solvent is by carrying out Monte Carlo simulations that gives the time-averaged structure, including the orientation of the solvent near a surface.[103] Explicit solvent simulations include insertion of all the solvent molecules explicitly and then running a molecular dynamics or Monte Carlo simulation. This yields an ensemble average of the property of interest. The explicit calculations employ periodic boundary conditions to account for long-range interactions. The disadvantage with the explicit calculations is that they are computationally expensive and consume enormous amount of computer time. A possible solution can be to simulate the solute quantum mechanically and the solvent with molecular dynamics. In order to reduce the computation time, calculations may be performed over a smaller number of solvent molecules, each starting with a different geometry. The resulting configuration can then be averaged out to give an ensemble average. Other solutions to the explicit simulation may be to use the more common continuum methods.

Consider the scenario where a polar solute is placed in a polar solvent. There will be a definite reorientation of the solvent molecules depending on the charge distribution on the solute. In addition, the inherent dipole of the solute will induce a dipole moment in nearby solvent molecules that adds on to the permanent dipole moment. As a result, the solvent is polarized in regions adjacent to the solute molecule. An electric field termed as the reaction field is generated as a result of this solvent polarization. As a result of the reaction field, the solute molecular wave function is perturbed and presents a different picture compared to its gas phase wave function.

Due to the induced dipole moment by the solvent's reaction field, the solute molecule will possess a larger dipole moment in the solvent than in the gas phase. Similarly the molecular wave function and other molecular properties differ significantly from the gas-phase calculations. In continuum methods, the solvent is modeled as a continuous dielectric that encapsulates a cavity containing the solute of interest. The continuous dielectric is characterized by the relative permittivity or the dielectric constant of the particular solvent at the temperature and pressure of the solution. In a quantum-mechanical treatment of the solute the electronic wave function of the solute is allowed to change as the transition from gas phase to solution phase is made. The motive is to achieve self-consistency between the charge distribution of the solute and the reaction field of the solvent. Calculations that employ self-consistency are termed as self-consistent-reaction-field (SCRF) models.

Poisson Equation

The Poisson equation relates the electrostatic potential as a function of the dielectric constant and the charge density.[104] The equation is valid for scenarios where the surrounding dielectric medium responds linearly to the embedding of the charge, and is given as:

$$\nabla^2 \phi(r) = - \frac{4\pi\rho(r)}{\epsilon} \quad (2-108)$$

where $\phi(r)$ is the electrostatic potential, $\rho(r)$ is the arbitrary charge density, and ϵ is the dielectric constant of the medium. The continuum models describe the solvent explicitly and the solute implicitly. The charge distribution of the solute is placed within a cavity that perturbs the otherwise homogenous dielectric medium. This approximation creates two distinct regions, an interior and exterior region with respect to the cavity. The Poisson equation may then be written as

$$\nabla \cdot \epsilon(r) \cdot \nabla \phi(r) = -4\pi\rho(r) \quad (2-109)$$

In the presence of electrolytes the Poisson equation is modified as the Poisson-Boltzmann equation, [105, 106] given as

$$\nabla \cdot \varepsilon(r) \nabla \phi(r) - \varepsilon(r) \lambda(r) \kappa^2 \frac{k_B T}{q} \sinh \left[\frac{q \phi(r)}{k_B T} \right] = -4 \pi \rho(r) \quad (2-110)$$

where q is the charge on the electrolyte ions, λ is a switching function depending on the accessibility of electrolyte, κ^2 is the Debye-Hückel parameter given as

$$\kappa^2 = \frac{8 \pi q^2 I}{\varepsilon k_B T} \quad (2-111)$$

where I is the ionic strength of the electrolyte solution. For given ideal cavity shapes such as spheres or cylinders, the Poisson-Boltzmann equation has analytical solutions.

Self-Consistent-Reaction-Field (SCRF) Models

Born-Kirkwood-Onsager SCRF Method. Also known as the dipole-in-a-sphere model, it approximates the molecular charge distribution as an electric dipole with electric dipole moment μ located at the cavity center.[107, 108] Onsager derived an expression for the electric field produced by the polarization of the solvent as [109]

$$E_R = \frac{2(\varepsilon_r - 1)}{(2\varepsilon_r + 1)a^3} \mu \quad (2-112)$$

where ε_r is the dielectric constant of the solvent and a is the radius of the sphere modeling the molecular cavity. The derivation is as follows: consider a conducting sphere of charge q , the

charge is uniformly distributed on the surface of the sphere and the charge density at any point is given as

$$\rho (s) = \frac{q}{4 \pi a^2} \quad (2-113)$$

where s is the surface point.

The work required to create the charge distribution in the cavity is given as

$$G = -\frac{1}{2} \int \rho(r) \phi(r) dr \quad (2-114)$$

where ρ is the charge density and ϕ is the electrostatic potential. The electrostatic potential on the surface of the conducting sphere is obtained by calculating from the exterior and is given as

$$\phi(r) = -\frac{q}{\epsilon |r|} \quad (2-115)$$

where q is a point charge and ϵ is the dielectric constant of the exterior. Taking the radius of the conducting sphere to be r , (2-114) becomes

$$G = -\frac{1}{2} \int \left(\frac{q}{4 \pi a^2} \right) \left(-\frac{q}{\epsilon |a|} \right) da = \frac{q^2}{2 \epsilon a} \quad (2-116)$$

The polarization energy is the difference in the work required in the gas phase and the condensed phase, we have

$$G_P = -\frac{1}{2} \left(1 - \frac{1}{\epsilon} \right) \frac{q^2}{a} \quad (2-117)$$

which is the Born equation for a monatomic ion. If the conducting sphere is replaced by an electric dipole (which is defined as the vector from the electric charges $+Q$ to $-Q$ separated by a distance b , with magnitude Qb), the equation can then be written as

$$G_P = -\frac{1}{2} \left(\frac{2(\epsilon - 1)}{(2\epsilon + 1)} \right) \frac{\mu^2}{a^3} \quad (2-118)$$

The potential energy of interaction between the dipole moment μ and the reaction field E_R is given as

$$V = -\hat{\mu} \cdot E_R \quad (2-119)$$

and the corresponding operator in atomic units is given as

$$\hat{V} = -\hat{\mu} \cdot E_R \quad (2-120)$$

where the dipole moment operator is defined as

$$\hat{\mu} = -\sum_i r_i + \sum_{\alpha} Z_{\alpha} R_{\alpha} \quad (2-121)$$

The procedure involves an initial guess for the electron probability density $\rho^{(0)}(r)$ for the isolated molecule using an *ab initio* technique such as HF or DFT. The electric dipole moment of the molecule is then calculated in vacuum as

$$\mu^{(0)} = -\int \rho^{(0)}(r) r dr + \sum_{\alpha} Z_{\alpha} R_{\alpha} \quad (2-122)$$

The calculated value for $\mu^{(0)}$ is then used in (2-112) to give an initial value for $E^{(0)}_R$ of the reaction field. Using the value for $E^{(0)}_R$, V_{int} is calculated as

$$\hat{V}_{int}^{(0)} = -\hat{\mu} \cdot E^{(0)}_R \quad (2-123)$$

using V_{int} the equations are solved to give an improved $\rho^{(1)}$. This process is carried out until self-consistency is achieved. The calculated value for V_{int} is included in the Hamiltonian to obtain the electronic energy $U^{(f)}$, which is given as

$$U^{(f)} = \left\langle \psi^{(f)} \left| \hat{H}_M + \hat{V}_{int} \right| \psi^{(f)} \right\rangle \quad (2-124)$$

where $\psi^{(f)}$ is the final electronic wave function resulting from self-consistency. $U^{(f)}$ should be corrected for another term which results from the polarization of the solvent due to the solute. This is given as

$$E_{pol} = -\frac{1}{2} \left\langle \psi^{(f)} \left| \hat{V}_{int} \right| \psi^{(f)} \right\rangle \quad (2-125)$$

Gibbs Energy of Solvation

The free energy of solvation ΔG_s^0 is the most important property describing the interaction of the solute and the solvent. Also known as the free energy of transfer, it refers to the free energy change when a molecule leaves the gas-phase and enters the condensed phase. According to Ben-Naim's definition of a solvation process, the embedding of a solute into a

given solvent can be defined as the process in which a particle of the solute is transferred from a fixed position in the gas phase into a fixed position in solution at constant temperature, pressure, and solvent composition.[110] Hence the Gibbs free energy of solvation is the reversible work needed to incorporate the solute, M, in solvent S. The free energy expression may then be given as

$$\Delta G_{solv} = W(M/S) + RT \ln \left[\frac{(q_{rot} q_{vib})_{gas}}{(q_{rot} q_{vib})_{sol}} \right] \quad (2-126)$$

where $W(M/S)$ is the coupling work of the solute in the solvent and, q_{rot} , q_{vib} denote the rotational and vibrational partition functions of the solute. There is however a difference in the momentum partition functions Λ_M that gives rise to a term defined as ‘liberation free-energy’ that has to be added to the free energy of solvation.

$$\Delta G_{lib} = -RT \ln \left[\frac{\Lambda_{M,gas}}{\Lambda_{M,sol}} \right] \quad (2-127)$$

Because the Gibbs free energy is a thermodynamic quantity, the standard states should be specified. For most calculations it is 1M in both the gas and condensed phases.

The free energy of solvation may be broken down into several components: (1) electrostatic contribution, (2) cavitation contribution, (3) dispersion contribution, (4) repulsion contribution, and (5) thermal contribution. In other words

$$\Delta G_s = \Delta G_{s,el} + \Delta G_{s,cav} + \Delta G_{s,dis} + \Delta G_{s,rep} + \Delta G_{s,mm} \quad (2-128)$$

Experimentally only the total free energy of solvation is measured, and the measurement of coupling between the different terms is difficult. Though the computational cost restricts the

calculation of the coupling terms, the most important contribution of the solvent reorganization effect arises from the cavitation and electrostatic terms. This gets magnified in the case of polar solvents.

Electrostatic contribution. The electrostatic contribution arises from the solute-solvent electrostatic interaction. The quantum mechanical treatment of the solute embedded in a continuum is given by the Schrödinger equation as

$$\left[\hat{H}_M^0(q, Q) + \frac{1}{2} \hat{V}_{elec}(q, Q, \rho_M, \varepsilon) \right] \varphi(q, Q) = U(Q) \varphi(q, Q) \quad (2-129)$$

where V_{ele} characterizes the electrostatic response of the solvent as a function of the dielectric constant ε , charge distribution of the solute ρ_M , and $U(Q)$ is the sum total of the electronic energy of the solute and the electrostatic contribution to the free energy of solvation. The work spent in polarizing the solvent accounts for half the solute-solvent interaction energy and hence a factor of $1/2$ is introduced into the expression.

$$\Delta G_{s,el}^0 = (U^{(f)} + E_{pol}) - U^{(0)} = U^{(f)} - \frac{1}{2} \left\langle \varphi^{(f)} \left| \hat{V}_{int} \right| \varphi^{(f)} \right\rangle - U^{(0)} \quad (2-130)$$

$$\Delta G_{s,el}^0 = \left\langle \varphi^{(f)} \left| \hat{H}_M^{(0)} + \frac{1}{2} \hat{V}_{int} \right| \varphi^{(f)} \right\rangle - \left\langle \varphi^{(0)} \left| \hat{H}_M^{(0)} \right| \varphi^{(0)} \right\rangle \quad (2-131)$$

Cavitation contribution. The cavitation contribution is the work required to create a cavity of appropriate volume and shape in the solvent that is occupied with solute molecules. Several methods are available for the calculation of the cavitation free energy depending on

solute properties such as its shape and size and on solvent properties such as surface tension, isothermal compressibility, number density, or the molecular radius.[111] A common theory employed is the scaled-particle-theory formulated by Pierotti for the calculation of cavitation free energy.[112] The free energy term is calculated from the radii of the solute and the solvent molecules, the number density of the solvent molecules, and the temperature and pressure. In this theory the molecules are assumed to be hard spheres and the free energy is expanded in powers of the radius of the sphere.

$$\Delta G_{cav} = K_0 + K_1 R_{MS} + K_2 R_{MS}^2 + K_3 R_{MS}^3 \quad (2-132)$$

where R_{MS} is the sum of the radii of the solvent and the solute, and the coefficients K contain terms such as R_s , the molecular radius, n_s the number density of the solvent, pressure P , and temperature T .

$$K_0 = RT \left[-\ln(1-y) + \frac{9}{2} \left(\frac{y}{1-y} \right)^2 \right] - \frac{4\pi R_s^3 P}{3} \quad (2-133)$$

$$K_1 = -\frac{3RT}{R_s} \left[\frac{y}{1-y} + 3 \left(\frac{y}{1-y} \right)^2 \right] + 4\pi R_s^2 P \quad (2-134)$$

$$K_2 = \frac{3RT}{R_s} \left[\frac{y}{1-y} + \frac{3}{2} \left(\frac{y}{1-y} \right)^2 \right] - 4\pi R_s P \quad (2-135)$$

$$K_3 = \frac{4\pi P}{3} \quad (2-136)$$

where $y = 4\pi R_s^3 n_s/3$. For models employing a nonspherical cavity, the scaled-particle theory was modified by Claverie to give the Pierotti-Claverie formula.[112] The free energy of cavitation for each atom was weighted by a factor proportional to the solvent-exposed surface of that atom.[112]

$$\Delta G_{cav} = \sum_i \frac{S_i}{4\pi R_i^2} \Delta G_{cav}(R_i) \quad (2-137)$$

Dispersion-repulsion contribution. The majority of the interactions that hold liquids together are the dispersion forces. This holds true even for solvent containing polar molecules. When a solute is inserted into a cavity, it will experience strong dispersion forces from the solvent molecules. These dispersion attractions between the solute and solvent are accounted for in the dispersion contribution term. Also it is dispersion alone that accounts for free energy transfer of a solute inserted into a solvent when neither of them have permanent electric dipole moments. The repulsion contribution also termed as the exchange-repulsion contribution arises from quantum-mechanical repulsions between the solute and the solvent. The average dispersion-repulsion contribution for a solute M surrounded by solvent S is given as

$$\langle U_{dis-rep} \rangle = n_S \sum_{s \in S} N_S \sum_{m \in M} \int U_{ms}(r_{ms}) g_{ms}(r_{ms}) dr_{ms}^3 \quad (2-138)$$

where

$$U_{ms} = \sum_k \alpha_{ms,k} r_{ms}^{-k} \quad (2-139)$$

where N_s is the number of fragments of type s in the solvent molecule, n_s is the density of the solvent molecules, and g_{ms} is the correlation function between fragments m and s .

Molecular Motion. The thermal or molecular motion contribution is given by:

$$\Delta G_{mm} = -RT \ln \left(\frac{q_{M,sol}}{q_{M,gas}} \right) \quad (2-140)$$

where $q_{M,sol}$ and $q_{M,gas}$ are the partition functions of the solute M in the solution and gas phases. The contribution arises from the difference in molecular motions on going from gas to condensed phase. The molecular partition function in the free energy expression is a product of the translational, rotational, vibrational, and electronic partition functions.

Classic Continuum-Solvent Methods

Solvent Accessible Surface Area (SASA). The primary assumption that is made in SASA is that the maximum interaction of the solvent is in the area close to the solute molecule. These interactions are taken into account by the determination of surface area for each atom or a group of atoms surrounding the solvent molecule. The free energy of solvation associated with the non-electrostatic solvation of any atom will be proportional to the solvent exposed surface area. The free energy expression is given as

$$\Delta G_S = \sum_i A_i \sigma_i \quad (2-141)$$

where A_i is the surface area and σ_i the atomic surface tension or atomic solvation parameter associated with the particular atom or group of atoms. By surface tension we mean the quantity that relates to energy per unit area rather than surface tension that is a macroscopic quantity. This method does not elucidate the various contributions of the free energy of solvation. In the simplest approach towards the construction of SASA, the solvent molecules are approximated as

spheres of certain radii. The SASA is then generated by the center of the solvent sphere overlapping on to the surface of the solute characterized by its Van der Waals radius. This is equivalent to having a SASA as the sum of the solvent radius plus the Van der Waals radius.

Generalized Born model. For arbitrary cavity shapes, numerical methods have to be employed to solve the Poisson equation. Alternatively the polarization free energy may be solved using an approximation to the Poisson equation, which is the Generalized Born approach, given as

$$G_P = -\frac{1}{2} \left(1 - \frac{1}{\epsilon} \right) \sum_{m, m'}^{atoms} q_m q_{m'} \gamma_{mm'} \quad (2-142)$$

where m, m' cover all the atoms, each having a charge q , and γ is an effective Coulomb integral given as

$$\gamma_{mm'} = \left(r_{mm'}^2 + \alpha_m \alpha_{m'} \exp \left(-\frac{r_{mm'}^2}{d_{mm'} \alpha_m \alpha_{m'}} \right) \right)^{-1/2} \quad (2-143)$$

where $r_{mm'}$ is the interatomic distance, α_m is the effective Born radius of atom m . The procedure involves fixing of the atomic radii for defining the cavity. The effective Born radius is then computed using certain techniques, after which the effective Coulomb integral is evaluated. The atomic charges are assigned and Equation 2-142 is solved to yield the polarization free energy.

Polarized-Continuum Model (PCM). The model proposed by Miertus, Scrocco, and Tomasi uses a molecular cavity more practical than a spherical or ellipsoidal shape.[113] Instead of having a charge distribution in the cavity, each atomic nuclei of the solute M is now encapsulated within a sphere of radius 1.2 times the Van der Waals radius of the atom. The volume occupied by these overlapping spheres is taken as the cavity size. An apparent surface

charge (ASC) develops on the surface of the molecular cavity. This is generated by the surface charge density (charge per unit surface area) that varies from region to region on the cavity. The electrostatic potential generated by the ASC is equal to the potential generated by the polarized dielectric continuum. The model relies on calculating the ASC that approximates the solvent's polarization with respect to the solute's charge distribution. The ASC is approximated by tessellating the solute cavity into a number of surface elements and an apparent charge Q_j placed at a distance r_j in the j^{th} region. The electrostatic potential due to the polarization of the dielectric in atomic units is given by:

$$\phi_{\sigma}(r) = \sum_j \frac{Q_j}{|r - r_j|} \quad (2-144)$$

where the apparent charges are:

$$Q_j = \left[\frac{(\epsilon_r - 1)}{4\pi\epsilon_r} \right] A_j \nabla \phi_{in}(r_j) \cdot n_j \quad (2-145)$$

where A_j is the area of the j^{th} region, $\nabla \phi_{in}(r_j)$ is the rate of change of electrostatic potential within the cavity, and n_j is the unit vector perpendicular to the cavity surface at r_j . The electrostatic potential within the cavity is:

$$\phi_{in} = \phi_{M,in} + \phi_{\sigma,in} \quad (2-146)$$

where $\phi_{M,in}$ is the charge distribution of the solute and $\phi_{\sigma,in}$ is the contribution from the polarized solvent. The apparent charges are found by an iterative process where ϕ_{in} is approximated as $\phi_{M,in}$ by neglecting $\phi_{\sigma,in}$. The first step involves calculating $\rho^{(0)}$ from the wave function, which is then used to evaluate $\phi_M^{(0)}$. The value obtained for the electrostatic potential

is then used to evaluate Q_j of the ASC using Equation 2-145. The electrostatic potential $\phi_\sigma(r)$ is then calculated using Equation 2-144. The new potential $\phi_{in} = \phi_{M,in} + \phi_{\sigma,in}$ is then calculated from the $\phi_\sigma(r)$ obtained from the earlier step. The improved ϕ_m is then used to calculate the improved charges Q_j . This process continues until self-consistency is achieved. The final apparent charges are then used to calculate the additional term in the Hamiltonian given as

$$\hat{V}_{int}^{(0)} = - \sum_i \phi_\sigma^{(final)}(r_i) + \sum_\alpha Z_\alpha \phi_\sigma^{(final)}(r_\alpha) \quad (2-147)$$

Conductor-like Solvation Model (COSMO). This model resembles PCM in that it uses practical solute-molecule cavities and employs surface charges on the cavity surface surrounded by the solvent medium.[114-116] The major difference being that the solvent medium is now an electrical conductor rather than a dielectric. The practical advantage results from the simplification of the electrostatic problem, facilitating the calculation of analytical gradients. Because in COSMO the solute charge distribution is surrounded by a conductor rather than a dielectric, the conductor-polarization free energy is scaled by a factor of $2(\epsilon-1)/(2\epsilon+1)$. The simplified approach makes the calculation of apparent charges computationally faster. COSMO has also been extended to model real solvents in what is termed as COSMO-RS (real solvent) method. In this model both the solvent and the solute are initially described by means of COSMO calculations. The solute is described by the screening charge density on the cavity surface.

Atomic Units

Theoretical calculations employ a system of units called atomic units to simplify the equations. This system was developed by setting many fundamental constants equal to 1. The greatest advantage is the reduction of computer time required to perform computations. The other advantage is that any changes in measured values of standard physical constants do not affect the theoretical calculations. The natural unit of mass is the mass of the electron, the unit of

charge is the magnitude of the charge of an electron or a proton. The natural unit of angular momentum on an atomic or molecular scale is \hbar . The natural unit of length is the Bohr radius defined as

$$a_0 = \frac{4\pi\epsilon_0\hbar^2}{m_e e^2} = 5.2918 \times 10^{-11} m \quad (2-148)$$

The natural unit of energy is called the Hartree and is denoted by E_h .

$$E_h = \frac{m_e e^4}{16\pi\epsilon_0^2 \hbar^2} = 27.211 eV = 4.3597 \times 10^{-18} J \quad (2-149)$$

The use of atomic units simplifies the equations used in atomic and molecular calculations. The Hamiltonian for a helium atom is written as

$$\hat{H} = -\frac{\hbar^2}{2m_e} \nabla_1^2 - \frac{\hbar^2}{2m_e} \nabla_2^2 - \frac{2e^2}{4\pi\epsilon_0 r_1} - \frac{2e^2}{4\pi\epsilon_0 r_2} + \frac{e^2}{4\pi\epsilon_0 r_{12}} \quad (2-150)$$

simplifies, in atomic units, to

$$\hat{H} = -\frac{1}{2} \nabla_1^2 - \frac{1}{2} \nabla_2^2 - \frac{2}{r_1} - \frac{2}{r_2} + \frac{1}{r_{12}} \quad (2-151)$$

Basis Sets

In order to obtain accurate molecular SCF wave functions, the spatial orbitals should be expanded as a linear combination of one-electron basis functions χ_s :

$$\varphi_i = \sum_{s=1}^b c_{si} \chi_s \quad (2-152)$$

The need for an efficient basis set is essential for success of the calculation. In other words, the basis set can be described as a set of atomic functions used to construct molecular orbitals. One of the early basis sets employed in the computational studies of polyatomic molecules consisted of the Slater type atomic orbitals abbreviated as STOs

$$S_{nlm}(r, \theta, \phi) = \frac{(2\xi)^{n+1/2}}{[(2n)!]^{1/2}} r^{n-1} e^{-\xi r} Y_l^m(\theta, \phi) \quad (2-153)$$

where ξ (zeta) is the orbital exponent. Hence each χ_s is a STO basis function and we have LC-STO MOs (Linear combinations of Slater type orbitals-molecular orbitals). For diatomic molecules the basis function are constructed by assigning a few atomic orbitals on one atom and the rest are centered on the other atom. However for polyatomic molecules, the STOs are centered on each atom. As we move to polyatomic molecules we need to deal with multi-center integrals. This creates some difficulties, as the evaluation of multi-center integrals is time consuming. However if we use Gaussian functions instead of Slater orbitals, the multicenter integrals are easy to evaluate. Boys proposed the use of Gaussian-type functions (GTFs) in 1950, [117] and a Cartesian Gaussian centered on atom a is defined as

$$g_{ijk} = N x_a^i y_a^j z_a^k e^{-\alpha r_a^2} \quad (2-154)$$

where i, j, k are nonnegative integers and α is the orbital exponent. The normalization constant is given as

$$N = \left(\frac{2\alpha}{\pi} \right)^{3/4} \left[\frac{(8\alpha)^{i+j+k} i! j! k!}{(2i)!(2j)!(2k)!} \right]^{1/2} \quad (2-155)$$

We can have different GTFs depending on the sum of the nonnegative integers. When the sum

$i + j + k = 0$, the GTF is known as a s-type Gaussian, when $i + j + k = 1$, we have a p-type Gaussian, and when $i + j + k = 2$, we have a d-type Gaussian. Any s atomic orbital is represented by a linear combination of Gaussians having the form $\exp(-ar_b^2)$ with different orbital exponents. Any atomic p_x orbital is given by a linear combination of Gaussians of the form $x_b \exp(-ar_b^2)$. The Gaussian orbital describes the Slater orbital reasonable well for values of $r > a_0$; however we have a poor approximation for $r < a_0$. Hence we need to have a linear combination of Gaussian functions to curve fit Slater orbitals.

A basis set consisting of one STO for each inner-shell and valence-shell of each atom is called the minimal (or minimum) basis set. For example, for C_2H_4 a minimal basis set consists of 1s, 2s, 2p_x, 2p_y, and 2p_z atomic orbitals on each carbon and a 1s STO on each hydrogen; hence they are 5 STOs on each carbon and one each on H, for a total of 14 basis functions. There are two distinct sets of s -type STOs and one set of p -type STO on the two carbon atoms and one s -type STO for the four hydrogen atoms.

Describing an atomic orbital with a finite number of Gaussian functions introduces several inadequacies in the calculations. The major limitations are as follows: because all the orbitals in a STO-NG (where N is the number of Gaussian functions describing the Slater orbital) basis set have the same orbital exponent, they have the same size. This cannot be a true picture as orbitals are diffused to different extents depending on the type of bonding. Hence different molecules have different orbital exponents. The other limitation lies in the fact that the STO-NG basis sets cannot predict anisotropic charge distributions. Depending on the directional nature of the bonding, electron densities diffuse to a different extent along the bonds. This leads to anisotropic distribution of the electron density that cannot be predicted by the STO-NG basis set as all the orbitals having the same angular momentum have the same radial dependence.

Variable functions were introduced into basis sets that could adjust the shape of the atomic orbital. Hence the size of the atomic orbital can now be optimized as part of the Hartree-Fock calculation. Each atomic orbital is now expressed as a linear combination of two Slater-type orbitals with different orbital exponents. For example, the 1s orbital can be written as

$$\varphi_{1s}(r) = \varphi_{1s}^{STO}(r, \xi_1) + d\varphi_{1s}^{STO}(r, \xi_2) \quad (2-156)$$

The two Slater orbitals represent two different size 2s orbitals. Using a linear combination of these orbitals with different orbital exponents, a new atomic orbital can be constructed by varying the constant d . The linear combination retains the desired symmetry of the original atomic orbital. Basis sets generated from a linear combination of two Slater orbitals with different exponents are called double-zeta (DZ) basis sets. A triple-zeta (TZ) basis set is generated by a linear combination of three STOs with different orbital exponents.

A split-valence (SV) basis set uses only one minimal basis set for the inner shell (core) atomic orbital but uses two (or more) for each valence atomic orbital. Hence a SV basis set is double zeta (or triple zeta) for the valence AOs and is minimal for the core AO. Split-valence sets are designated valence double zeta (DVZ), valence triple zeta (VTZ) depending on the number of STOs used for the valence AO.

In order to facilitate the evaluation of the secular determinant the split-valence basis sets are expressed in terms of Gaussian functions.

$$\chi_r = \sum_u d_{ur} g_u \quad (2-157)$$

where g_u 's are the normalized Cartesian Gaussians given by Equation 2-154 and are called primitive Gaussians. The term d_{ur} corresponds to contracted coefficients that are held constant during a calculation. In Equation 2-157, χ_r is called a contracted Gaussian-type function (CGTF). Hence each of the two Slater orbitals in Equation 2-156 are expressed as a linear combination of Gaussian functions. The notation used to express the number of Gaussian functions is N-MPG, where N is the number of Gaussian functions employed for the core orbitals; hyphen indicates the use of split-valence basis set; M and P are used to describe the number of Gaussians used for the orbitals with different orbital exponents. By convention M corresponds to the number of

Gaussian functions used to express the smaller Slater orbital and P corresponds to the larger Slater orbital. G simply indicates the usage of Gaussian functions.

During the formation of molecules, the atomic orbitals distort upon overlap and there is a shift in their charge centers. This effect is termed as polarization and one should account for this phenomenon in the basis set. To account for the polarization effects a correction to the basis set is made by adding a STO whose l quantum numbers are greater than the maximum l of the valence shell of the ground state atom. Such basis sets are termed polarized (P) basis sets. For example, the double-zeta plus polarization set (DZ + P or DZP) adds to the valence double zeta a set of five $3d$ functions to each second row atoms and a set of three $2p$ functions on each hydrogen atom. This is also indicated by an asterisk *, for example 6-31G* that indicates the addition of $3d$ orbitals to the $2p$ orbitals of the atoms of the second row elements. A double asterisk (6-31G**) indicates the application of polarization to the hydrogen atoms by the addition of $2p$ orbitals. The 3-21G* is an exception in that the d functions are added only to 2nd row elements.

One or two plus signs can also be added such as 6-31+G* or 6-31++G*. A plus sign is added to indicate the addition of diffuse functions; a single plus sign indicates that diffuse functions have been added to atoms other than hydrogen. A second plus sign indicates the addition of diffuse functions to all atoms. The diffuse functions are primitives with small orbital exponents that describe the shape of the wave function for orbitals far away from nucleus. The other applications of diffuse functions involve the description of basis sets for anions. They are also used for simulating long range interactions such as Van der Waals interactions. Basis sets employing diffuse functions are known as augmented basis sets.

An extension of the VDZ notation is the aug-cc-pVDZ, where 'aug' indicates that this is an augmented basis set implying the addition of diffuse functions. Electron correlation has also been accounted for and hence the term 'cc'. The term 'p' denotes the inclusion of polarization functions in the basis sets. These basis sets are commonly employed for high-accuracy electron correlation calculations.

CHAPTER 3

RESULTS AND DISCUSSION

Computational Details

Geometry optimization and single point energy calculations were performed using NWChem 5.1 from the Molecular Sciences Laboratory Software Group of Pacific Northwest National Laboratory.[118, 119] The Extensible Computational Chemistry Environment (Eccé) software, version 4.5.1, was used to manage the calculations and pictorial representations. All calculations were performed at the DFT level of theory, [99] employing the 6-31G* basis set [120] and the B3LYP hybrid exchange correlation functional.[121]

The calculations were performed on a eight node Fedora Core 4 Linux base computer cluster consisting of a HP DL 145 G2 master node (dual AMD Opteron 246'S 3GB RAM, 160 SATA HDD) and a file server node (DL 145, dual Opteron 242'S, 2GB RAM~1TB U230 SCSI/SATA RAID 5 drives array). The nodes were connected using a dual switched gigabit Ethernet network.

Solvent effects were calculated using the Conductor-like Solvation Model (COSMO).[114-116]

Input Files

The structure of the input file directs the launching of the job in NWChem. Before the calculation begins NWChem reads through the input file (see Tables 3 and 4) to search for start-up directives that indicate the type of job, the memory usage, identifying the directories for storing the output, etc. The start-up directives include commands like START, SCRATCH_DIR, MEMORY, ECHO, etc. After the file has been reviewed for start-up directives, the file is re-read until the TASK directive is reached. The TASK directive issues a command for the commencement of the calculation at the requested level of theory.

Table 3. NWChem input file of DMPO

```
scratch_dir /scr/sai
permanent_dir /home/sai/nw_work/Spin-traps/DMPO-RDFT-6-31G
Title "DMPO-RDFT-6-31G"

Start DMPO-RDFT-6-31G

echo

charge 0

geometry autosym units angstrom
C      1.28314      3.28424      -0.954581
H      0.432444      3.94761      -1.06987
C      2.41265      3.20858      -1.91389
C      3.32595      2.13385      -1.31176
C      2.60248      1.65216      -0.0259173
N      1.39962      2.46809      0.0344717
O      0.479779      2.36835      0.998348
H      3.47620      1.31041      -2.04467
H      4.32465      2.57269      -1.09056
H      2.04048      2.90662      -2.91631
H      2.93135      4.18894      -1.97053
C      2.21523      0.167214      -0.128128
H      3.12368      -0.467967      -0.204572
H      1.63660      -0.145941      0.767828
H      1.58539      -0.00325839      -1.02801
C      3.46462      1.89861      1.22354
H      4.46045      2.29812      0.934816
H      2.96936      2.63256      1.89526
H      3.61142      0.953023      1.78795
```


Table 3 (continued)

end

```
ecce_print /home/sai/nw_work/Spin-traps/DMPO-RDFT-6-31G/ecce.out
```

```
basis "ao basis" cartesian print
```

```
  H library "6-31G*"
```

```
  O library "6-31G*"
```

```
  C library "6-31G*"
```

```
  N library "6-31G*"
```

```
END
```

```
dft
```

```
  mult 1
```

```
  XC b3lyp
```

```
  iterations 200
```

```
  mulliken
```

```
end
```

```
driver
```

```
  gmax 0.00045
```

```
  grms 0.0003
```

```
  xmax 5e-05
```

```
  xrms 0.0012
```

```
  maxiter 100
```

```
end
```

```
task dft optimize
```

Table 4. NWChem input file of DMPO solvation using COSMO model

```
scratch_dir /scr/sai
permanent_dir /home/sai/nw_work/Spin-traps/DMPO-RDFT-COSMO-1
Title "DMPO-RDFT-COSMO-1"

Start DMPO-RDFT-COSMO-1

echo

charge 0

geometry autosym units angstrom
C      0.953659      1.38186      -0.0671880
H      1.91000      1.88732      -0.104842
C     -0.388225      1.97269      0.222300
C     -1.35421      0.809028     -0.122296
C     -0.497766     -0.473188     -0.0642258
N      0.917990      0.0830835     -0.221829
O      1.87675     -0.717911     -0.424313
H     -2.20933      0.758502      0.558069
H     -1.74597      0.944766     -1.13579
H     -0.473095      2.27806      1.27659
H     -0.593526      2.86897     -0.375373
C     -0.541071     -1.17791      1.29744
H     -1.50555     -1.67898      1.43267
H      0.256264     -1.92464      1.35176
H     -0.405255     -0.465539      2.11908
C     -0.753954     -1.45370     -1.20570
H     -0.694454     -0.949616     -2.17635
H     -0.00857352    -2.25246     -1.18748
```

Table 4 (continued)

H -1.75289 -1.89173 -1.10465

end

ecce_print /home/sai/nw_work/Spin-traps/DMPO-RDFT-COSMO-
1/ecce.out

basis "ao basis" cartesian print

 H library "6-31G*"

 O library "6-31G*"

 C library "6-31G*"

 N library "6-31G*"

END

dft

 mult 1

 XC b3lyp

 iterations 200

 mulliken

end

driver

 gmax 0.00045

 grms 0.0003

 xmax 5e-05

 xrms 0.0012

 maxiter 100

end

cosmo

end

task dft optimize

Examining the different lines in Tables 3 and 4, TITLE directive is used to specify the job title. The start-up directive ECHO is a way of printing the input file in the output of the calculation. The CHARGE directive defines the total charge of the system. The GEOMETRY directive defines the geometry in default units which is in Cartesian coordinates in Angströms. The basis sets are defined for the atoms in the molecule, after which the level of theory is mentioned. For example, the above input file performs the calculation at DFT level of theory, employing the 6-31G* basis set and the B3LYP hybrid exchange correlation functional. The input file ends with a TASK directive that issues a command for geometry optimization of the molecule under consideration. Solvation studies using COMSO are done by incorporating the key word 'COSMO' in the input file and the default value of the dielectric constant is equated to 78.4D.

Discussion of Results

The spin traps under investigation are the cyclic type DMPO and linear type PBN nitrones. To improve the selectivity of the spin traps, details of the reaction mechanism must be properly understood so that the relevant structure property relationships may be elucidated. *In vivo* studies require a good understanding of the mechanism in an aqueous environment. Prior work [122], involving calculations of these spin traps in gas phase does not match the experimental data (see Table 5).

Table 5. Dipole moments of DMPO-type and the PBN-type Spin Traps at the DFT/B3LYP/6-31G*/COSMO level.

Compounds	Calculated dipole moment (D)	Literature values [123]
DMPO	5.34	3.72
PBN	4.20	n/a
DMPO-OH	3.57	2.5
PBN-OH	4.48	n/a

The difference indicates that there are significant changes in structure and energy of the spin traps in solution. To model these systems more accurately, computational solution models are needed. Existing continuum solvation models like COSMO (Conductor like Solvation Model) [114-116] that treat the solvent as a uniform dielectric, describe only the physics of solvation and fail to account for chemical effects like hydrogen bonding. The COSMO model incorporates the molecule in a cavity of approximately 1.2 times the Van der Waals radius. The disadvantage with standard COSMO is that the spin trap and the water molecule surrounding it are encapsulated in separate cavities. This model is unable to account for short range interactions like hydrogen bonding as the cavities are separated by a uniform dielectric.

Accurate local chemistry is vital because of the importance to molecular geometry of both intra and intermolecular hydrogen bonding. These hydrogen bonding interactions are crucial in stabilizing the spin trap and its radical adduct in solution. The properties in the gas phase do not match with those in the condensed phase as a result of the chemical interactions with the solvent. The alternative is to use a full quantum mechanical approach that explicitly includes the solvent molecules in the calculation. The adequate description of the long range, predominately physics, effects on a solvated molecule may require dozens or even hundreds of solvent molecules. Because the calculation time scales with the number of electrons to the fourth power (N^4), these calculations are often infeasible, requiring access to computer superclusters with thousands of processors.

Practical solutions lie in the development of hybrid models. The hybrid models consist of surrounding the molecule of interest (radical, spin trap, or adduct) with a limited number of solvent molecules to account for the short range chemical effects and use continuum models such as COSMO to account for the long range physics. This hybrid model should accurately reflect the biological environment at a reasonable computational cost. One of the first questions that must be answered is just how many water molecules must be included in the hybrid model.

DMPO Solvation Studies

Intermolecular hydrogen bonding plays a significant role in the stabilization of DMPO (see Figure 2). The hybrid model consists of surrounding the spin trap with discrete water molecules (see Figure 3). The idea behind the hybrid model is to approximate the number of water molecules surrounding the spin trap, in order to describe the chemical properties.

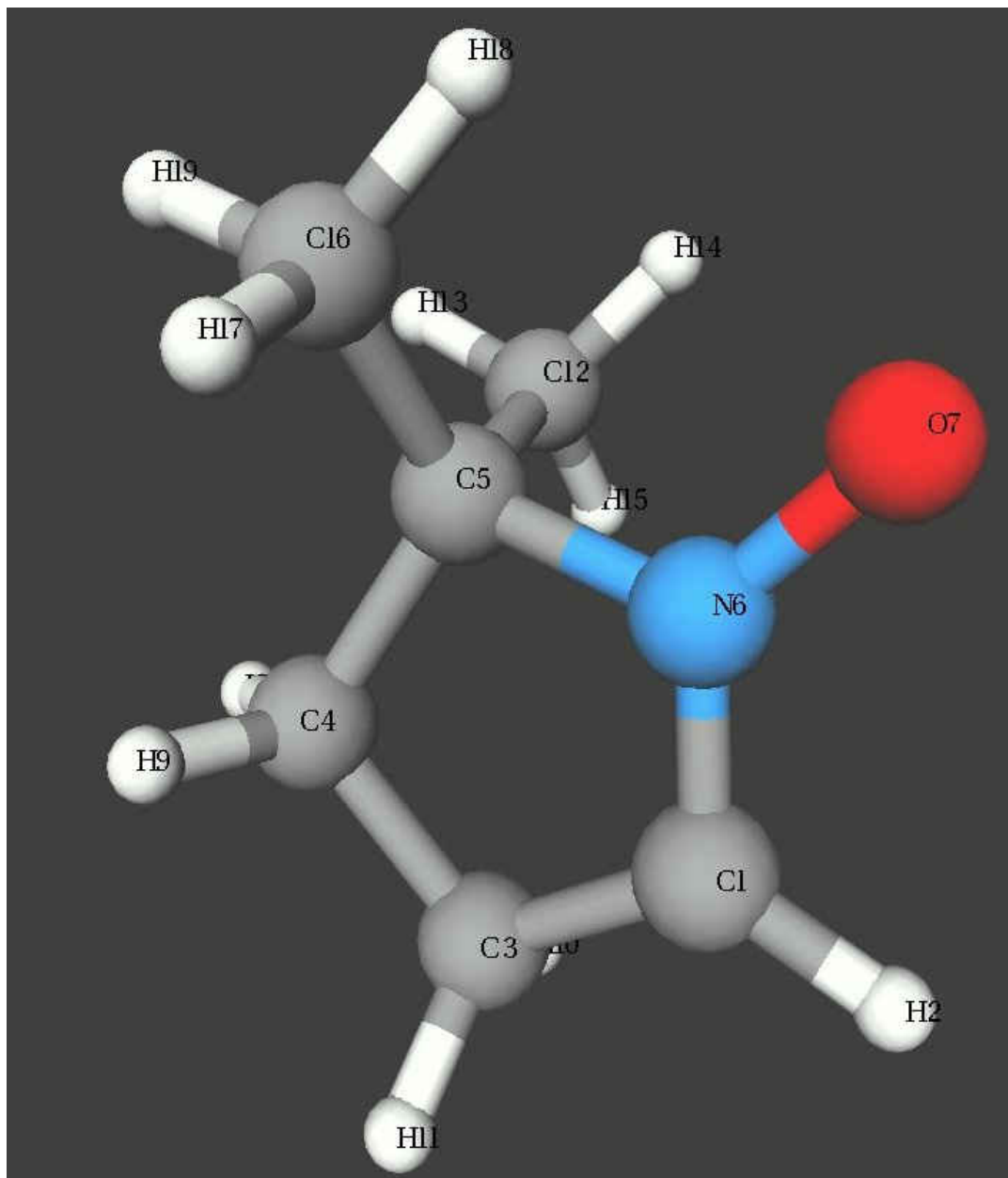


Figure 2. DMPO spin trap.

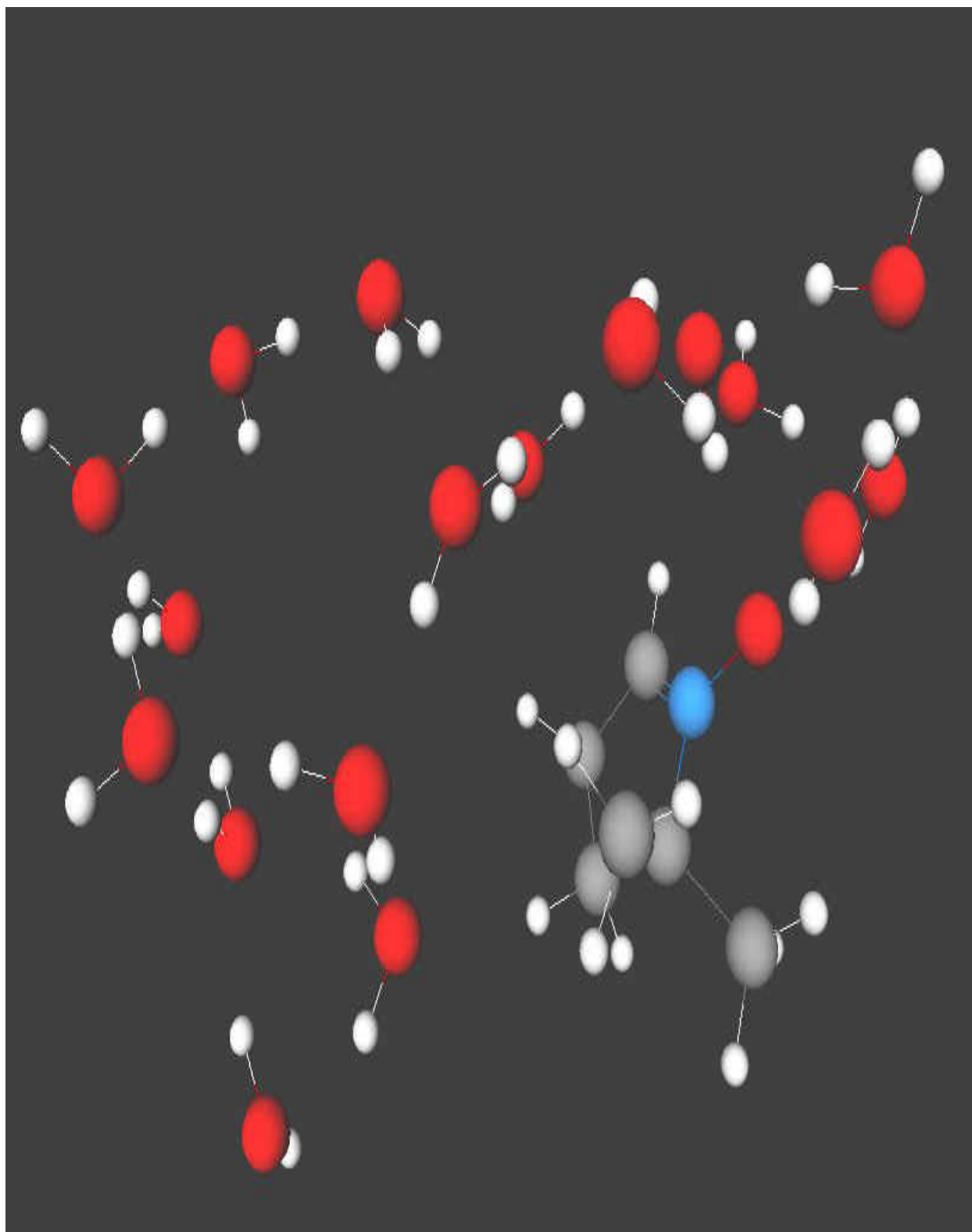


Figure 3. DMPO spin trap surrounded by water molecules (a representation of the hybrid model).

As indicated by Figure 4, the single point energy starts to level off after a limited number, indicating that the effects due to the water molecules are saturated. As a result, further addition of water molecules will only result in cluster formation with the existing water molecules without inducing additional significant changes in the DMPO.[124]

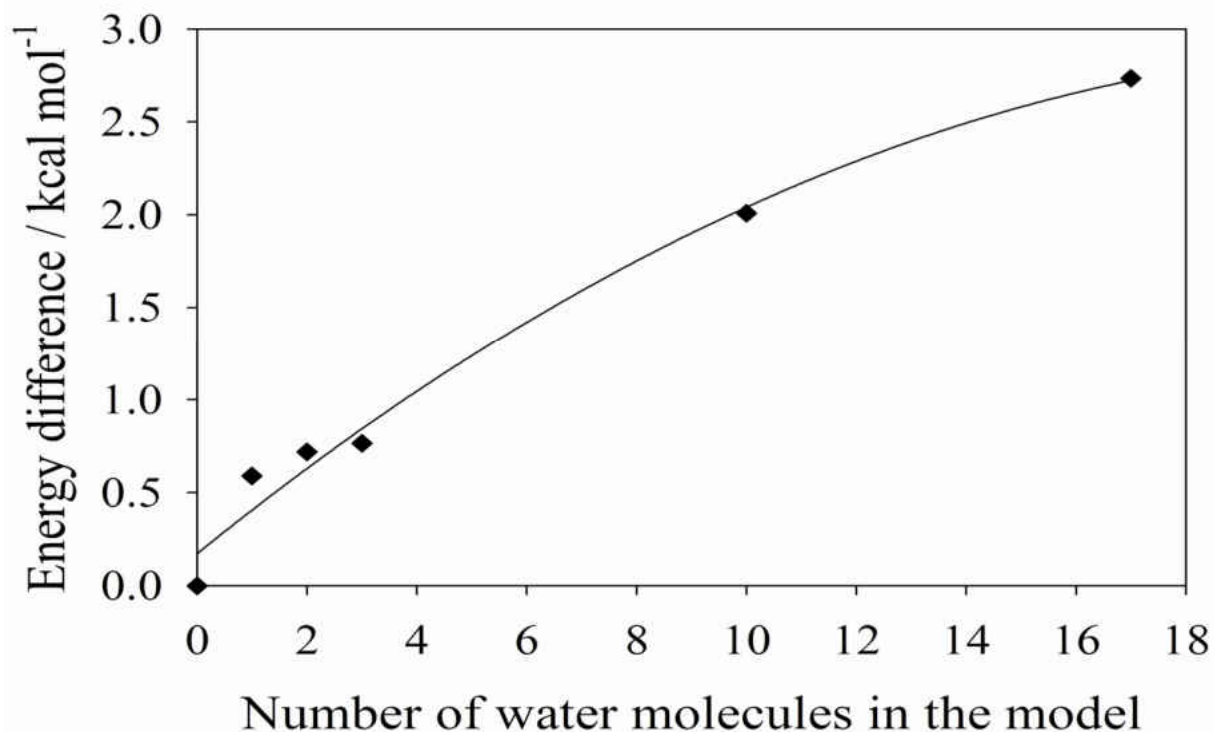


Figure 4. Plot of the difference in the single point energy of DMPO as a function of the number of water molecules in the hybrid model.

As a result, additional water molecules will only increase the computational complexity without providing further changes in the properties of the spin trap. This greatly simplifies the work, as we can obtain a true picture while saving time and also by reducing the complexity of the problem. The effects of intermolecular hydrogen bonding are evident in Table 6.

Table 6. Geometry changes (trends in bond lengths and bond and bond angles) in DMPO.

System	6N-1C	6N-5C	7O-6N	1C-3C-10H	6N-5C-12C	1C-6N-5C	1C-6N-7O	5C-12C-13H	5C-12C-14H
DMPO	1.30844	1.52926	1.26563	111.37	106.54	111.97	128.79	110.16	109.71
DMPO + 1 water molecule	1.30396	1.52988	1.2767	111.15	107.62	112.26	126.88	109.16	110.91
DMPO + 2 water molecules	1.30774	1.52918	1.26815	110.8	106.46	111.73	128.94	110.14	109.74
DMPO + 3 water molecules	1.29971	1.52522	1.29403	110.68	108.11	113.12	126.38	111.97	108.83
DMPO + 10 water molecules	1.29181	1.52207	1.31574	109.01	107.11	113.5	126.65	108.83	110.12
DMPO + 17 water molecules	1.29093	1.51623	1.31776	108.2	108.34	114.52	125.87	108.97	111.49

*All the bond lengths are in Angströms (Å) and the bond angles in degrees (°).

As indicated in Table 6, intermolecular hydrogen bonding with the oxygen atom (7O) of the nitroxide group has led to an elongation of the N-O bond (7O-6N). Another evidence of strong hydrogen bonding interaction is the increase in the 6N-5C-12C bond angle. The presence of water molecules around the N-O bond increases the steric interaction with the methyl substituent on the 5C resulting in an increase in 6N-5C-12C bond angle. The same reasoning can be given for the trends in 1C-6N-5C bond angle, 7O-6N-5C-12C and the 7O-6N-5C-16C torsion angles (see Table 7).

Table 7. Trends in torsion angles in DMPO.

System	1-6-5-12	1-6-5-16	3-4-5-6	4-5-12-14	6-5-4-8	6-5-12-14	7-6-5-12	7-6-5-16
DMPO	-106.0225	134.1624	-20.48112	-166.47325	-143.22754	-55.01548	71.45362	-48.36145
DMPO + 3 water molecules	-103.0388	135.3609	-22.38403	-178.47139	-145.24109	-55.15206	74.78137	-46.819
DMPO + 17 water molecules	-114.4504	124.8427	-9.28145	-179.86733	-130.46899	-67.89855	62.87527	-57.83164

*All the bond angles are in degrees (°).

As indicated by the changes in bond lengths, bond angles, and torsion angles, there are significant geometry changes in the presence of water molecules arising from strong hydrogen bonding and other interactions. The hydrogen bonding in the DMPO hybrid model is as follows (see Table 8)

Table 8. Hydrogen bond lengths in DMPO hybrid model.

System	Intermolecular H-bonding	Intramolecular H-bonding(with other water molecules)
DMPO	n/a	n/a
DMPO + 1	1.84	
DMPO + 2	1.755	1.798
DMPO + 3	1.785	1.806
	1.886	
DMPO + 10	1.663	1.798
	1.803	1.971
DMPO + 17	1.778	
	1.894	
	1.901	

*All the bond lengths are in Angströms (Å).

Changes in the local geometry are also reflected in the change in dipole moments for the DMPO spin trap (see Table 9).

Table 9. Trends in dipole moments for the DMPO spin trap.

System	Dipole moments (D)
DMPO	3.721
DMPO + 1 water molecule	3.862
DMPO + 2 water molecules	3.737
DMPO + 3 water molecules	3.963
DMPO + 10 water molecules	4.038
DMPO + 17 water molecules	4.084

PBN Solvation Studies

Unlike the spin traps, the adducts are capable of forming intramolecular as well as intermolecular hydrogen bonds. For PBN-OH, the *cis*-adduct is stabilized by the strong intramolecular hydrogen bonding between the N-O and the O-H functional groups (see Figure 5). The *trans* adduct is stabilized by the intermolecular hydrogen bonds with water, which as expected significantly changes the dipole moment and other properties (see Figure 6). The *trans*-conformation is not found using the COSMO model, as the spin trap is surrounded by a uniform dielectric incapable of forming the needed hydrogen bonds.

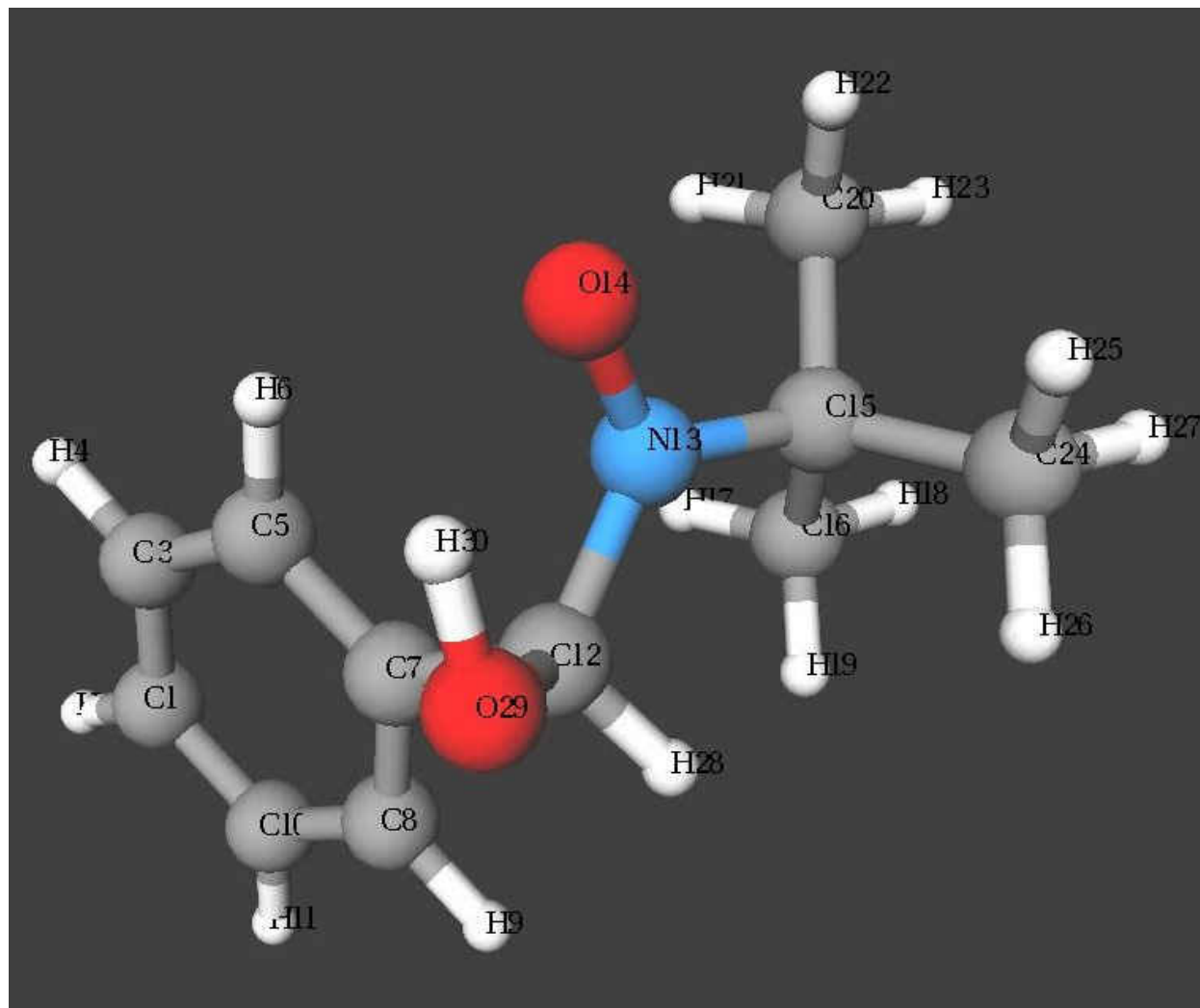


Figure 5. PBN-OH adduct in the *cis* conformation with respect to the nitroxide group.

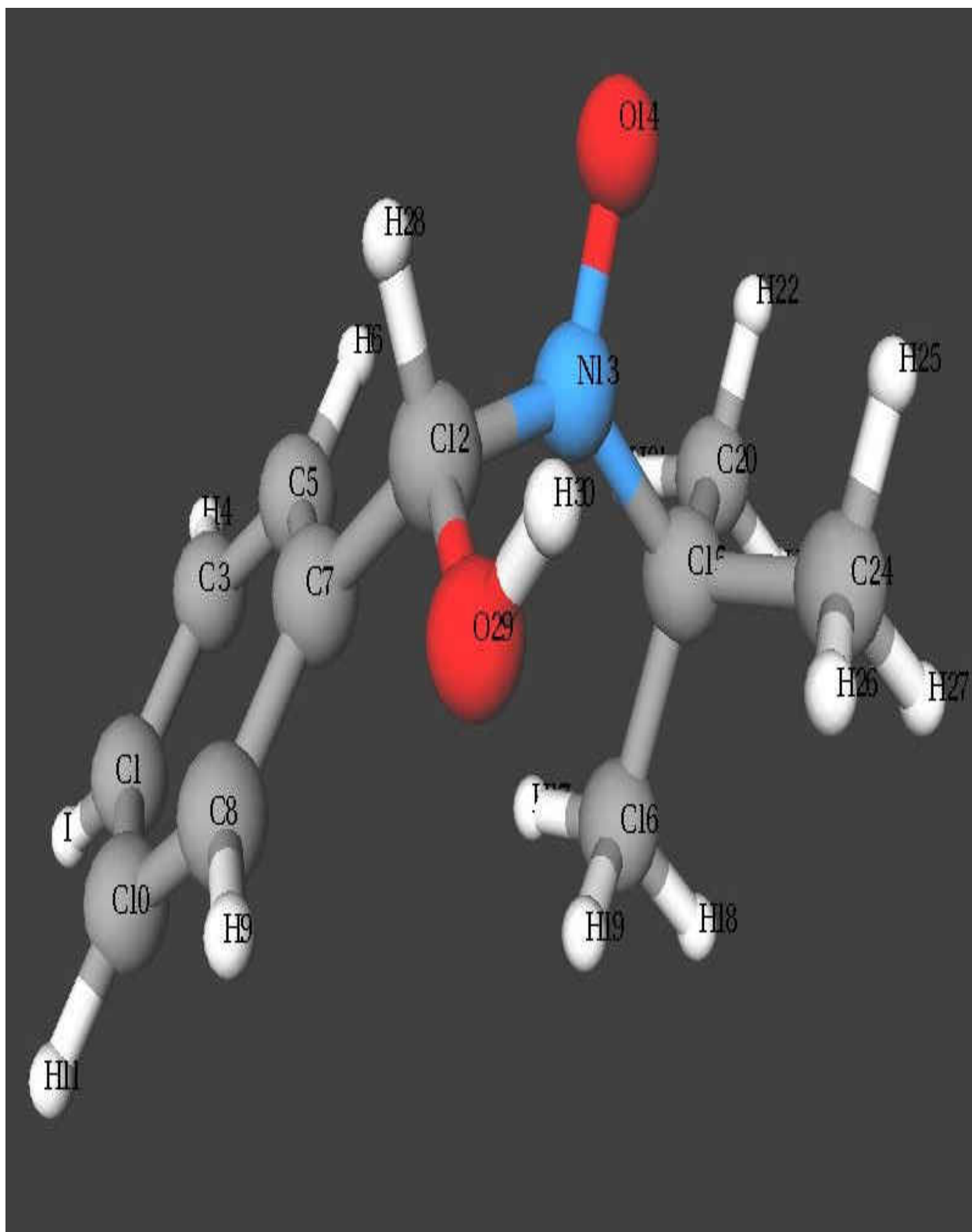


Figure 6. PBN-OH adduct in the *trans* conformation with respect to the nitroxide group.

As indicated in Table 10, there are distinct changes in properties like dipole moment as the geometry of the adduct changes from *cis* to *trans*.

Table 10. Calculated single point energies and dipole moments for the hydroxyl radical, spin trap and two adduct conformers at the B3LYP/6-31G* level.

Molecule	Molecular energy / E_h^*	Dipole moment (D)
OH	-75.686	1.773
PBN	-558.125	3.036
PBN-OH (<i>cis</i>)	-633.930	3.053
PBN-OH (<i>trans</i>)	-633.920	1.809

*All the energies are in hartrees and 1 hartree is 2625.500 kJ/mol.

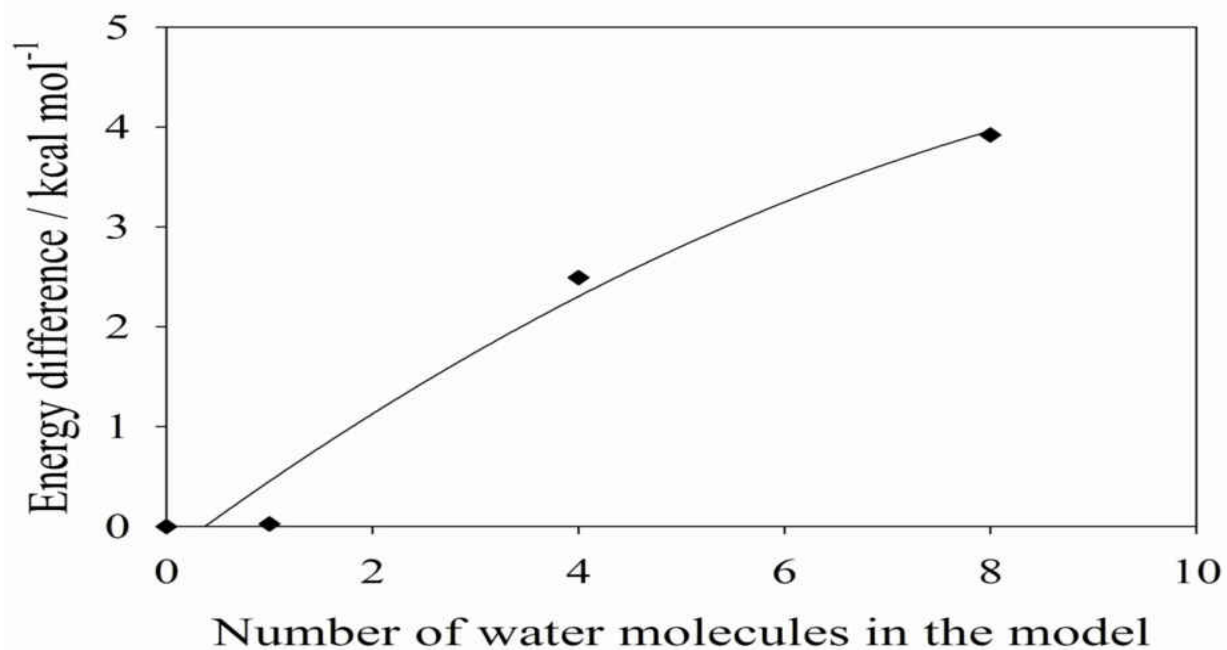


Figure 7. Plot of the difference in single point energies of the PBN-OH *cis*-adduct as a function of the number of water molecules.

As may be seen in Figure 7, the energy difference starts to level off after the addition of 9-10 water molecules. The presence of additional water molecules will have an insignificant effect on the geometry of the molecule thereby simplifying the problem at hand. The hybrid model for the PBN-OH adduct involves surrounding the adduct with discrete water molecules as in Figures 8 and 9. The effect of intramolecular and intermolecular interactions is evident in Table 11.

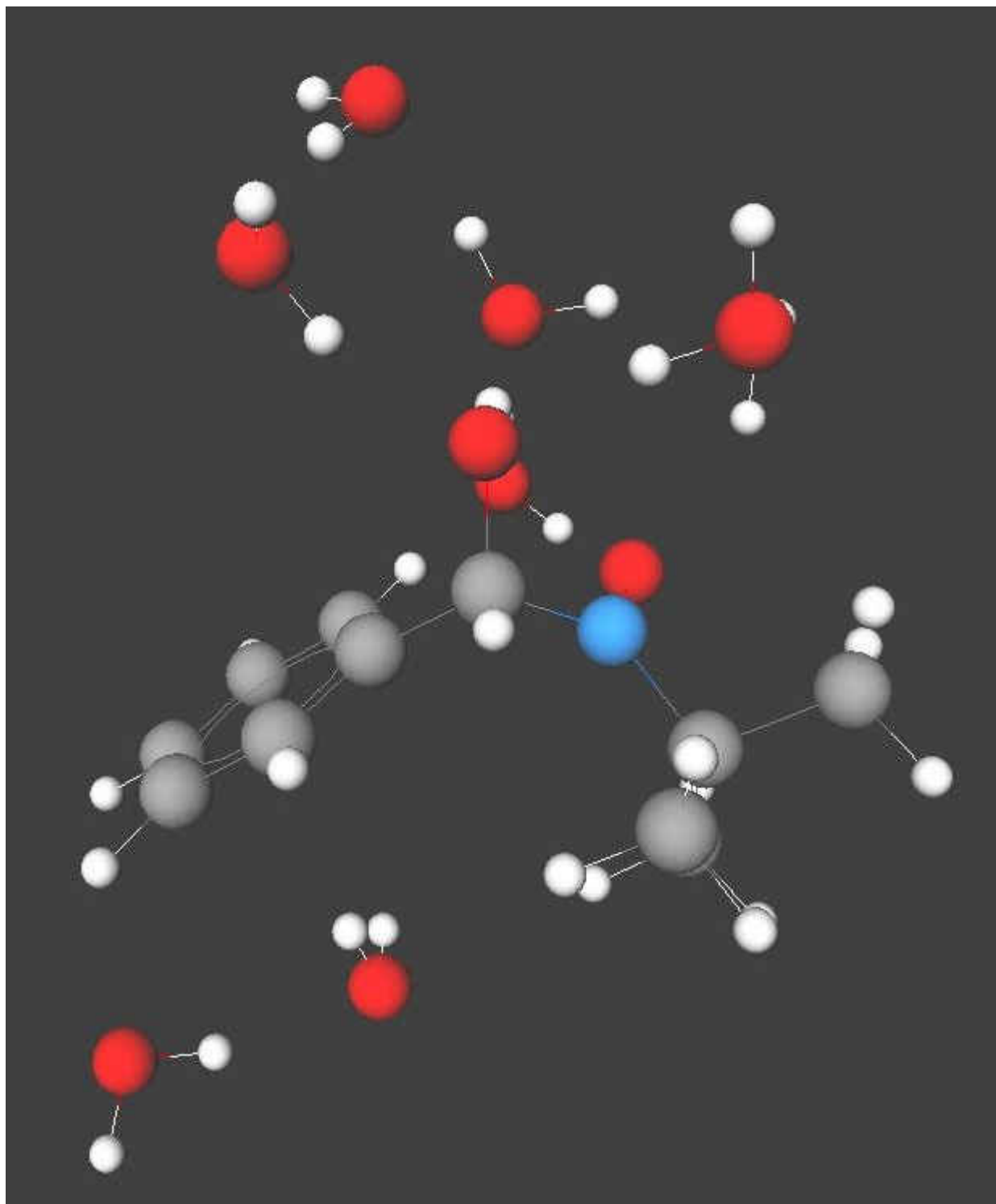


Figure 8. PBN-OH *cis* adduct surrounded by water molecules.

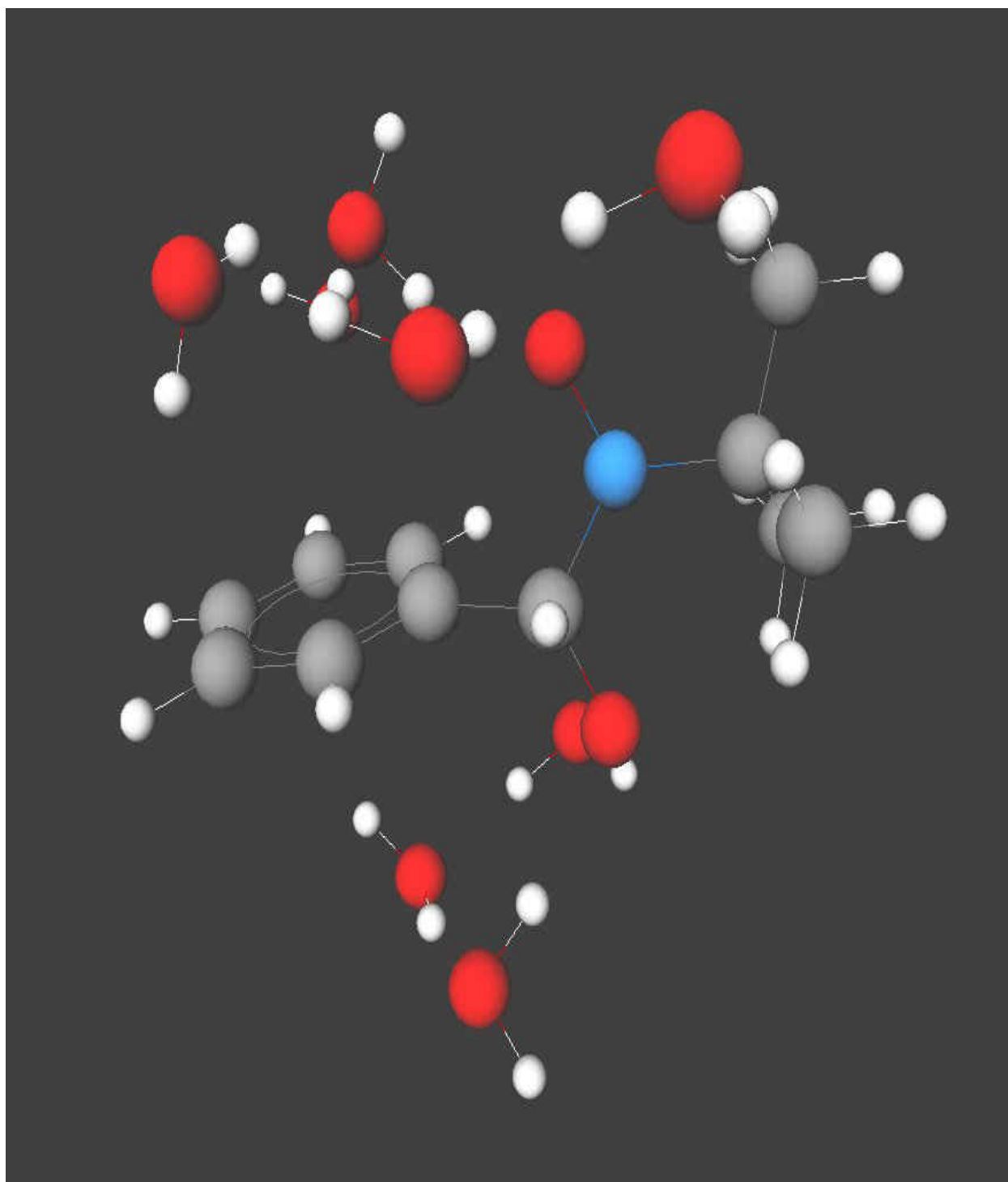


Figure 9. PBN-OH *trans* adduct surrounded by water molecules.

Table 11. Geometry changes (trends in bond lengths and bond angles) in PBN-OH *cis* adduct.

System	290-12C	30H-290	7C-12C-13N	13N-12C-28H	28H-12C-290	12C-13N-15C	13N-15C-16C	13N-15C-24C	16C-15C-24C	12C-290-30H
PBN-OH	1.39892	0.98045	110.46	108.13	107.65	123.69	109.77	108.02	111.08	104.03
PBN-OH + 1 water molecule	1.41683	0.98214	112.29	108.45	106.53	126.86	110.31	106.82	110.9	103.52
PBN-OH + 4 water molecules	1.41123	0.98471	112.88	106.04	104.77	126.03	111.06	106.71	109.91	110.49
PBN-OH + 8 water molecules	1.41684	1.02347	112.83	106.69	105.62	126.22	111.24	106.76	109.88	113.02

*All the bond lengths are in Angströms (Å) and the bond angles in degrees (°).

As seen in Table 11, there is an elongation of the 20O-12C bond as the intramolecular hydrogen bonding gets stronger. There is also a considerable change in the 12C-29O-30H bond angle as the hydrogen atom (30H) on the hydroxyl radical is involved in strong intermolecular hydrogen bond interactions with the water molecules surrounding it. The effect of intermolecular hydrogen bond interactions can also be seen in the variation of 7C-12C-13N-14O torsion angle given in Table 12. As more water molecules cluster around the nitroxide functionality it results in a steric interaction with the tert-butyl group on the atom adjacent to the nitrogen atom. This observation is reflected in an increase in the 7C-12C-13N-15C torsion angle from -101.58996° to -81.8889° . As is evident in Table 13, the adduct is initially stabilized by intramolecular hydrogen bonds, however as the number of water molecules are increased from 0 to 8 the intermolecular hydrogen bonds start playing a dominant role over the intramolecular hydrogen bonds. This is reflected in an increase in the 14O-13N-12C-29O torsion angle. The trend in 28H-12C-29O-30H torsion angle also reflects the strength of the intermolecular hydrogen bond interactions.

Table 12. Trends in torsion angles for the PBN-OH *cis* adduct.

System	5-7-12- 29	7-12-13- 14	7-12-13-15	12-13-15- 20	13-12-29- 30	14-13-12- 28	14-13-12- 29	14-13-15- 20	28-12-29- 30
PBN-OH	75.24932	96.55436	-101.58996	161.12872	29.805	-143.73417	-27.31288	-37.66055	146.53528
PBN-OH + 1 water molecule	74.32034	84.42158	-91.12573	112.83136	35.92951	-153.74493	-39.36371	-62.57459	151.60487
PBN-OH + 4 water molecules	78.32146	75.70435	-101.4521	117.38281	70.07795	-164.9281	-51.89831	-59.82544	176.08349
PBN-OH + 8 water molecules	64.91069	78.09934	-95.55464	112.81694	57.45741	-162.70852	-49.08169	-60.79361	171.78023
PBN-OH + 11 water molecules	62.2839	78.27381	-81.8889	95.9016	61.91076	-161.6407	-47.0934	-63.88429	177.0782

*All the bond lengths are in Angströms (Å) and the bond angles in degrees (°).

Table 13. Hydrogen bond lengths in PBN-OH *cis* adduct.

System	Intramolecular H-bonding	Intermolecular H-bonding	Type
PBN-OH	1.939		
PBN-OH + 1 water molecule	1.976	1.946	
PBN-OH + 4 water molecules	2.634	1.895	(N-O...H ₂ O)
		1.731	(H-O...H ₂ O)
		1.863	(O-H...OH ₂)
PBN-OH + 11 water molecules	2.432	1.739	(O-H...OH ₂)
		1.979	(H-O...H ₂ O)
		2.029	(N-O...H ₂ O)

*All the bond lengths are in Angströms (Å).

As is evident from Table 13, as the number of water molecules increase the intermolecular hydrogen bonds become stronger than the intramolecular hydrogen bonds, and are the stabilizing forces for the *cis* adduct. The notable geometry changes in the *trans* adduct are given in Table 14. As seen in Table 15, the *trans* adduct is stabilized by extensive intermolecular hydrogen bonding. The geometry changes in going from the *cis* to *trans* configuration are given in Table 16.

Table 14. Geometry changes (trends in bond angles) in PBN-OH *trans* adduct.

System	13N-12C-29O	12C-13N-14O	17H-16C-19H
PBN-OH	110.94	115.44	109.1
PBN-OH + 2 water molecules	113.2	113.2	107.94
PBN-OH + 8 water molecules	110.94	115.44	109.1

*All the bond angles in degrees (°).

Table 15. Hydrogen bond lengths in PBN-OH *trans* adduct.

System	Intramolecular H-bonding	Intermolecular H-bonding	Type
PBN-OH	2.255		(N-O...H-C)
PBN-OH + 2 water molecules	2.588	1.827	(O-H...OH ₂)
		1.937	(N-O...H ₂ O)
PBN-OH + 8 water molecules	2.766	1.666	(O-H...OH ₂)
		1.839	(H-O...H ₂ O)
		1.834	(N-O...H ₂ O)
		1.923	(N-O...H ₂ O)

*All the bond lengths are in Angströms (Å).

Table 16. Torsion angle comparison between *cis* and *trans* PBN-OH adducts.

Torsion angle	PBN-OH <i>cis</i>	PBN-OH <i>trans</i>
5-7-12-28	-165.03912	68.12331
5-7-12-29	75.24392	-170.73522
7-12-13-14	96.55436	127.31184
7-12-29-30	-92.73116	-165.72241
8-7-12-28	17.60245	-108.04876
8-7-12-29	-102.1091	13.09271
14-13-12-28	-143.73417	10.42836
14-13-12-29	-27.31288	-107.57613
15-13-12-28	18.12151	167.92049
15-13-12-29	134.5428	49.91601
28-12-29-30	146.53528	-45.49754

*All the bond angles in degrees (°).

As is indicated in Table 16, there are huge changes in going from *cis* to *trans* configuration, most notable being that of 14O-13N-12C-290 torsion angle. The other marked changes that reflect the difference in geometries are the 14O-13N-12C-28H, 15C-13N-12C-28H torsion angles. Changes in the local geometry are also reflected in the change in dipole moments for the adduct (see Table 17).

Table 17. Trends in dipole moment for the PBN-OH *cis* adduct.

System	Dipole moments (D)
PBN-OH	3.053
PBN-OH + 1 water molecule	3.157
PBN-OH + 4 water molecules	2.412
PBN-OH + 8 water molecules	2.475

PBN-Me Adduct

It is known that C-centered radicals are trapped efficiently by PBN type nitrones. It was shown that addition of methyl radical was thermodynamically and kinetically more favored than proton abstraction from the PBN spin trap.[125] Hybrid models were tested on the PBN-Me adduct (see Figures 10,11 and 12) and the optimum number of water molecules were found.

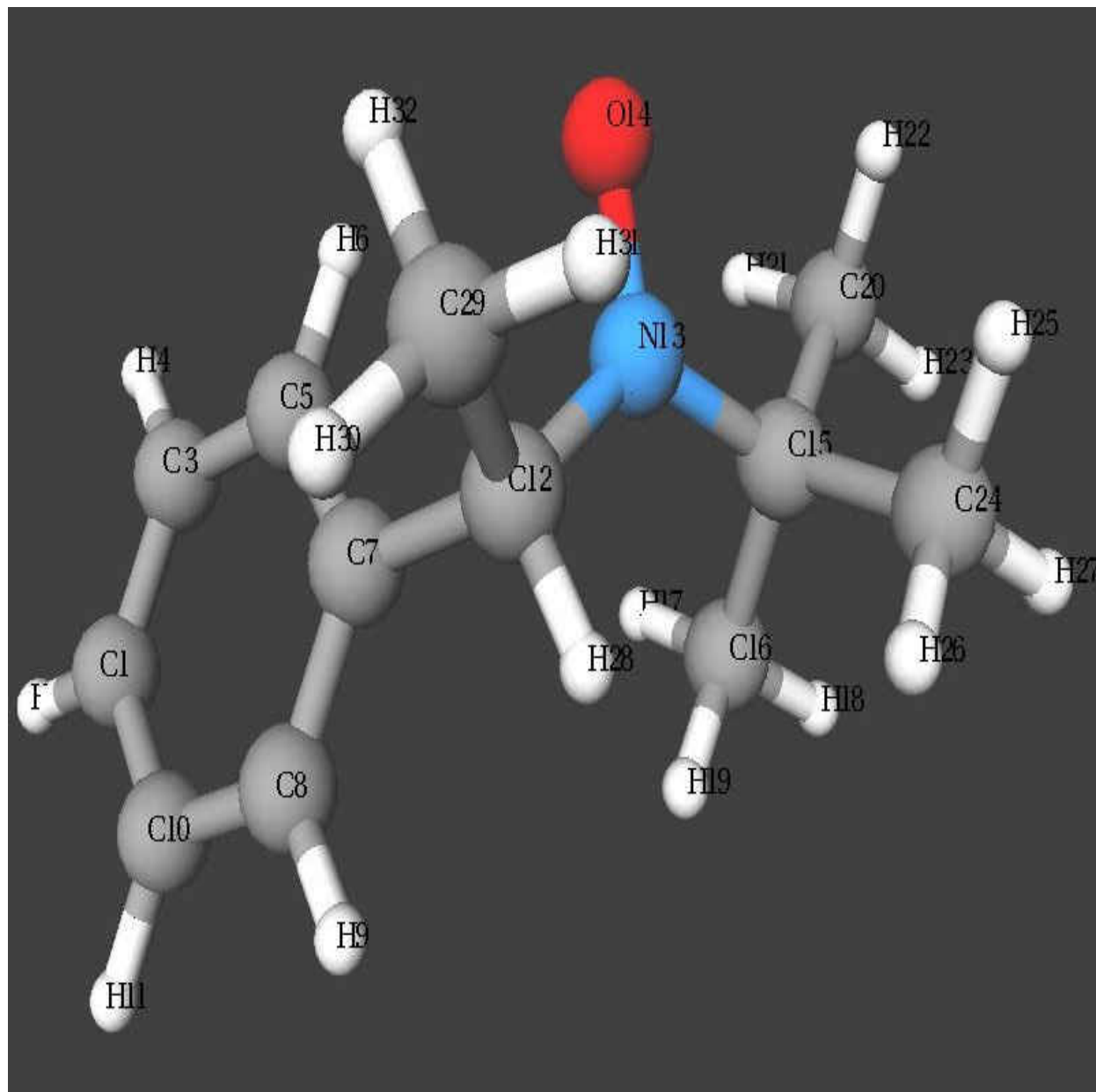


Figure 10. PBN-Me *cis* adduct.

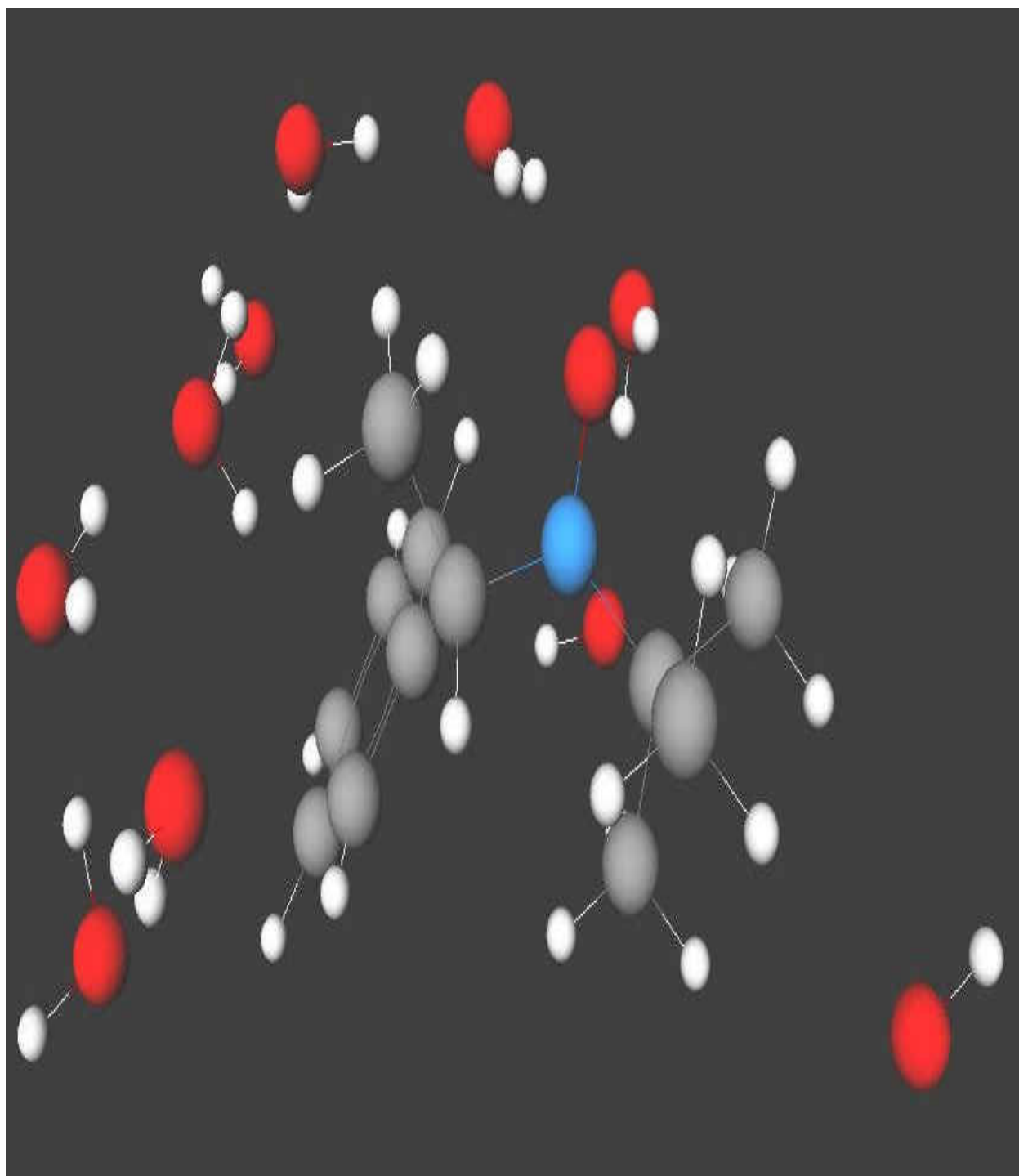


Figure 11. PBN-Me *cis* adduct surrounded by water molecules.

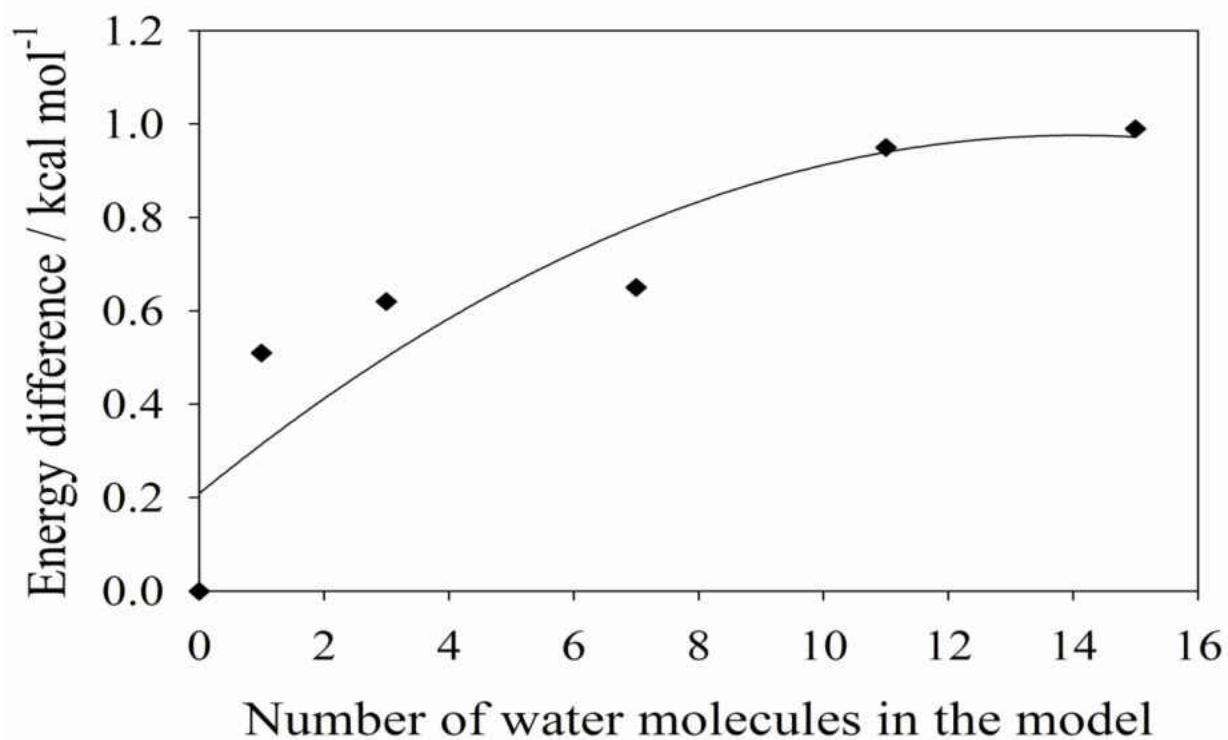


Figure 12. Plot of the difference in single point energies of the PBN-Me adduct as a function of the number of water molecules.

As may be seen in Figure 12, the energy difference starts to level off after the addition of 14-15 water molecules. The geometry changes in the PBN-Me adduct are given in Table 18.

Table 18. Geometry changes (trends in bond angles) in PBN-Me adduct.

System	12C-13N-14O	14O-13N-15C	13N-15C-24C
PBN-Me	117.78	119.83	108.89
PBN-Me + 1 water molecule	116.39	119.65	109.13
PBN-Me + 3 water molecules	116.3	119.55	109.71
PBN-Me + 7 water molecules	117.09	120.2	108.53
PBN-Me + 11 water molecules	118.27	118.75	108.56
PBN-Me + 15 water molecules	118.1	117.27	107.69

*All the bond angles in degrees (°).

As seen in Table 18, the geometry changes in PBN-Me adduct are not as drastic as in the case of PBN-OH adduct due to the lack of electronegative atoms capable of forming hydrogen bonds. This evidence is another clear indication of the significant role played by hydrogen bonds. The only major changes in the torsion angles are those of 5C-7C-12C-13N and 5C-7C-12C-28H (see Table 19). The variation in the former is due to steric hindrance between the methyl radical and the water molecules coordinating to the oxygen atom of the nitroxide functionality. The hydrogen bond lengths in the PBN-Me adduct are shown in Table 20.

Table 19. Trends in torsion angles for the PBN-Me adduct.

System	5-7-12-13	5-7-12-28	7-12-13-14	7-12-13-15	14-13-12-29	14-13-15-20
PBN-Me	-43.5935	-160.65614	82.79394	-102.24427	-42.14396	13.78235
PBN-Me + 1 water molecule	-59.2868	-176.78823	67.45257	-100.47551	-57.97173	17.11221
PBN-Me + 3 water molecules	-59.0834	-175.84482	66.40486	-100.55583	-58.8308	20.591
PBN-Me + 7 water molecules	-45.712	-163.1211	86.19289	-106.41098	-38.81324	20.50226
PBN-Me + 11 water molecules	-48.4851	-164.83694	94.01939	-99.09039	-31.64201	22.96879
PBN + Me + 19 water molecules	-18.776	-135.6101	91.81832	-99.32507	-33.69921	38.21685

*All the bond angles in degrees (°).

Table 20. Hydrogen bond lengths in PBN-Me *cis* adduct.

System	Intramolecular H-bonding	Intermolecular H-bonding	Type
PBN-Me	2.535	n/a	(N-O...H-CH ₂)
PBN-Me + 1 water molecule	2.571	1.953	(N-O...H ₂ O)
PBN-Me + 3 water molecules	2.566	1.939	(N-O...H ₂ O)
PBN-Me + 7 water molecules	2.507	1.902	(N-O...H ₂ O)
		1.996	
PBN-Me + 11 water molecules	2.487	2.049	(N-O...H ₂ O)
		2.023	
			(CH ₂ -H...OH ₂)
PBN-Me + 19 water molecules	2.501	1.864	(N-O...H ₂ O)
		2.177	

*All the bond lengths are in Angströms (Å).

As seen in Table 20, the PBN-Me adduct is stabilized predominantly by intermolecular hydrogen bonding. Changes in the local geometry are also reflected in the change in dipole moments for the adduct (see Table 21).

Table 21. Trends in dipole moment for PBN-Me adduct.

System	Dipole moments (D)
PBN-Me	2.642
PBN-Me + 1 water molecule	2.572
PBN-Me + 3 water molecules	2.577
PBN-Me + 7 water molecules	2.693
PBN-Me + 11 water molecules	2.646
PBN-Me + 19 water molecules	2.706

PPN Solvation Studies

The presence of electronegative atoms in the PPN spin trap allows for extensive hydrogen bonding interactions (see Figure 13).

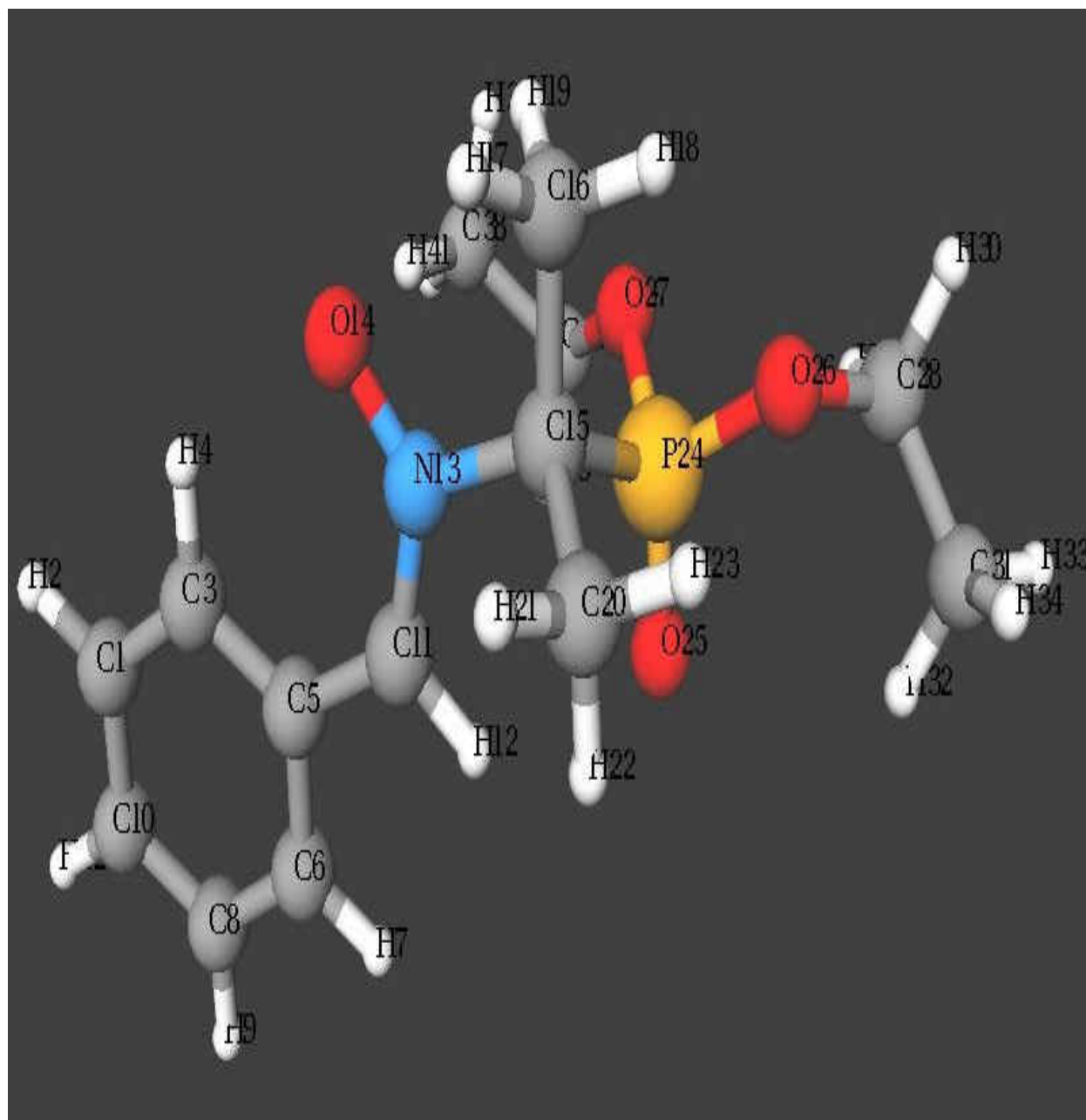


Figure 13. PPN spin trap.

The results of incorporating PPN in the hybrid model (see Figures 14 and 15) are as follows

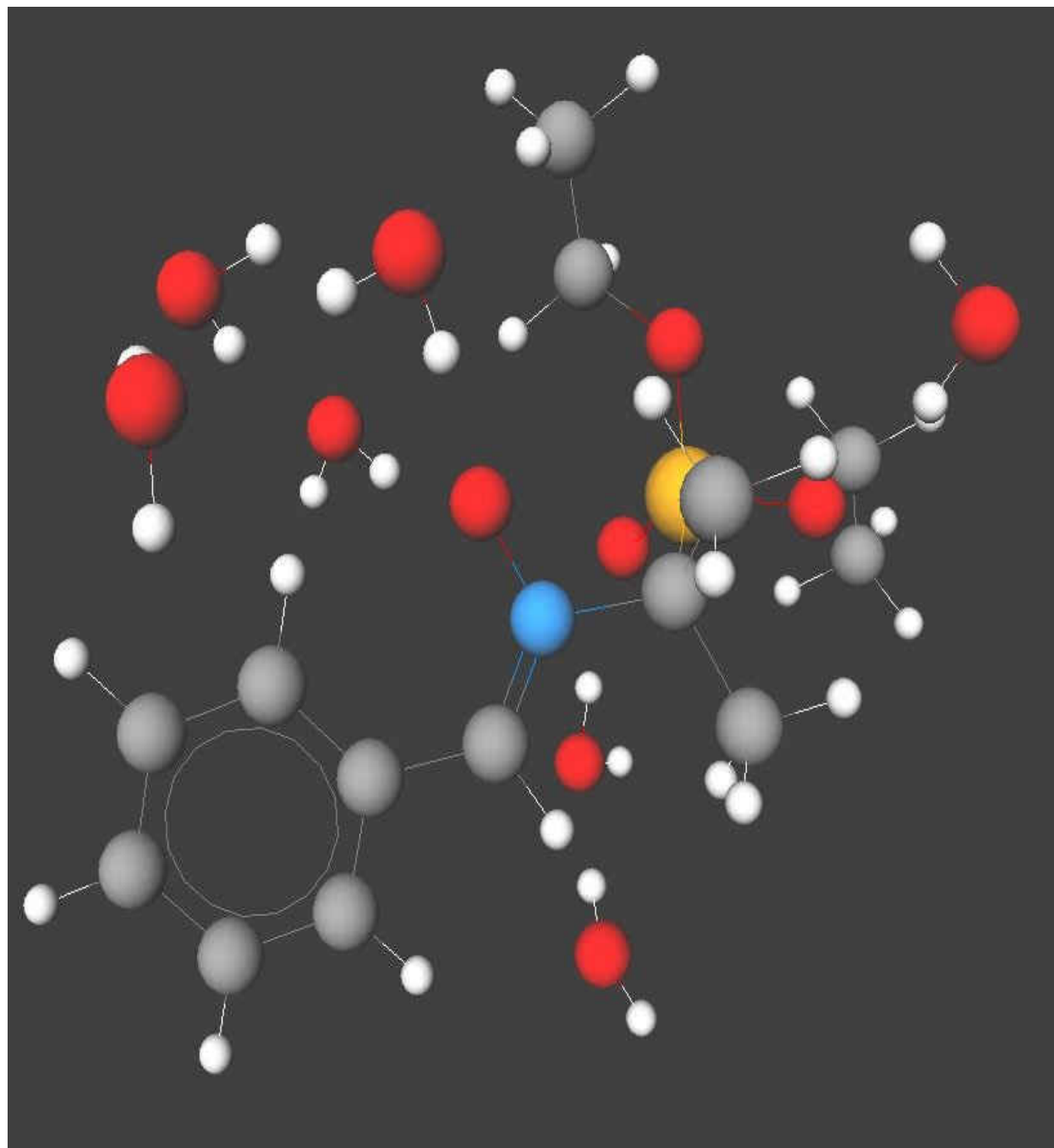


Figure 14. PPN spin trap surrounded by water molecules.

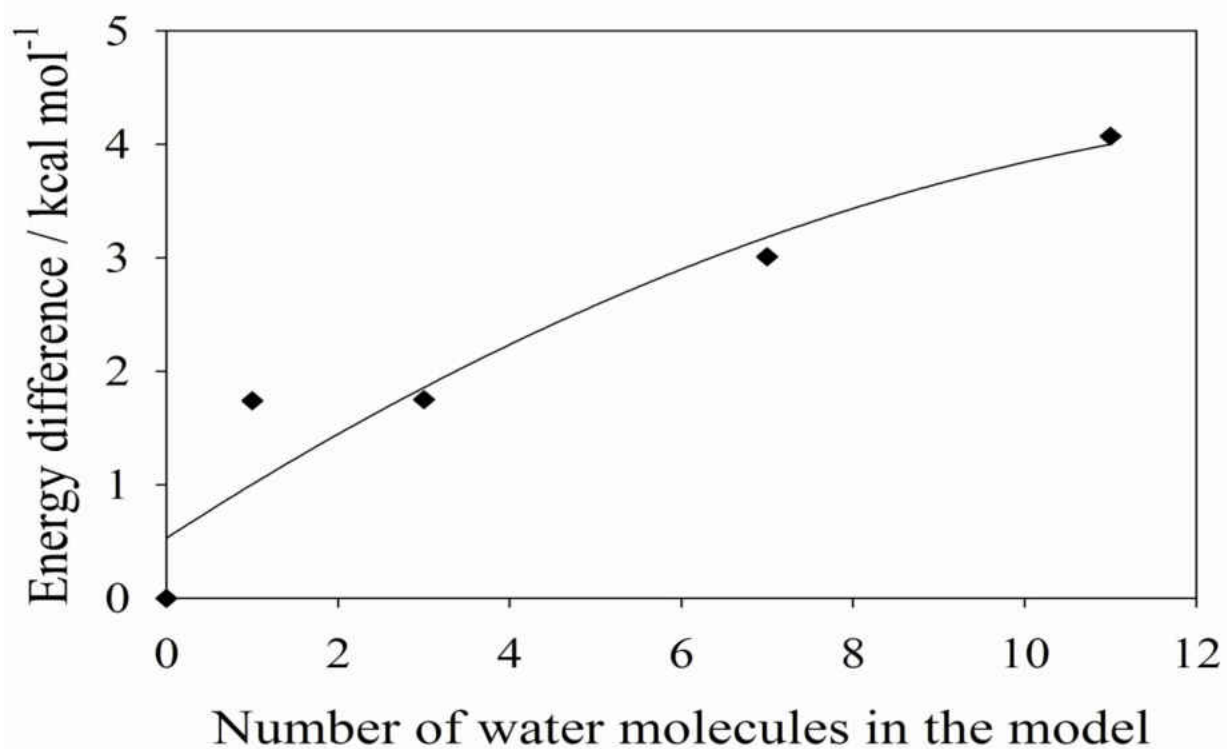


Figure 15. Plot of the difference in single point energies of PPN as a function of the number of water molecules.

The same trend is observed as expected in that the single point energy levels off after 12 water molecules (see Figure 15). The geometry changes in the PPN spin trap when surrounded by water molecules is given in Tables 22 and 23. The hydrogen bond lengths in the PPN spin trap are given in Table 24.

Table 22. Geometry changes (trends in bond lengths and bond angles) in PPN spin trap.

System	140-13N	25O-24P	4H-3C-5C	5C-11C-12H	13N-15C-24P	15C-24P-25O	15C-24P-26O	25O-24P-26C
PPN	1.28007	1.48998	118.87	117.98	107.44	114.84	99.59	116.87
PPN + 1 water molecule	1.29322	1.49127	118.97	117.93	110.04	115.17	98.69	116.68
PPN + 3 water molecules	1.29668	1.5019	119.01	116.66	105.52	112.85	99.91	115.56
PPN + 7 water molecules	1.31263	1.49568	120.18	116.91	102.88	114.18	99.19	114.86
PPN + 11 water molecules	1.31281	1.50585	120.6	116.13	103.7	113.81	99.72	113.37
PPN + 15 water molecules	1.31394	1.52334	120.41	116.93	105.65	119.55	97.31	112.56

*All the bond lengths are in Angströms (Å) and the bond angles in degrees (°).

Table 23. Trends in torsion angles for the PPN spin trap.

System	3-5-11-13	11-13-15-16	11-13-15-24	13-15-24-25	14-13-15-24
PPN	-3.14198	177.50027	62.55547	-62.95405	-117.89763
PPN + 1 water molecule	-2.71396	172.25014	52.1821	-56.06231	-132.2844
PPN + 3 water molecules	-7.25038	150.7226	88.6996	-63.69195	-88.16699
PPN + 7 water molecules	-14.7763	119.17489	122.03015	-43.25273	-56.63881
PPN + 11 water molecules	1.91084	103.13058	139.09963	-45.68774	-44.57424
PPN + 15 water molecules	-23.2346	81.49892	161.64064	-53.60714	-19.30663

*All the bond angles in degrees (°).

Table 24. Hydrogen bond lengths in PPN spin trap.

System	Intramolecular H-bonding	Type
PPN	2.18	(N-O...H-Benzene)
	2.935	(P=O...H-C-NO)
PPN + 1 water molecule	1.837	(N-O...H ₂ O)
PPN + 3 water molecules	1.868	(N-O...H ₂ O)
	2.168	(P=O...H ₂ O)
	1.894	
PPN + 7 water molecules	1.851	(N-O...H ₂ O)
	1.81	
	1.795	(P=O...H ₂ O)
	1.984	(OH ₂ ...OEt)
PPN + 11 water molecules	1.883	(N-O...H ₂ O)
	1.823	
	1.727	(P=O...H ₂ O)
	1.887	
PPN + 15 water molecules	1.579	(N-O...H ₂ O)
	1.381	(P=O...H ₂ O)

*All the bond lengths are in Angströms (Å).

The trends in PPN are more drastic due to the presence of additional electronegative atoms in the form of the phosphorus atom and the 3 additional oxygen atoms that are capable of forming hydrogen bonds. As indicated in the Tables 22, 23, and 24, we have additional hydrogen bonding with the oxygen atom of the P=O functionality resulting in an increase in the 15C-24P-25O bond angle. The same reasoning can be attributed for an increase in the 11C-13N-15C-24P torsion angle from 62.55547° to 161.64064°. Another interesting observation is that of the water molecule coordinating simultaneously with the N-O and P=O functionality reflected in a major decrease in the 14O-13N-15C-24P torsion angle from -117.89763° to -19.30663°. As is indicated in Table 24, the hydrogen bonds get stronger with an increase in the number of water molecules surrounding the spin trap. The dipole moment changes are given as follows (see Table 25)

Table 25. Trends in dipole moment for PPN spin trap.

System	Dipole Moments (D)
PPN	2.084
PPN + 1 water molecule	2.932
PPN + 7 water molecules	2.935
PPN + 11 water molecules	2.904
PPN + 15 water molecules	3.865

Aprotic solvent studies

A similar theory was applied to aprotic solvents to confirm the dominant role played by polar protic solvents like water in stabilizing the spin traps (see Figure 16).

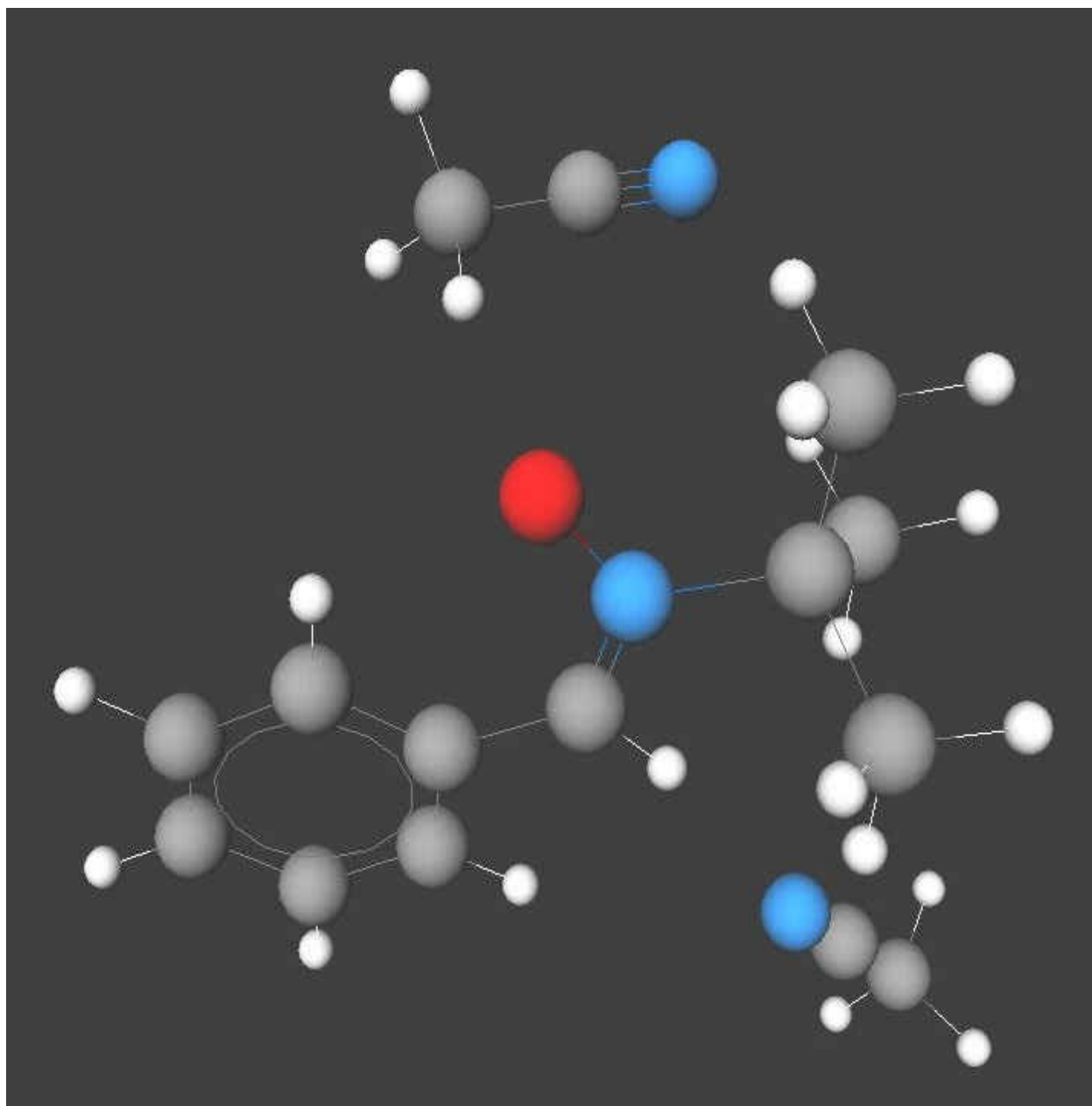


Figure 16. PBN spin trap surrounded by acetonitrile molecules.

As indicated in Table 26 there is no stabilization by acetonitrile (dipole moment: $4.5 \pm 0.1D$ [126]) which further consolidates the role of polar protic solvents like water in stabilizing the spin traps.

Table 26. Molecular energies of PBN in acetonitrile.

System	Molecular Energy/ E_h
PBN +1 water molecule	-634.58
PBN + 1 acetonitrile molecules	-558.125
PBN + 2 acetonitrile molecules	-558.122

Conclusion

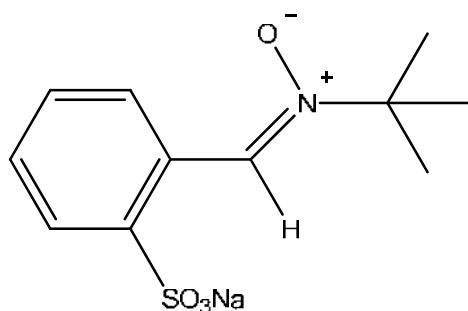
As indicated by the data, polar protic solvents like water play an important role in the stabilization of spin traps. The studies from hybrid model indicate that there is a limited number of water molecules that influence the properties of the spin trap, and that there is a negligible effect upon further addition of water molecules. The intermolecular hydrogen bonding between the solvent and the PBN-OH spin trap adduct is responsible for two distinct adduct conformers. This has a profound effect on the dipole moment as compared to the calculated value in the gas phase. Hydrogen bonding interactions are dominant forces in the phosphorylated analogue of PBN, thereby supporting the role of hydrogen bonds in stabilizing the spin trap and the adduct. The dipole moment as calculated by the hybrid model of DMPO is 4.08 as compared to the literature value of 3.72 and COSMO value of 5.34 (see Table 5).[124, 127, 128]

CHAPTER 4

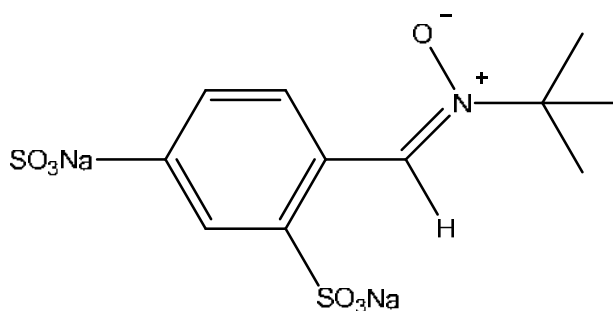
FUTURE WORK

Spin traps provide offer a broad scope for research. The synthesis of phosphorylated analogues of various nitrones has widened the applicability of spin traps in biological systems. Computational studies on the phosphorylated analogues of spin traps is however very limited. In view of this, the following ideas can be considered for future research.

1. Comparative DFT study of the spin trapping of hydroxy, methyl, hydroperoxyl, mercapto radicals by various phosphorylated PBN analogues, notably PPN, 4-OHPPN, 4-PyOPN.[129]
2. Comparison of the radical trapping ability of phosphorylated analogues vs. S-PBN and NXY-059.



S-PBN



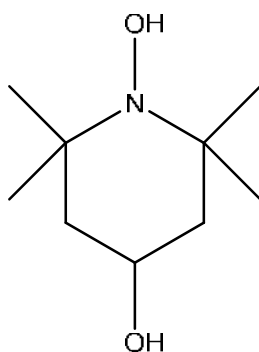
NXY-059

S-PBN and NXY-059 also trap carbon and oxygen-centered radicals effectively and their spin trapping efficiency should be compared with the phosphorylated analogues of PBN. [130, 131]

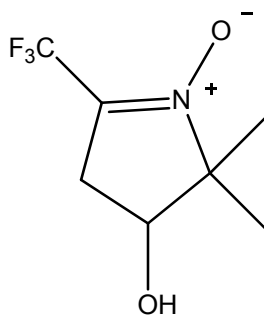
3. DFT study of spin trapping of phenyl, carbon dioxide, carbonate radical species by phosphorylated PBN analogues.

There are some newly discovered spin traps that are reported in literature that are suitable candidates for theoretical investigation.

1. Computational investigation of the spin trapping capabilities of new class of spin trap 1-hydroxy-2,2,6,6-tetramethyl-4-oxo-piperidine hydrochloride (TEMPONE-H), given the fact that the sensitivity of TEMPONE-H in the detection of peroxynitrite and superoxide radicals was about 10-fold higher than DMPO.[132]



2. Computational investigation of a new class of fluorinated nitrones, for e.g. FDMPO. [133-135]



5. Application of the hybrid solvation models to the above mentioned exotic spin traps.

REFERENCES

1. Lai, C.; Piette, L. H. *Biochem. Biophys. Res. Commun.* **1977**, *78*, 51-59.
2. Bilenko, M. V. *Ischemia and Reperfusion of Various Organs*; Nova Science Pub. Inc.: Huntington, New York, **2001**.
3. Roberfroid, M.; Calderon, P. B. *Free Radicals and Oxidation Phenomena in Biological Systems*; MerceL Dekker: New York, 1995.
4. Halliwell, B.; Gutteridge, J. M. C. *Free Radicals in Biology and Medicine*; Oxford University Press: Oxford, 1999.
5. Bilenko, M. V. *Ischemic and Reperfusion of Various Organs: Injury, Mechanisms, Methods of Prevention and Treatment*; Nova Science Pub. Inc.: Huntington, New York, 2001.
6. Fenton, H. J. H. *J. Chem. Soc.* **1894**, *65*, 899.
7. Dixon, W. T.; Norman, R. O. C. *J. Chem. Soc.* **1963**, 3119.
8. Jefcoate, C. R. E.; Lindsay-Smith, J. R.; Norman, R. O. C. *J. Chem. Soc. (B)* **1969**, 1013.
9. Ogata, Y.; Furuta, K. *The Chemistry of Peroxides*, Wiley: New York, 1983.
10. Saito, I.; Takayama, M.; Matsuura, T.; Matsugo, S.; Kawanishi, S. *J. Am. Chem. Soc.* **1990**, *112*, 883.
11. Dixon, W. T.; Norman, R. O. C. *J. Chem. Soc.* **1963**, 3119.
12. Walling, C. *Acc. Chem. Res.* **1975**, *8*, 125.
13. Hayon, E.; Iyata, T.; Lichtin, N. N.; Simic, M. *J. Am. Chem. Soc.* **1970**, *92*, 3898.
14. Walling, C.; El-Taliawi, G. M. *J. Am. Chem. Soc.* **1973**, *95*, 848.
15. Walling, C.; El-Taliawi, G. M.; Johnson, R. A. *J. Am. Chem. Soc.* **1974**, *96*, 133.
16. Nofre, C.; Le Roux, Y.; Gondot, L.; Cier, A. *Bull. Soc. Chim. Fr.* **1964**, 2451.

17. Janzen, E. G.; Blackburn, B. J. *J. Am. Chem. Soc.* **1968**, *90*, 5909-5910.
18. Swartz, H. M. *Bull. Magn. Reson.* **1986**, *8*, 172-175.
19. Pou, S.; Pou, W. S.; Brecht, D. S.; Snyder, S. H.; Rosen, G. M. *J. Biol. Chem.* **1992**, *267*, 24173-24176.
20. Harbour, J. R.; Bolton, J. R. *Biochem. Biophys. Res. Commun.* **1975**, *64*, 803-807.
21. Rosen, G. M.; Britigan, B. E.; Cohen, M. S.; Ellington, S. P.; Barber, M. J. *Biochim. Biophys. Acta.* **1988**, *969*, 236-241.
22. Iwamura, M.; Inamoto, N. *Bull. Chem. Soc. Jap.*, **1967**, *40*, 702-703.
23. Iwamura, M.; Inamoto, N. *Bull. Chem. Soc. Jap.*, **1970**, *43*, 856-860.
24. Janzen, E. G.; Blackburn, B. J. *J. Am. Chem. Soc.* **1969**, *91*, 4481-4490.
25. Janzen, E. G.; Gerlock, J. L. *Nature* **1969**, *222*, 867-868.
26. Lagercrantz, C.; Forchult, S. *Nature* **1968**, *218*, 1247-1248.
27. Lagercrantz, C.; Torssell, K. *Acta Chem. Scand.* **1968**, *22*, 1935-1941.
28. Chalfont, G. R.; Perkins, M. J.; Horsfield, A. *J. Am. Chem. Soc.* **1968**, *90*, 7141-7142.
29. Leaver, I. H.; Ramsey, G. C. *Tetrahedron* **1969**, *25*, 5669-5675.
30. Terabe, S.; Konaka, R. *J. Am. Chem. Soc.* **1969**, *91*, 5665-5657.
31. Janzen, E. G. *Acc. Chem. Res.* **1981**, *4*, 31.
32. Cheng, J. D.; Shine, H. J. *J. Org. Chem.* **1974**, *39*, 336.
33. Janzen, E. G.; Liu, P. *J. Magn. Reson.* **1973**, *9*, 510.
34. Wargon, J. A.; Williams, F. *J. Chem. Soc., Chem. Commun.* **1975**, 947.
35. Tordo, P.; Boyer, M.; Friedmann, A.; Santero, O.; Pujol, L. *J. Phys. Chem.* **1978**, *82*, 1742.
36. Gowenlock, B. G.; McCullough, K. J.; Manson, R. B. *J. Am. Chem. Soc. Perkin Trans. (II)*. **1988**, 701-703.

37. Mackor, A.; Wajer, Th. A. J. W.; de Boer, Th. J. *Tetrahedron Lett.* **1966**, 2115-2123.
38. Wajer, Th. A. J. W.; Mackor, A.; de Boer, Th. J.; Van Voorst, J. D. W. *Tetrahedron.* **1967**, 23, 4021-4026.
39. Kalyanaraman, B.; Perez-Reyes, E.; Mason, R. P.; *Tetrahedron Lett.* **1979**, 4809-4812.
40. Fischer, V.; Mason, R. P. *Chem. Biol. Interact.* **1986**, 57, 129-142.
41. Maender, O. W.; Janzen, E. G. *J. Org. Chem.* **1969**, 34, 4072-4082.
42. Hata, Y.; Watanabe, T. K.; Hirata, M.; *Chem-Biol. Interact.* **1987**, 63, 171-184.
43. Becker, A. R.; Sternson, L. A. *Proct. Natl. Acad. Sci.* **1981**, 78, 2003-2007.
44. Hampton, M. J.; Floyd, R. A.; Janzen, R. A.; Shetty, R. V. *Mutation Res.* **1981**, 91, 279-283.
45. Sies, H.; Mehlhorn, R. *Arch. Biochem. Biophys.* **1986**, 251, 393-396.
46. Martinie-Humbrouck, J.; Rassat, A. *Tetrahedron.* **1974**, 30, 433-436.
47. Castellano, A. L.; Griller, D.; Ingold, K. U. *Can. J. Chem.* **1982**, 60, 1501-1503.
48. Bullock, A. T.; Gavin, D. L.; Ingram, M. D. *J. Chem. Soc. Chem. Commun.* **1980**, 327-328.
49. Bowman, D. F.; Gillan, D. L.; Ingold, K. U. *J. Am. Chem. Soc.* **1970**, 93, 6555-6561.
50. Bowman, D. F.; Brokenshire, J. L.; Gillan, D. L.; Ingold, K. U. *J. Am. Chem. Soc.* **1970**, 93, 6551-6555.
51. Bowman, D. F.; Gillan, D. L.; Ingold, K. U. *J. Am. Chem. Soc.* **1970**, 93, 902-908.
52. Janzen, E. G.; Zhang, Y. K.; Arimura, M. *Chem. Lett.* **1993**, 497-500.
53. Kalyanaraman, B.; Mottley, C.; Mason, R. P. *J. Biol. Chem.* **1983**, 258, 3855-3858.
54. Rosen, G. M.; Rauckman, E. J. *Mol. Pharmacol.* **1980**, 17, 233-238.
55. Janzen, E. G.; Krygsman, P. H.; Lindsay, D. A.; Haire, D. L. *J. Am. Chem. Soc.* **1990**, 112, 8279-8284.
56. Sang, H.; Janzen, E. G.; Lewis, B. H. *J. Org. Chem.* **1996**, 61, 2358-2363.

57. Harbour, J. R.; Chow, V.; Bolton, J. R. *Can. J. Chem.* **1974**, *52*, 3549-3553.
58. Finkelstein, E.; Rosen, G. M.; Rauckman, E. J.; Paxton, J. *Mol. Pharmacol.* **1979**, *16*, 676.
59. Kalyanaraman, B.; Perez-Reyes, E.; Mason, R. P. *Biochem. Biophys. Acta.* **1980**, *630*, 119.
60. Finkelstein, E.; Rosen, G. M.; Rauckman, E. J.; Paxton, J. *Mol. Pharmacol.* **1980**, *102*, 4994.
61. Finkelstein, E.; Rosen, G. M.; Rauckman, E. J. *Mol. Pharmacol.* **1982**, *21*, 676-685.
62. Janzen, E. G.; Zhang, Y. K.; Arimura, M. *J. Org. Chem.* **1995**, *60*, 5434-5440.
63. Janzen, E. G.; Hinton, R. D.; Kotake, Y. *Tetrahedron Lett.* **1992**, *33*, 1257-1260.
64. Janzen, E. G.; Kotake, Y.; Hinton, R. D. *Free. Rad. Biol. Med.* **1992**, *12*, 169-173.
65. Janzen, E. G. *Free Rad. Biol.* **1980**, *4*, 115- 151.
66. Tordo, P.; Boyer, M.; Vila. F.; Pujol, L. *Phosphorus Sulfur*, **1977**, *3*, 43-45.
67. Tordo, P.; Boyer, M.; Vila. F.; Cerri, V. *Phosphorus Sulfur*, **1977**, *3*, 373-376.
68. Tordo, P.; Boyer, M.; Friedmann, A.; Santero, O.; Pujol, L. *J. Phys. Chem.* **1978**, *82*, 1742.
69. Kaena, J. F.; Van Nice, F. L. *Physiol. Chem. Phys. Med. NMR*, **1984**, *16*, 477-480.
70. Finkelstein, E.; Rosen, G. M.; Rauckman, E.; Paxton, J. *Mol. Pharmacol.* **1979**, *16*, 676-685.
71. Zeghdaoui, A.; Tuccio, B.; Finet, J. P.; Cerri, V.; Tordo, P. *J. Chem. Soc. Perkin Trans. 2.* **1995**, *12*, 2087-2089.
72. Tuccio, B.; Zeghdaoui, A.; Finet, J. P.; Cerri, V.; Tordo, P. *Res. Chem. Intermed.* **1996**, *22*, 393-404.
73. Liu, Y.P.; Wang, L. F.; Zhou, N.; Ji, Y. Q.; Liu, Y.; Liu, K. J.; Tian, Q. *J. Org. Chem.* **2006**, *71*, 7753-7762.
74. Jones, R. C. F.; Matin, J. N. *Chem. Heterocycl. Compd.* **2002**, *59*, 1-81.
75. Janzen, E. G.; Haire, D. L. *Adv. Free. Radical Chem.* **1990**, *1*, 253-295.
76. Swartz, H. M. *Bull. Magn. Reson.* **1986**, *8*, 172-175.

77. Naik, N.; Brasalu, R. *Tetrahedron*. **1998**, *54*, 667-696.
78. Hawker, C. J.; Bosman, A. W.; Harth, E. *Chem. Rev.* **2001**, *101*, 3661-3688.
79. Berliner, L. J. In *Spectroscopy in Biochemistry*; Bell, J. E., Ed.; CRC: Boca Raton, Fla, 1981; Vol. 2, pp 1-56.
80. Misik, V.; Reisz, P. *Ultrason. Sonochem.* **1996**, *3*, S173.
81. Stolze, K.; Udilova, N.; Nohl, H. *Free Radical Biol. Med.* **2000**, *29*, 1005.
82. Zhang, L.-Y.; Stone, K.; Pryor, W. A. *Free Radical Biol. Med.* **1995**, *19*, 161.
83. Ma, Z.; Zhao, B.; Yuan, Z. *Anal. Chim. Acta.* **1999**, *389*, 213.
84. Sankarapandi, S.; Zweier, J. *J. Biol. Chem.* **1999**, *274*, 34576.
85. Zweier, J. L.; Kuppusamy, P.; Lutty, G. A. *Proc. Natl. Acad. Sci. U.S.A.* **1987**, *84*, 1404.
86. Schrodinger, E. *Ann. Phys.* **1926**, *79*, 361-376.
87. Schrodinger, E. *Ann. Phys.* **1926**, *79*, 489-527.
88. Schrodinger, E. *Ann. Phys.* **1926**, *80*, 437-490.
89. Schrodinger, E. *Ann. Phys.* **1926**, *81*, 109-139.
90. Born, M. *Zeitschrift für Physik.* **1926**, *37*, 863-867.
91. Heisenberg, W. *Zeitschrift für Physik.* **1927**, *43*, 172-198.
92. Pauli, W. *Zeit. Phys.* **1925**, *31*, 765.
93. Born, M.; Oppenheimer, R. *Annalen der Physik.* **1927**, *84*, 457-484.
94. Hartree, D. R. *Proc. Cambridge. Philos.* **1928**, *24*, 89.
95. Fock, V. A. *Z. Phys.* **1930**, *61*, 126.
96. Fock, V. A. *Z. Phys.* **1930**, *62*, 795.
97. Slater, J. C. *Phys. Rev.* **1930**, *36*, 57.
98. Roothaan, C. C. J. *Rev. Mod. Phys.* **1951**, *23*, 69-89.

99. Hohenberg, P.; Kohn, W. *Phys. Rev.* **1964**, *136*, B864.
100. Kohn, W.; Sham, L. J. *Phys. Revs.* **1965**, *140*, 1133.
101. Slater, J. C. *Phys. Rev.* **1929**, *34*, 1293-1322.
102. Condon, E. U. *Phys. Rev.* **1930**, *36*, 1121-1133.
103. Jorgensen, W. L. *Encycl. Comput. Chem.* **1998**, *4*, 2826.
104. Poisson, S. D. *Nouveau Bulletin des Sciences par la Societ  Philomathique de Paris.* **1813**, *3*, 388-392.
105. Guoy, G. L. *de Phys.* **1910**, *9*, 457.
106. Chapman, D. L. *Philos. Mag.* **1913**, *25*, 475.
107. Born, M. Z. *Phys.* **1925**, *1*, 45.
108. Kirkwood, J. G. *J. Chem. Phys.* **1934**, *2*, 351.
109. Onsager, L. *J. Am. Chem. Soc.* **1936**, *58*, 1486.
110. Ben-Naim, A. *Solvation Thermodynamics*, Plenum, New York, 1987.
111. Tunon, I., Silla, J. L., *Chem. Phys. Lett.*, **1993**, *203*, 289.
112. Claverie, P. *Intermolecular Interactions: From Dynamics to Biomolecules*, ed. Pullman, B., Wiley, Chichester, 1978.
113. Miertus, S.; Scrocco, E.; Tomasi, J. *Chem. Phys.* **1981**, *55*, 117.
114. Klamt, A.; Sch urmann. *J. Chem. Soc. Perkin Trans 2.* **1993**, *2*, 799-805.
115. Klamt, A. *J. Phys. Chem.* **1995**, *99*, 2224-2235.
116. Klamt, A.; Jonas, Volker.; B rger, T.; Lohrenz, J. C. W. *J. Phys. Chem. A.* **1998**, *102*, 5074-5085.
117. Boys, S. F. *Proc. R. Soc. London Ser A.* **1950**, *200*, 542.

118. E. J. Bylaska, W. A. de Jong, N. Govind, K. Kowalski, T. P. Straatsma, M. Valiev, D. Wang, E. Apra, T. L. Windus, J. Hammond, P. Nichols, S. Hirata, M. T. Hackler, Y. Zhao, P.-D. Fan, R. J. Harrison, M. Dupuis, D. M. A. Smith, J. Nieplocha, V. Tipparaju, M. Krishnan, Q. Wu, T. Van Voorhis, A. A. Auer, M. Nooijen, E. Brown, G. Cisneros, G. I. Fann, H. Fruchtl, J. Garza, K. Hirao, R. Kendall, J. A. Nichols, K. Tsemekhman, K. Wolinski, J. Anchell, D. Bernholdt, P. Borowski, T. Clark, D. Clerc, H. Dachsel, M. Deegan, K. Dyllal, D. Elwood, E. Glendening, M. Gutowski, A. Hess, J. Jaffe, B. Johnson, J. Ju, R. Kobayashi, R. Kutteh, Z. Lin, R. Littlefield, X. Long, B. Meng, T. Nakajima, S. Niu, L. Pollack, M. Rosing, G. Sandrone, M. Stave, H. Taylor, G. Thomas, J. van Lenthe, A. Wong, and Z. Zhang, "NWChem, A Computational Chemistry Package for Parallel Computers, Version 5.1" (2007), Pacific Northwest National Laboratory, Richland, Washington 99352-0999, USA.

119. "High Performance Computational Chemistry: An Overview of NWChem a Distributed Parallel Application," Kendall, R.A.; Apra, E.; Bernholdt, D.E.; Bylaska, E.J.; Dupuis, M.; Fann, G.I.; Harrison, R.J.; Ju, J.; Nichols, J.A.; Nieplocha, J.; Straatsma, T.P.; Windus, T.L.; Wong, A.T.; *Computer Phys. Comm.* 2000, 128, 260-283.

120. Gordon, M. S.; Binkley, S. J.; Pople, J. A.; Pietro, W. J.; Hehre, W. J. *J. Am. Chem. Soc.* **1982**, 104, 2797-2803.

121. Becke, A. D. *J. Chem. Phys.* **1993**, 98, 1372-1377.

122. Tande, Jacob F. A Computational Study of Spin Traps, East Tennessee State University, **2007**, Master's Thesis.

123. Villamena, F.; Hadad, C. M.; Zweier, J. L. *J. Am. Chem. Soc.* **2004**, 126, 1816-1829.

124. Konda, Sai Sriharsha; Kirkby, Scott J. *Computational Investigation of Spin Traps Using Hybrid Solvation Models*. Abstracts, 60th Southeast Regional Meeting of the American Chemical Society, Nashville, TN, United States, November 12-15 (2008), SERM-115, American Chemical Society, Washington, D.C.
125. Boyd, S. L.; Boyd, R. J. *J. Phys. Chem.* **2001**, *105*, 7096-7105.
126. Ohba, T.; Ikawa, S. *Mol. Phys.* **1991**, *73*, 985.
127. Sriharsha Konda, Sai; Kirkby, Scott J. *Computational Investigation of Spin Traps Using Hybrid Solvation Models*. Abstracts of Papers, 237th ACS National Meeting, Salt Lake City, UT, United States, March 22-26 (2009), COMP-077, American Chemical Society, Washington, D. C.
128. Sai Sriharsha Konda, Scott, J. Kirkby, *Computational Investigation of Spin Traps Using Hybrid Solvation Models*. Abstracts, Appalachian Student Research Forum, East Tennessee State University, Johnson City, TN, United States, April 09 (2009), 88.
129. Villamena, F.; Hadad, C. M.; Zweier, J. L. *J. Phys. Chem.* **2005**, *109*, 1662-1674.
130. Maples, K. R.; Ma, F.; Zhang, Y. K. *Free Rad. Res.* **2000**, *34*, 417-426.
131. Williams, H. E.; Claybourn, M.; Green, R. *Free Rad. Res.* **2007**, *41*, 1047-1052.
132. Khramtsov, V. V.; Reznikov, V. A.; Berliner, L. J.; Litkin, A. K.; Grigor'ev, I. A.; Clanton, T. L. *Free Rad. Biol. Med.* **2001**, *30*, 1099-1107.
133. Selinsky, B. S.; Levy, L. A.; Motten, A. G.; London, R. E. *J. Magn. Reson.* **1989**, *81*, 57-67.
134. Janzen, E. G.; Zhang, Y. K.; Arimura, M. *J. Org. Chem.* **1995**, *60*, 5434-5440.
135. Zhao, C. X.; He, H. Y. *J. Fluorine Chem.* **1995**, *72*, 215-223.

APPENDICES

APPENDIX A: Single Point Energy Tables

Table 27. Difference in single point energies of DMPO when surrounded by water molecules.

Molecule	Energy difference (kcal/mol)
DMPO	0
DMPO + 1 water molecule	0.589
DMPO + 2 water molecules	0.719
DMPO + 3 water molecules	0.766
DMPO + 10 water molecules	2.008
DMPO + 17 water molecules	2.736

Table 28. Difference in single point energies of PBN *cis*-adduct when surrounded by water molecules.

Molecule	Energy difference (kcal/mol)
PBN adduct	0
PBN adduct + 1 water molecule	0.0251
PBN adduct + 4 water molecules	2.4906
PBN adduct + 8 water molecules	3.9213

Table 29. Difference in single point energies of PBN-Me adduct when surrounded by water molecules.

Molecule	Energy Difference (kcal/mol)
PBN- Me	0
PBN- Me + 1 water molecules	0.5141
PBN- Me + 3 water molecules	0.6154
PBN- Me + 7 water molecules	0.6456
PBN- Me + 11 water molecules	0.9453
PBN-Me + 15 water molecules	0.9900

Table 30. Difference in single point energies of PPN when surrounded by water molecules.

Molecule	Energy Difference (kcal/mol)
PPN	0
PPN + 1 water molecule	1.744
PPN + 3 water molecules	1.752
PPN + 7 water molecules	3.005
PPN + 11 water molecules	4.006

APPENDIX B: Structural Details of DMPO

1. Input file for DMPO geometry optimization.

```
=====
scratch_dir /scr/sai
permanent_dir /home/sai/nw_work/Spin-traps/DMPO-RDFT-6-31G
Title "DMPO-RDFT-6-31G"
```

```
Start DMPO-RDFT-6-31G
```

```
echo
```

```
charge 0
```

```
geometry autosym units angstrom
```

C	1.28314	3.28424	-0.954581
H	0.432444	3.94761	-1.06987
C	2.41265	3.20858	-1.91389
C	3.32595	2.13385	-1.31176
C	2.60248	1.65216	-0.0259173
N	1.39962	2.46809	0.0344717
O	0.479779	2.36835	0.998348
H	3.47620	1.31041	-2.04467
H	4.32465	2.57269	-1.09056
H	2.04048	2.90662	-2.91631
H	2.93135	4.18894	-1.97053
C	2.21523	0.167214	-0.128128
H	3.12368	-0.467967	-0.204572
H	1.63660	-0.145941	0.767828
H	1.58539	-0.00325839	-1.02801
C	3.46462	1.89861	1.22354
H	4.46045	2.29812	0.934816


```
H      2.96936      2.63256      1.89526
H      3.61142      0.953023     1.78795
```

```
end
```

```
ecce_print /home/sai/nw_work/Spin-traps/DMPO-RDFT-6-31G/ecce.out
```

```
basis "ao basis" cartesian print
```

```
  H library "6-31G*"
```

```
  O library "6-31G*"
```

```
  C library "6-31G*"
```

```
  N library "6-31G*"
```

```
END
```

```
dft
```

```
  mult 1
```

```
  XC b3lyp
```

```
  iterations 200
```

```
  mulliken
```

```
end
```

```
driver
```

```
  gmax 0.00045
```

```
  grms 0.0003
```

```
  xmax 5e-05
```

```
  xrms 0.0012
```

```
  maxiter 100
```

```
end
```

```
task dft optimize
```

```
=====
```

APPENDIX C: Structural Details of PBN/PBN-OH

1. Input file for PBN geometry optimization.

```
=====
scratch_dir /scr/sai
permanent_dir /home/sai/nw_work/Spin-traps/PBN/PBN
Title "PBN"
```

Start PBN

echo

charge 0

geometry autosym units angstrom

C	0.126771	0.0561804	0.00160139
H	-0.788961	-0.522775	0.0125691
C	0.0634188	1.46461	-0.0247405
H	-0.897060	1.96924	-0.0163045
C	1.25046	2.22662	-0.0729991
H	1.15577	3.30158	-0.135154
C	2.52679	1.59392	-0.0430856
C	2.57708	0.164760	-0.0144289
H	3.52903	-0.358724	0.000294584
C	1.38177	-0.597964	-0.000628249
H	1.41955	-1.68247	0.00721104
C	3.80226	2.38372	-0.0187180
N	3.84261	3.66579	0.223547
H	4.72796	1.81461	-0.0143679
O	2.97353	4.12058	1.11105
C	5.06514	4.46671	0.0614132
C	5.83372	4.13714	-1.24476
H	5.22864	4.40692	-2.13771
H	6.77482	4.72733	-1.28704

```
H      6.11384      3.06733      -1.31312
C      4.72603      5.97956      0.0162774
H      4.12664      6.22756     -0.887103
H      4.15445      6.30012      0.913648
H      5.65885      6.58395     -0.0152634
C      5.96335      4.20705      1.28498
H      5.41455      4.47915      2.21531
H      6.22819      3.12968      1.34796
H      6.89354      4.80649      1.23798
```

end

```
ecce_print /home/sai/nw_work/Spin-traps/PBN/PBN/ecce.out
```

```
basis "ao basis" cartesian print
```

```
  H library "6-31G*"
```

```
  O library "6-31G*"
```

```
  C library "6-31G*"
```

```
  N library "6-31G*"
```

```
END
```

```
dft
```

```
  mult 1
```

```
  XC b3lyp
```

```
  iterations 200
```

```
  mulliken
```

```
end
```

```
driver
```

```
  default
```

```
  maxiter 100
```

```
end
```

```
task dft optimize
```

```
=====
```

2. Input file for PBN-OH cis adduct geometry optimization.

```
=====
scratch_dir /scr/sai
permanent_dir /home/sai/nw_work/Spin-traps/PBN/PBN-adduct
Title "PBN-adduct"

Start PBN-adduct
echo
charge 0

geometry autosym units angstrom
C      -0.00710432      -3.67877      -0.780622
H      -0.139851       -4.64104      -1.25786
C      -0.907584       -3.25822       0.220842
H      -1.73159        -3.89753       0.509858
C      -0.737371       -2.00202       0.842864
H      -1.44379        -1.69197       1.60252
C      0.345150        -1.15780       0.474190
C      1.23812         -1.58702      -0.542899
H      2.06245         -0.958076      -0.853320
C      1.06377         -2.84350      -1.16346
H      1.75061         -3.16531      -1.93549
C      0.517148        0.205410       1.10852
N      -0.373438        1.17405       0.453540
O      -1.69138        0.954079       0.533009
C      0.130310        2.40014       -0.211233
C      1.09082         2.02416       -1.35758
H      0.600351        1.30612       -2.04941
H      1.38498         2.92667       -1.93596
H      2.02233         1.56082       -0.973474
```

C	-1.04241	3.20942	-0.811268
H	-1.59272	2.60078	-1.56110
H	-1.75440	3.51720	-0.0151658
H	-0.673632	4.12886	-1.31582
C	0.857764	3.29147	0.815120
H	0.183545	3.52302	1.66759
H	1.76501	2.79378	1.21538
H	1.17694	4.24816	0.347602
H	1.57833	0.520479	0.999076
O	0.211444	0.154623	2.47830
H	0.959994	-0.323404	2.92292

end

ecce_print /home/sai/nw_work/Spin-traps/PBN/PBN-adduct/ecce.out

basis "ao basis" cartesian print

H library "6-31G*"

O library "6-31G*"

C library "6-31G*"

N library "6-31G*"

END

dft

mult 2

XC b3lyp

iterations 200

mulliken

end

driver

default

maxiter 100

end

task dft optimize

APPENDIX D: Structural Details of PBN-Me

4. Input file for PBN-Me adduct geometry optimization.

```
=====
scratch_dir /scr/sai
permanent_dir /home/sai/nw_work/PBN-Me/PBN-Me-adduct
Title "PBN-Me-adduct"
```

```
Start PBN-Me-adduct
```

```
echo
```

```
charge 0
```

```
geometry autosym units angstrom
```

```
C      -0.840052      -3.65708      0.543024
H      -1.18299      -4.59947      0.951999
C       0.179195      -2.93589      1.19918
H       0.619988      -3.32660      2.10801
C       0.633629      -1.70993      0.665143
H       1.42828      -1.18417      1.17610
C       0.0573581     -1.18308     -0.523562
C      -0.958935     -1.92605     -1.18095
H      -1.39725     -1.55909     -2.09950
C      -1.40728     -3.15449     -0.647510
H      -2.18008     -3.71708     -1.15526
C       0.552347      0.116882     -1.12638
N       0.690601      1.15507     -0.0852553
O       1.85155      1.23858      0.576968
C      -0.314842      2.22729      0.105444
C      -1.75211      1.66288      0.0236993
H      -1.86871      0.801747      0.715881
```

H	-2.49540	2.44123	0.301650
H	-2.00645	1.32847	-1.00237
C	-0.140256	2.86791	1.49998
H	-0.237936	2.09556	2.29364
H	0.857608	3.34735	1.59679
H	-0.910685	3.64883	1.67560
C	-0.112626	3.30887	-0.970261
H	0.919752	3.71794	-0.913503
H	-0.264915	2.89007	-1.98721
H	-0.829900	4.14574	-0.826601
H	-0.169881	0.460249	-1.89581
C	1.87244	-0.109314	-1.87364
H	1.71445	-0.836404	-2.70017
H	2.23076	0.847257	-2.31067
H	2.65332	-0.509591	-1.19351

end

ecce_print /home/sai/nw_work/PBN-Me/PBN-Me-adduct/ecce.out

basis "ao basis" cartesian print

H library "6-31G*"

O library "6-31G*"

C library "6-31G*"

N library "6-31G*"

END

dft

mult 2

XC b3lyp

iterations 200

mulliken

end

```
driver
  default
  maxiter 100
end
```

```
task dft optimize
```

```
=====
```


APPENDIX E: Structural Details of PPN

5. Input file for PPN geometry optimization.

```
=====
scratch_dir /scr/sai
```

```
permanent_dir /home/sai/nw_work/PPN/PPN-1
```

```
Title "PPN-1"
```

```
Start PPN-1
```

```
echo
```

```
charge 0
```

```
geometry autosym units angstrom
```

C	-0.510622	4.91974	0.0457371
H	-1.38133	5.56905	0.00295667
C	-0.644633	3.57864	-0.309462
H	-1.59668	3.17768	-0.627059
C	0.475368	2.71981	-0.262773
C	1.71643	3.25582	0.149696
H	2.58687	2.60527	0.191703
C	1.83749	4.59373	0.504486
H	2.80168	4.98302	0.820451
C	0.721229	5.43432	0.453954
C	0.464854	1.31268	-0.612689
H	1.39430	0.764815	-0.539608
N	-0.583711	0.597203	-0.970792
O	-1.77877	1.04820	-1.05450
C	-0.394448	-0.888034	-1.33189
C	-1.75008	-1.45309	-1.76610
H	-2.11764	-0.905124	-2.63679

H	-1.62245	-2.50631	-2.02705
H	-2.49331	-1.36795	-0.973669
C	0.638863	-1.01346	-2.46494
H	0.314255	-0.412738	-3.32134
H	1.63573	-0.685819	-2.16183
H	0.710343	-2.05872	-2.77936
P	0.234640	-1.75832	0.192919
O	1.56511	-1.29239	0.675421
O	0.136337	-3.28638	-0.310261
O	-0.949416	-1.68657	1.28846
C	0.602787	-4.36648	0.544478
H	0.418840	-4.10590	1.59219
H	-0.0362563	-5.21681	0.291813
C	2.06963	-4.67288	0.292285
H	2.69144	-3.81102	0.549117
H	2.38026	-5.52816	0.904085
H	2.23449	-4.92517	-0.760350
C	-0.935152	-0.736568	2.39391
H	-0.00576799	-0.161726	2.36250
H	-0.933009	-1.34039	3.30700
C	-2.16362	0.152785	2.31650
H	-3.07817	-0.446010	2.38231
H	-2.15647	0.861920	3.15277
H	-2.18486	0.714426	1.37740
H	0.813193	6.48128	0.730637

end

ecce_print /home/sai/nw_work/PPN/PPN-1/ecce.out

basis "ao basis" cartesian print

H library "6-31G*"

O library "6-31G*"

```
C library "6-31G*"
N library "6-31G*"
P library "6-31G*"
END
```

```
dft
  mult 1
  XC b3lyp
  iterations 200
  mulliken
end
```

```
driver
  default
  maxiter 100
end
```

```
task dft optimize
```

```
=====
```

APPENDIX F: COSMO Files

6. Input file for COSMO calculation of DMPO.

```
=====
scratch_dir /scr/sai
permanent_dir /home/sai/nw_work/Spin-traps/DMPO-RDFT-COSMO-1
Title "DMPO-RDFT-COSMO-1"

Start DMPO-RDFT-COSMO-1

echo

charge 0

geometry autosym units angstrom
C      0.953659      1.38186      -0.0671880
H      1.91000      1.88732      -0.104842
C     -0.388225      1.97269      0.222300
C     -1.35421      0.809028     -0.122296
C     -0.497766     -0.473188     -0.0642258
N      0.917990      0.0830835     -0.221829
O      1.87675     -0.717911     -0.424313
H     -2.20933      0.758502      0.558069
H     -1.74597      0.944766     -1.13579
H     -0.473095      2.27806      1.27659
H     -0.593526      2.86897     -0.375373
C     -0.541071     -1.17791      1.29744
H     -1.50555     -1.67898      1.43267
H      0.256264     -1.92464      1.35176
H     -0.405255     -0.465539      2.11908
C     -0.753954     -1.45370     -1.20570
H     -0.694454     -0.949616     -2.17635
```

```
H      -0.00857352      -2.25246      -1.18748
H      -1.75289       -1.89173       -1.10465
end

ecce_print /home/sai/nw_work/Spin-traps/DMPO-RDFT-COSMO-
1/ecce.out

basis "ao basis" cartesian print
  H library "6-31G*"
  O library "6-31G*"
  C library "6-31G*"
  N library "6-31G*"
END
dft
  mult 1
  XC b3lyp
  iterations 200
  mulliken
end

driver
  gmax 0.00045
  grms 0.0003
  xmax 5e-05
  xrms 0.0012
  maxiter 100
end
cosmo
end

task dft optimize
```

```
=====
```

2. Input file for the COSMO calculation of PBN-OH cis adduct.

```
=====

scratch_dir /scr/sai
permanent_dir /home/sai/nw_work/Spin-traps/PBN/cosmo-PBN-adduct
Title "cosmo-PBN-adduct"

Start cosmo-PBN-adduct

echo

charge 0

geometry autosym units angstrom
C      -0.937782      -3.56333      0.172604
H      -1.22287      -4.54147      0.536839
C      -0.0436775     -2.76727      0.917640
H       0.358746     -3.13779      1.85064
C       0.339594     -1.49560      0.439197
H       1.05183      -0.924379     1.01542
C      -0.194742     -0.991989     -0.779041
C      -1.08990     -1.80761     -1.52146
H      -1.49832     -1.45985     -2.46175
C      -1.45729     -3.08571     -1.04844
H      -2.13785     -3.69905     -1.62446
C       0.234484      0.349891     -1.34572
N       0.307579      1.38814     -0.299451
O       1.42847      1.47072      0.426653
C      -0.748449      2.41432     -0.122837
C      -2.12293      1.73618      0.0470555
H      -2.41353      1.16600     -0.860834
```

```
H    -2.91374    2.49478    0.230887
H    -2.09940    1.03925    0.911420
C    -0.470401   3.25784    1.14360
H    -0.410789   2.60357    2.04056
H    0.490950    3.80534    1.04733
H    -1.27611    4.00591    1.31033
C    -0.775975   3.36101    -1.33976
H    0.227905    3.80858    -1.50426
H    -1.07925    2.82792    -2.26325
H    -1.50401    4.18507    -1.17858
H    -0.507926   0.654186   -2.11029
O    1.46530     0.235272   -2.01332
H    2.12515     -0.125702  -1.36629
```

end

```
ecce_print /home/sai/nw_work/Spin-traps/PBN/cosmo-PBN-
adduct/ecce.out
```

```
basis "ao basis" cartesian print
```

```
  H library "6-31G*"
```

```
  O library "6-31G*"
```

```
  C library "6-31G*"
```

```
  N library "6-31G*"
```

END

```
dft
```

```
  mult 2
```

```
  XC b3lyp
```

```
  iterations 200
```

```
  mulliken
```

end

```
driver
  default
  maxiter 100
end
```

```
cosmo
end
```

```
task dft optimize
```

```
=====
```


APPENDIX G: OUTPUT COORDINATES FOR THE OPTIMIZED SPIN TRAPS

1. Output coordinates for DMPO spin trap.

Output coordinates in angstroms (scale by 1.889725989 to convert to a.u.)

No.	Tag	Charge	X	Y	Z
1	C	6.0000	0.95365936	1.38186194	-0.06718796
2	H	1.0000	1.90999970	1.88732081	-0.10484168
3	C	6.0000	-0.38822459	1.97269217	0.22230038
4	C	6.0000	-1.35421453	0.80902805	-0.12229574
5	C	6.0000	-0.49776626	-0.47318794	-0.06422578
6	N	7.0000	0.91799001	0.08308349	-0.22182910
7	O	8.0000	1.87675051	-0.71791104	-0.42431271
8	H	1.0000	-2.20932856	0.75850200	0.55806931
9	H	1.0000	-1.74597294	0.94476572	-1.13578866
10	H	1.0000	-0.47309466	2.27805678	1.27658895
11	H	1.0000	-0.59352551	2.86896753	-0.37537327
12	C	6.0000	-0.54107145	-1.17790792	1.29744107
13	H	1.0000	-1.50554849	-1.67898178	1.43266995
14	H	1.0000	0.25626418	-1.92464447	1.35175516
15	H	1.0000	-0.40525514	-0.46553878	2.11907755
16	C	6.0000	-0.75395367	-1.45370333	-1.20570287
17	H	1.0000	-0.69445429	-0.94961637	-2.17635422
18	H	1.0000	-0.00857352	-2.25245998	-1.18748091
19	H	1.0000	-1.75288662	-1.89172588	-1.10465159

2. Output coordinates for PBN spin trap.

Output coordinates in angstroms (scale by 1.889725989 to convert to a.u.)

No.	Tag	Charge	X	Y	Z
1	C	6.0000	-0.23222150	-4.10396129	-0.02789435
2	H	1.0000	-0.39026431	-5.17831648	0.01461741
3	C	6.0000	-1.20119714	-3.22897701	0.46636559
4	H	1.0000	-2.11830790	-3.62382712	0.89599143
5	C	6.0000	-1.01274794	-1.84871216	0.41933041
6	H	1.0000	-1.76047190	-1.16827340	0.80117677
7	C	6.0000	0.17105721	-1.31540975	-0.13449684

8	C	6.0000	1.14218645	-2.21336953	-0.63077173
9	H	1.0000	2.06027463	-1.81871110	-1.06110796
10	C	6.0000	0.94450987	-3.58792431	-0.57873665
11	H	1.0000	1.70682765	-4.25807257	-0.96722289
12	C	6.0000	0.47931803	0.09961502	-0.23885635
13	N	7.0000	-0.27415688	1.10332685	0.16032853
14	H	1.0000	1.42274647	0.36702568	-0.68961015
15	O	8.0000	-1.42010564	0.97210216	0.71352592
16	C	6.0000	0.16415989	2.56295616	-0.00504023
17	C	6.0000	1.53719247	2.71135961	-0.66814368
18	H	1.0000	1.55526655	2.29893898	-1.68250868
19	H	1.0000	1.76613944	3.77933834	-0.74570466
20	H	1.0000	2.33539279	2.24806069	-0.07857561
21	C	6.0000	-0.91805596	3.23342892	-0.86562302
22	H	1.0000	-0.92152484	2.81876420	-1.88003902
23	H	1.0000	-1.90150575	3.07464567	-0.42026271
24	H	1.0000	-0.72237762	4.30861360	-0.93451764
25	C	6.0000	0.18937619	3.15883713	1.41110810
26	H	1.0000	-0.77281621	3.00028746	1.90077675
27	H	1.0000	0.97263254	2.68974652	2.01727729
28	H	1.0000	0.39402834	4.23318041	1.35669789

3. Output coordinates for PBN-OH cis adduct.

Output coordinates in angstroms (scale by 1.889725989 to convert to a.u.)

No.	Tag	Charge	X	Y	Z
1	C	6.0000	-0.82524173	-3.66469945	0.54659216
2	H	1.0000	-1.15572915	-4.61332694	0.96120519
3	C	6.0000	0.16997882	-2.92560033	1.19258774
4	H	1.0000	0.61471769	-3.29906400	2.11130556
5	C	6.0000	0.59486253	-1.70770219	0.66469660
6	H	1.0000	1.36291289	-1.13006764	1.17116584
7	C	6.0000	0.02728643	-1.21436035	-0.51793904
8	C	6.0000	-0.96771550	-1.95805004	-1.15856218
9	H	1.0000	-1.40911983	-1.58362317	-2.07999181
10	C	6.0000	-1.39399271	-3.17868832	-0.63069182
11	H	1.0000	-2.16852412	-3.74707055	-1.13884801
12	C	6.0000	0.51980375	0.08629827	-1.14359921
13	N	7.0000	0.65874158	1.15040169	-0.09833122
14	O	8.0000	1.84649013	1.29706541	0.37415110

15	C	6.0000	-0.34007948	2.24359800	0.11041746
16	C	6.0000	-1.76421117	1.67369427	0.00558939
17	H	1.0000	-1.91831366	0.85855842	0.71908291
18	H	1.0000	-2.48204636	2.46882519	0.23266660
19	H	1.0000	-1.99783393	1.30292003	-0.99727837
20	C	6.0000	-0.11375805	2.81861425	1.51613686
21	H	1.0000	-0.26716730	2.04899788	2.27963984
22	H	1.0000	0.90012856	3.20761332	1.62216781
23	H	1.0000	-0.82705445	3.63019520	1.69402411
24	C	6.0000	-0.09507866	3.32476932	-0.96152771
25	H	1.0000	0.93009403	3.70038123	-0.88985358
26	H	1.0000	-0.24745133	2.92842900	-1.97169560
27	H	1.0000	-0.78599453	4.16330508	-0.81940385
28	H	1.0000	-0.20659766	0.43099653	-1.88596347
29	O	8.0000	1.75128233	-0.05949774	-1.79104365
30	H	1.0000	2.41010872	0.17755634	-1.10472617

4. Output coordinates for PBN-OH trans adduct.

Output coordinates in angstroms (scale by 1.889725989 to convert to a.u.)

No.	Tag	Charge	X	Y	Z
1	C	6.0000	-0.56807972	3.70106080	0.36918794
2	H	1.0000	-0.92335713	4.67778807	0.68656506
3	C	6.0000	-1.43702345	2.81085139	-0.26672775
4	H	1.0000	-2.47089205	3.09233181	-0.44832051
5	C	6.0000	-0.98069807	1.55758018	-0.67264996
6	H	1.0000	-1.65635005	0.86562269	-1.16858964
7	C	6.0000	0.34838855	1.17839425	-0.44280993
8	C	6.0000	1.21836979	2.07639195	0.18208022
9	H	1.0000	2.25000036	1.78840877	0.34939282
10	C	6.0000	0.75846132	3.33058825	0.58991480
11	H	1.0000	1.44174500	4.01886023	1.08050236
12	C	6.0000	0.83404812	-0.16711044	-0.95562677
13	N	7.0000	-0.11668970	-1.28020151	-0.70675641
14	O	8.0000	-0.42499269	-1.97421345	-1.74967896
15	C	6.0000	-0.34977617	-1.94262560	0.62696470
16	C	6.0000	-0.07775962	-0.98595933	1.79556113
17	H	1.0000	-0.74804760	-0.12255021	1.77859056
18	H	1.0000	-0.25223480	-1.52973067	2.73084050
19	H	1.0000	0.95443381	-0.62877381	1.79955832

20	C	6.0000	-1.82076532	-2.39114854	0.64756651
21	H	1.0000	-2.48981466	-1.52522082	0.59576467
22	H	1.0000	-2.03543921	-3.04539441	-0.19983906
23	H	1.0000	-2.02940904	-2.93103824	1.57749198
24	C	6.0000	0.58054046	-3.16949755	0.71097400
25	H	1.0000	0.43481216	-3.81045250	-0.16332238
26	H	1.0000	1.62931837	-2.85843697	0.75534285
27	H	1.0000	0.35952215	-3.75152244	1.61255650
28	H	1.0000	0.85842971	-0.14500399	-2.05150289
29	O	8.0000	2.12286860	-0.43549187	-0.43470637
30	H	1.0000	2.49275631	-1.17040323	-0.94910570

5. Output coordinates for PBN-Me cis adduct.

Output coordinates in angstroms (scale by 1.889725989 to convert to a.u.)

No.	Tag	Charge	X	Y	Z
1	C	6.0000	-0.65387276	-3.77620442	0.35936252
2	H	1.0000	-1.01862226	-4.76793984	0.61343107
3	C	6.0000	-0.12941513	-2.94421893	1.35129199
4	H	1.0000	-0.08513081	-3.28798347	2.38158315
5	C	6.0000	0.34049849	-1.67063627	1.02967347
6	H	1.0000	0.74307192	-1.02086185	1.80053156
7	C	6.0000	0.28622275	-1.20927548	-0.29264508
8	C	6.0000	-0.24422264	-2.04801598	-1.28011652
9	H	1.0000	-0.29355253	-1.70071616	-2.31064660
10	C	6.0000	-0.70953975	-3.32462268	-0.95964116
11	H	1.0000	-1.11993455	-3.96159122	-1.73900285
12	C	6.0000	0.83327144	0.16328890	-0.67853406
13	N	7.0000	0.44590310	1.20801157	0.29642630
14	O	8.0000	1.15564081	1.32654050	1.36086821
15	C	6.0000	-0.66021776	2.18269909	0.02544756
16	C	6.0000	-1.93124400	1.42049001	-0.39461752
17	H	1.0000	-2.23965117	0.71725888	0.38510037
18	H	1.0000	-2.74675339	2.13372599	-0.55852253
19	H	1.0000	-1.79456395	0.85849843	-1.32373416
20	C	6.0000	-0.92963002	2.96469807	1.31696255
21	H	1.0000	-1.21655885	2.29256430	2.13028774
22	H	1.0000	-0.04570088	3.51928813	1.63733813
23	H	1.0000	-1.74800640	3.67103889	1.14016079
24	C	6.0000	-0.21174829	3.14997329	-1.09004479

25 H	1.0000	0.69898547	3.68029469	-0.79322629
26 H	1.0000	-0.01457794	2.62526206	-2.03163017
27 H	1.0000	-0.99462226	3.89214047	-1.28356497
28 H	1.0000	0.38585024	0.44691427	-1.63623249
29 C	6.0000	2.36079438	0.14349203	-0.84531184
30 H	1.0000	2.64082070	-0.61663909	-1.58131257
31 H	1.0000	2.72418751	1.11852614	-1.18748403
32 H	1.0000	2.84208071	-0.08965537	0.10626920

6. Output coordinates for PPN spin trap.

Output coordinates in angstroms (scale by 1.889725989 to convert to a.u.)

No.	Tag	Charge	X	Y	Z
1 C		6.0000	0.49361425	-4.89327603	-0.11634541
2 H		1.0000	1.29669109	-5.54878805	-0.44334104
3 C		6.0000	0.50742836	-3.55499410	-0.50552489
4 H		1.0000	1.30026878	-3.16229082	-1.12618550
5 C		6.0000	-0.52826562	-2.68824520	-0.09297623
6 C		6.0000	-1.56228027	-3.21349992	0.71482713
7 H		1.0000	-2.36530748	-2.55673057	1.04105919
8 C		6.0000	-1.56402858	-4.54868394	1.09928162
9 H		1.0000	-2.36871476	-4.92964586	1.72248306
10 C		6.0000	-0.53307074	-5.39722978	0.68418351
11 C		6.0000	-0.62873112	-1.28310153	-0.43640234
12 H		1.0000	-1.47754249	-0.72841031	-0.06063799
13 N		7.0000	0.24312467	-0.57674776	-1.12961317
14 O		8.0000	1.33929185	-1.03640904	-1.60488017
15 C		6.0000	-0.04893017	0.90788931	-1.41723538
16 C		6.0000	1.08602605	1.46130169	-2.28396777
17 H		1.0000	1.13846736	0.90629229	-3.22348747
18 H		1.0000	0.88351346	2.51402376	-2.49475557
19 H		1.0000	2.05112082	1.37512019	-1.78521955
20 C		6.0000	-1.40114039	1.03459518	-2.14022960
21 H		1.0000	-1.38459472	0.42725978	-3.05156199
22 H		1.0000	-2.24071163	0.71540732	-1.51878768
23 H		1.0000	-1.56861787	2.07869953	-2.42009198
24 P		15.0000	-0.12750597	1.79039866	0.22391842
25 O		8.0000	-1.22212237	1.33612037	1.12695934
26 O		8.0000	-0.19601729	3.31512262	-0.29421480

27	O	8.0000	1.35447077	1.71632802	0.86083866
28	C	6.0000	-0.34444869	4.40284763	0.65948136
29	H	1.0000	0.17838061	4.14654318	1.58706416
30	H	1.0000	0.17710169	5.24748406	0.20138545
31	C	6.0000	-1.80964592	4.71785632	0.91068779
32	H	1.0000	-2.31352653	3.86156290	1.36705518
33	H	1.0000	-1.89355869	5.57842021	1.58500833
34	H	1.0000	-2.31624420	4.96574842	-0.02778668
35	C	6.0000	1.70647999	0.77222238	1.91407871
36	H	1.0000	0.81750841	0.20343755	2.19940088
37	H	1.0000	2.01251262	1.38077816	2.77102480
38	C	6.0000	2.83433506	-0.12571046	1.43684829
39	H	1.0000	3.72090911	0.46734593	1.18876762
40	H	1.0000	3.10404040	-0.83034370	2.23246638
41	H	1.0000	2.53778220	-0.69245494	0.54878516
42	H	1.0000	-0.53216547	-6.44208580	0.98316479

VITA
SAI SRIHARSHA MANOJ KONDA

Personal Data: Date of Birth: April 04, 1985
 Place of Birth: Eluru, India
 Marital Status: Single

Education: Public Schools, Visakhapatnam, India
 B. Sc. Chemistry (Hons.), Sri Sathya Sai University, Prasanthi
 Nilayam, India 2005
 M. Sc. Chemistry, Sri Sathya Sai University, Prasanthi
 Nilayam, India 2007
 M. S. Chemistry, East Tennessee State University,
 Johnson City, Tennessee 2009

Professional Experience Graduate Teaching Assistant, East Tennessee State University,
 Department of Chemistry, 2007- 2009

Honors and Awards Outstanding Teaching Assistant, East Tennessee State University,
 College of Arts and Science, 2007- 2008
 Outstanding Teaching Assistant, East Tennessee State University,
 School of Graduate Studies, 2008-2009
 Research Grant Award, East Tennessee State University,
 School of Graduate Studies, 2008-2009